

AD 746031

ANNUAL REPORT

31 December 1971

POST-DOCTORAL RESEARCH IN SEISMOLOGY

PREPARED FOR

Geophysics Division

Air Force Office of Scientific Research

Arlington, Virginia 22209

by

Department of Earth and Planetary Sciences

Massachusetts Institute of Technology

Cambridge, Massachusetts 02139

SEE AD 714112

Sponsored by

Advanced Research Project Agency

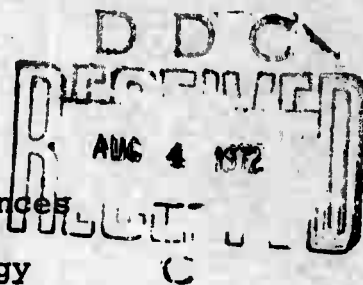
Nuclear Test Detection Office

Project Vela-Uniform

ARPA Order 292 67

Approved for public release;  
distribution unlimited.

Reproduced by  
NATIONAL TECHNICAL  
INFORMATION SERVICE  
U S Department of Commerce  
Springfield VA 22151



R  
151

**BEST  
AVAILABLE COPY**

### AVAILABILITY

Qualified requestors may obtain additional copies from the Defense Documentation Center, all others should apply to the Clearinghouse for Federal Scientific and Technical Information.

Distribution of this document is unlimited.

ACCESSION NO.	
RTIC	White Section <input checked="" type="checkbox"/>
DDC	Blue Section <input type="checkbox"/>
UNCLASSIFIED	<input type="checkbox"/>
JUSTIFICATION.....	
BY.....	
DISTRIBUTION/AVAILABILITY CODES	
Dist.	Avail. S.O. or SPECIAL
A	

## DOCUMENT CONTROL DATA - R &amp; D

(Security classification of title, body of abstract and indexing annotation must be entered when the overall report is classified)

1. ORIGINATING ACTIVITY (Corporate author) Massachusetts Institute of Technology Department of Earth and Planetary Sciences Cambridge, Massachusetts 02139		2a. REPORT SECURITY CLASSIFICATION UNCLASSIFIED	
		2b. GROUP	
3. REPORT TITLE  Post-Doctoral Research in Seismology			
4. DESCRIPTIVE NOTES (Type of report and inclusive dates) Scientific:.....Interim			
5. AUTHOR(S) (First name, middle initial, last name) Frank Press M. Nafi Toksöz (Keiiti Aki)			
6. REPORT DATE 31 December 1971	7a. TOTAL NO. OF PAGES 149	7b. NO. OF REFS 100	
6a. CONTRACT OR GRANT NO. AF49/638/1763	9a. ORIGINATOR'S REPORT NUMBER(S)		
b. PROJECT NO. 8652			
c. 62701D	9b. OTHER REPORT NO(S) (Any other numbers that may be assigned this report) AEOSR - TR - 72 - 1324		
d.			
10. DISTRIBUTION STATEMENT  Approved for public release; distribution unlimited.			
11. SUPPLEMENTARY NOTES  TECH, OTHER		12. SPONSORING MILITARY ACTIVITY Air Force Office of Scientific Research (NPG) 1400 Wilson Boulevard Arlington, Virginia 22209	
13. ABSTRACT <p>Research has been carried out on observations of surface and body waves from explosions and earthquakes, array processing of seismic data, source properties of earthquakes, theoretical and experimental studies of body wave propagation, and structure and dynamics of the crust and upper mantle.</p> <p>The spectra of waves generated by earthquakes and underground explosions have been studied using the Large Aperture Seismic Array (LASA) in Montana and the M.I.T. tiltmeter in Harvard, Massachusetts.</p> <p>Shear waves generated by large underground explosions have been used to estimate the magnitude of tectonic strain release accompanying the explosions.</p> <p>Near-field observations of the Parkfield earthquakes are fitted by a gliding-edge dislocation model. Seismic data were used to investigate the focal depth of earthquakes and core waves.</p> <p>Theoretical studies of body wave propagation have been done using finite differences, complex frequency, and generalized ray theory. Non-linear loss mechanisms are being treated numerically.</p> <p>The structure of the crust and upper mantle has been studied using seismic travel-times and spectral ratios. Numerical simulations have been done on the thermal behavior of a downgoing slab and on the thermal and viscous flow behavior at mid-ocean ridges.</p>			

14.

## KEY WORDS

Seismology  
Body waves  
Surface waves  
Array  
Seismic source  
Seismic discrimination  
Crustal structure  
Upper mantle structure

LINK A

LINK B

LINK C

ROLE

WT

ROLE

WT

ROLE

WT

Department of Earth and Planetary Sciences  
Massachusetts Institute of Technology  
Cambridge, Massachusetts 02139

POST-DOCTORAL RESEARCH IN SEISMOLOGY

Annual Report

to

Air Force Office of Scientific Research

1 July 1969 - 30 June 1971

ARPA Order No. 292 67

Project Code No. 8652

Name of Contractor - Massachusetts Institute of Technology

Date of Contract - 1 July 1966

Amount of Contract - \$377,755.

Contract No. AF49(638)-1763

Contract Termination Date - 30 June 1972

Project Scientists - Frank Press 617/864-6900, ext. 3382  
M. Nafi Toksöz 617/864-6900, ext. 6382  
(Keiiti Aki 617/864-6900, ext. 6397)

Short Title of Work - Post-Doctoral Research in Seismology

Approved for public release;  
distribution unlimited.

## ABSTRACT

Research has been carried out on observations of surface and body waves from explosions and earthquakes, array processing of seismic data, source properties of earthquakes, theoretical and experimental studies of body wave propagation, and structure and dynamics of the crust and upper mantle.

The spectra of waves generated by earthquakes and underground explosions have been studied using the Large Aperture Seismic Array (LASA) in Montana and the M.I.T. tiltmeter in Harvard, Massachusetts.

Shear waves generated by large underground explosions have been used to estimate the magnitude of tectonic strain release accompanying the explosions.

Near-field observations of the Parkfield earthquakes are fitted by a gliding-edge dislocation model. Seismic data were used to investigate the focal depth of earthquakes and core waves.

Theoretical studies of body wave propagation have been done using finite differences, complex frequency, and generalized ray theory. Non-linear loss mechanisms are being treated numerically.

The structure of the crust and upper mantle has been studied using seismic travel-times and spectral ratios. Numerical simulations have been done on the thermal behavior of

a downgoing slab and on the thermal and viscous flow behavior at mid-ocean ridges.

## TABLE OF CONTENTS

	Page
I. INTRODUCTION . . . . .	1
II. OBSERVATIONS OF SURFACE AND BODY WAVES . . . . . FROM EXPLOSIONS AND EARTHQUAKES	8
III. ARRAY PROCESSING OF SEISMIC DATA . . . . .	10
IV. SOURCE PROPERTIES OF EARTHQUAKES . . . . .	25
V. THEORETICAL AND EXPERIMENTAL STUDIES OF . . . . . BODY-WAVE PROPAGATION	45
VI. STRUCTURE AND DYNAMICS OF THE CRUST AND . . . . . UPPER MANTLE	68
VII. LIST OF PUBLICATIONS FOR THE PERIOD . . . . . 1969 THROUGH 1971	134
VIII. RESEARCH ASSOCIATES SUPPORTED BY CON- . . . . . TRACT NO. AF49(638)-1763	136

I.

INTRODUCTION

This report summarizes research carried out under the Post-Doctoral Program in Seismology during the period 1 July 1969 to 30 June 1971. Staff members of the Department of Earth and Planetary Sciences and Lincoln Laboratory participated in this program.

The work described here is divided into five categories:

1) observations of surface and body waves from earthquakes and explosions, 2) properties of earthquake sources, 3) array processing of seismic data, 4) theoretical and experimental studies of body wave propagation, and 5) studies of the structure and dynamical behavior of the crust and upper mantle.

Rayleigh waves from underground nuclear explosions and earthquakes in western North America recorded by a mercury tube tiltmeter and a conventional long-period vertical seismometer at Harvard, Massachusetts, have been used to investigate possible spectral ratio techniques for discrimination between explosions and earthquakes. The ratio of the spectral amplitudes in the bands from 15 to 22 sec and 22 to 60 sec is found to provide complete discrimination for events in the western United States, but not for the Milrow explosion in the Aleutians. Regional source effects appear to significantly influence spectral ratios and should be studied further.

Frequency-wave number spectra of Rayleigh waves from ex-

plosions and earthquakes in the western United States have been studied using the Montana LASA. A loss of coherent signals for periods near 50 sec has been found for the NTS explosions, but not for earthquakes or the Colorado explosion, Rulison. This phenomenon is not well understood, but may be related to the shallow source depth of NTS explosions. Various tests have indicated that these observations are probably not significantly affected by non-linear behavior of the instruments for large signals.

Frequency-wave number spectra of Rayleigh waves from the Milrow explosion show that significant 'multipathing' occurred at periods in the range 20 to 25 sec. No 'multipathing' was observed at longer periods.

Shear waves generated by the large underground nuclear explosions Greeley, Boxcar, and Benham have been studied with the aim of determining the characteristics of strain release in the focal region. Shear waves alone do not furnish sufficient information to uniquely specify the strength and orientation of a double-couple source assumed to coincide with the explosions; two of four parameters must be determined from other types of observations. If this is done by assuming that faulting is of the vertical strike-slip type, it is found that the strength of the double-couple, relative to the explosion, is  $0.75 \pm 0.06$  for Greeley,  $0.20 \pm 0.02$  for Boxcar, and  $0.44 \pm 0.04$  for Benham.

For an interpretation of near-field seismic motions, a propagating, vertical strike-slip fault may be modeled approximately as a uniformly-gliding edge dislocation. In such a model, the perpendicular and parallel components of motion at the fault's surface are simply related. Further, the amplitude of the displacement is sensitive to the ratios of rupture-to-shear wave velocity and shear-to-compressional wave velocity. A layer of low-velocity sediments, for instance, may produce a large effect. The fault model is applied successfully to near-field observations of the 1966 Parkfield, California, earthquake.

The focal depth of the three largest earthquakes in the Parkfield, California, sequence was determined using first and second P arrivals at Berkeley, California. Data were insufficient to determine whether the second arrival corresponds to refraction along a discontinuity within the crust or to a complicated source-time function. With either interpretation, however, the focal depths for the three earthquakes apparently increased with time through the sequence.

A study of core waves shows that reflection at a discontinuity in the outer core, near the inner-core boundary, produces precursors to PKIKP observed between  $130^{\circ}$  and  $142^{\circ}$ . Neither reflections in the outer-core nor higher-mode, diffracted waves can produce the tail of the diffracted P waves

observed between  $105^\circ$  and  $125^\circ$ . It appears that reflections or multiple paths in the upper mantle must be responsible.

Two independent methods for solving wave-propagation problems in heterogeneous media, numerical integration of equations of motion using finite-difference techniques and complex-frequency solutions obtained by the approximate wave theoretical method of Aki and Larner (1970), are compared for several problems and are found to be in excellent agreement. The techniques are applied to the response of soft sedimentary basins to shear waves and underscore the need to account realistically for structural heterogeneities to properly estimate surface motion and earthquake risk near such structures.

The propagation of acoustic waves in a fluid medium consisting of two homogeneous half-spaces separated by a linear transition layer has been studied in the frequency domain. The solutions obtained are exact and are evaluated by numerical contour integration in the complex wave number plane. The solutions are compared with approximate solutions obtained by the saddle point method and the sense in which the approximate solutions are asymptotic ones is discussed. The contribution from complex poles is found to be significant for waves near the critical distance.

The extension of generalized ray theory from plane-parallel to spherical layers is straightforward for pulses of short duration because plane-wave reflection and transmission coeffi-

cients can then be used. Synthetic seismograms can then be calculated using the Cagniard-de Hoop theory. The upper limit of pulse duration for applicability of this generalized ray technique to body wave propagation in the deep mantle is 75 sec for S waves and 40 sec for P waves. The technique has been used to obtain preliminary velocity models beneath North America.

Numerical calculations have been made of the expected thermal behavior of a slab of lithosphere as it sinks into the mantle, as is thought to happen beneath island arcs. The relative effects of lattice and radiative thermal conductivity and viscous, radioactive, compressive and latent heating have been investigated. Seismic wave travel-times and amplitudes are the measurable quantities most affected by slab structure and potentially most useful for further refining thermal models. Waves propagating down the slab from shallow earthquakes are advanced by as much as 4 sec. Further, strong focusing and shadow-zone effects are produced in the radiation pattern of earthquakes near or within the slab.

Compressional waves observed along a profile extending from the western United States to the Great Lakes have been studied to resolve details of the structure in the upper 1000 km of the mantle. The best fitting model satisfies the observed travel-times and waveforms. Synthetic seismograms

are constructed using the Cagniard-de Hoop method. Large observed later arrivals are in excellent agreement with calculated waves related to discontinuities near 430 km and 660 km depths. In addition, a rather high velocity gradient near the 550 km depth is needed to explain large arrivals at about 21° distance.

The crustal structure beneath LASA has been investigated using the spectral ratio of vertical-to-horizontal displacements of long-period P waves. The period of the lowest frequency peak in the spectral ratio, related to the vertical P wave travel-time in the crust, is quite variable over the area spanned by the array. Variations in crustal thickness of about 7 km are implied. The Moho generally shoals from the northeast to the southwest across the array and exhibits a synclinal structure with the axis plunging toward the northeast in the southwest quadrant of LASA.

A numerical simulation of upper mantle convection has been constructed using a two-dimensional time-dependent model that allows large viscosity variations. The method has been applied to sea-floor spreading with the objective of examining the driving mechanism of mid-ocean ridges. Counterflow below the plates is confined to depths less than 340 km. It is found that for a spreading velocity of 1.2 cm/yr, the ridge can produce compressive stress in the lithosphere out to a

distance of 1600 km. For a spreading rate of 6 cm/yr, however, this model is clearly excluded for it requires an excessively large stress in the lithosphere. Therefore, upwelling material must cross the seismic discontinuity at the 400 km depth.

Numerical calculations are being made of a spherically symmetrical wave due to explosions in a number of rock types. Propagation in the range of peak stress below 1 kb is calculated starting from the pulse shape calculations of earlier works. An anelastic material model is used with shear hysteresis independent of the rate, corresponding to a nominal  $Q$  for P waves of 180. Preliminary results indicate that small irreversibilities have a larger effect on surface waves than on body waves.

Some of the work discussed herein has already been published. The summary for such work is given below in abstract form. The complete results may be found by consulting the appropriate reference given in Section VII of this report.

#### Reference

Aki, K. and K. Larner, Surface motion of a layered medium having an irregular interface due to incident plane SH waves, J. Geophys. Res., 75, 933-954, 1970.

II.

OBSERVATIONS OF SURFACE AND BODY WAVES FROM EXPLOSIONS AND  
EARTHQUAKES

II.1 Discriminations of Earthquakes and Explosions by the  
Rayleigh-Wave Spectral Ratio by John S. Derr (Abstract)

Limited data from a long-period vertical seismometer and the prototype of a new mercury tiltmeter at the station, Harvard, Massachusetts, tend to confirm that the Rayleigh-wave spectral ratio of a short- to long-period energy provides a useful discriminant for underground explosions in the Western United States at distances of from  $28^\circ$  to  $38^\circ$  in the magnitude range of  $3.5 < M_S < 5.6$ . This corresponds to discrimination in the range of  $5.0 < m_b < 6.3$ . The same spectral ratio, however, does not discriminate the large Milrow event in the Aleutians from earthquakes in the same region, possibly because of differences in earthquake source mechanisms in different regions and because this explosion released significant tectonic strain. The Rayleigh spectral ratio complements the  $M_S - m_b$  discriminant by providing a clear separation of earthquakes and explosions in some geographical regions where earthquakes are of low stress drop and generally strike-slip in mechanism.

II. 2 Radiation Patterns of S Waves from Underground Nuclear  
Explosions by Tomowo Hirasawa (Abstract)

Use is made of polarization angles of S waves from the

Greeley, Boxcar, and Benham events to determine focal mechanisms of earthquakes presumably triggered almost instantaneously by the events. Although other possibilities are not completely excluded, the observed S waves are interpreted as mixed waves of direct S phase and reflected phases (sS,pS) from a composite source of explosion and double-couple force. Assuming a vertical strike slip, the strike of the P-wave nodal plane and the relative strength of the double-couple source compared with that of the explosion are determined. The seismic moments of triggered earthquakes are calculated as  $3.9 \sim 6.3 \times 10^{23}$  dyne cm for Boxcar and  $1.4 \sim 2.3 \times 10^{24}$  dyne cm for Benham. Particularly in the case of Benham, the rise time of about 2 sec together with the seismic moment of  $2.3 \times 10^{24}$  dyne cm is compatible with the observations of seismic waves. The possibility of estimating the pre-existing tectonic shear stress is suggested in the case of Boxcar. The tectonic stress is estimated at 130 bars from the assumption of stress relaxation due to a cavity created by the nuclear detonation.

III.

ARRAY PROCESSING OF SEISMIC DATA

III. 1 Twenty- to Eighty-Second Period Characteristics of Nuclear Explosions Recorded at LASA by Harry Mack

Abstract

Surface waves recorded at LASA generated by several NTS events have been subjected to frequency-wavenumber analysis. All the spectra show a loss of signal at 0.02 Hz but there appears to exist coherent propagation at lower frequencies, producing a notch in the normalized peak wavenumber spectrum at 0.02 Hz. Several earthquakes and the deeply-buried Colorado nuclear explosion RULISON do not exhibit this notch. This may indicate that the frequency-wavenumber characteristics peculiar to NTS events is a result of shallow source depth.

Frequency-wavenumber (F-K) spectra have been calculated for the vertical components of several NTS events recorded at LASA. For explosions in the low-intermediate yield range the wavenumber spectra exhibit common features. There is a loss of coherent signal at 0.02 Hz but there is apparent coherent propagation at lower frequencies.

Figures 1a, 1b, and 1c show high-resolution F-K spectra (Capon, 1969) for the event LANPHER at frequencies of 0.05 Hz,

0.02 Hz, and 0.015 Hz. The loss of signal at 0.02 Hz is obvious from the lack of a coherent peak in the wavenumber plane (Figure 1b). The return of coherent propagation at an apparently lower frequency is illustrated by the peak in Figure 1c which has a phase velocity of 4.2 km/sec which is about right for Rayleigh waves at this period. The apparent direction of propagation is further west than the true back azimuth. However, the resolution of the array is poor at these low frequencies and there may be quite a large error in velocity shown in Figure 2 for LANPHER. The average power is the power spectrum averaged over the individual sensors of LASA and has contributions from both coherent and incoherent disturbances. The values are normalized to the power at a frequency of 0.05 Hz.

There is an increase in power at frequencies lower than 0.02 Hz. The lower curve in the same figure, associated with the right-hand scale, is the normalized peak value of the wavenumber spectrum at each frequency and is a measure of the ratio of coherent power to total power as determined by F-K analysis. A distinct drop is seen in this value at frequencies around 0.02 Hz corresponding to the absence of coherent propagation illustrated in Figure 1b. The curve then rises again towards the lower frequencies and is maximum at a frequency of 0.015 Hz agreeing with the coherent peak in Figure 1c.

The frequency-wavenumber characteristics of LANPHER have been found for six other events of the low-intermediate yield

range. The body wave magnitude range ( $m_b$ ) of these events was 5.2 to 5.8. So far, this apparent energy at long periods has not been observed at LASA for smaller events. This, however, may be a signal-to-noise problem. For illustration, Figures 3a and 3b show the average power and peak wavenumber spectra for the events SLED and ZAZA. The shapes of the wavenumber spectra are seen to be very similar, both with the notch at 0.02 Hz.

F-K analysis of earthquakes located in Nevada, California, Baja, California, and off the coast of Oregon has failed to produce a wavenumber spectrum with a notch. The spread of surface wave amplitudes at 0.03 Hz for the earthquakes is the same as for the NTS events. Figure 4 shows the average power and peak wavenumber spectrum for the event from Baja, California. Both curves are smooth compared with those shown in the previous figures. The wavenumber spectrum curves for the earthquakes were not all similar but none exhibited a notch at any frequency.

The analysis procedures were designed such that frequency or wavenumber windowing could not produce a null at 0.02 Hz. Analysis of the high amplitude calibration recording rules out non-linearities in the amplitude range observed. There is still the possibility of high frequency surface waves causing spurious movements of the long-period seismometer mass (Berkhemer and Schneider, 1964). The argument is that these surface waves

would propagate across the array and produce a long-period transient from each seismometer. F-K analysis of these transients would produce apparent coherent propagation at low frequencies with low phase velocity. Some measured phase velocities were low and this would agree with the above arguments. However, this is not always the case as can be seen from the velocity of 4.2 km/sec shown in Figure 1c. This higher velocity is hard to reconcile with expected phase and group velocities of short-period surface waves. Also, the short-period surface waves from the earthquakes produced no such effect.

The nuclear event RULISON, located in Colorado, produced F-K spectra similar to the earthquakes. Figure 5 shows the power and wavenumber spectrum for RULISON. Coherent propagation exists at 0.02 Hz and disappears at lower frequencies. Although RULISON had a body wave magnitude of 5.3, the surface wave displacement at LASA was greater than most of the other NTS events because the detonation site was nearer. RULISON was buried more deeply than is normal at NTS. This fact, coupled with the earthquake spectra, may indicate that the wavenumber spectra peculiar to NTS events, whether real or not, is a result of shallow source depth.

#### References

Berckhemer, H. and Schneider, G., Near earthquakes recorded with long-period seismographs, Bull. Seism. Soc. Am., 54,

973-987, 1964.

Capon, J., High-resolution frequency-wavenumber spectrum  
analysis, Proc. I.E.E.E., 57, 1408-1418, 1969.

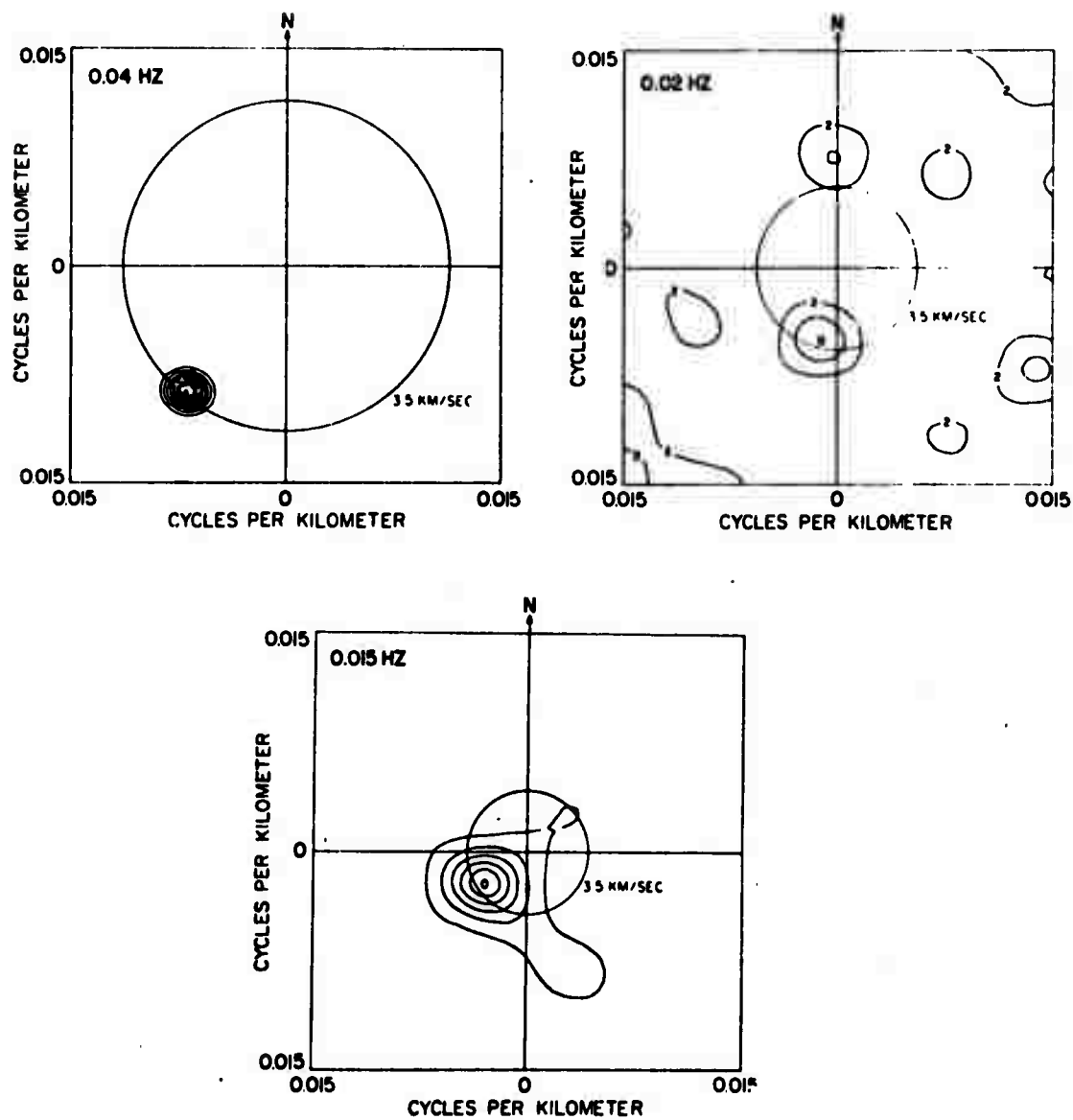


Figure 1. High resolution F-K spectra for the event LANPIER recorded at LASA at frequencies of 1a) 0.05 Hz, 1b) 0.02 Hz, and 1c) 0.015 Hz. The contours are in dB.

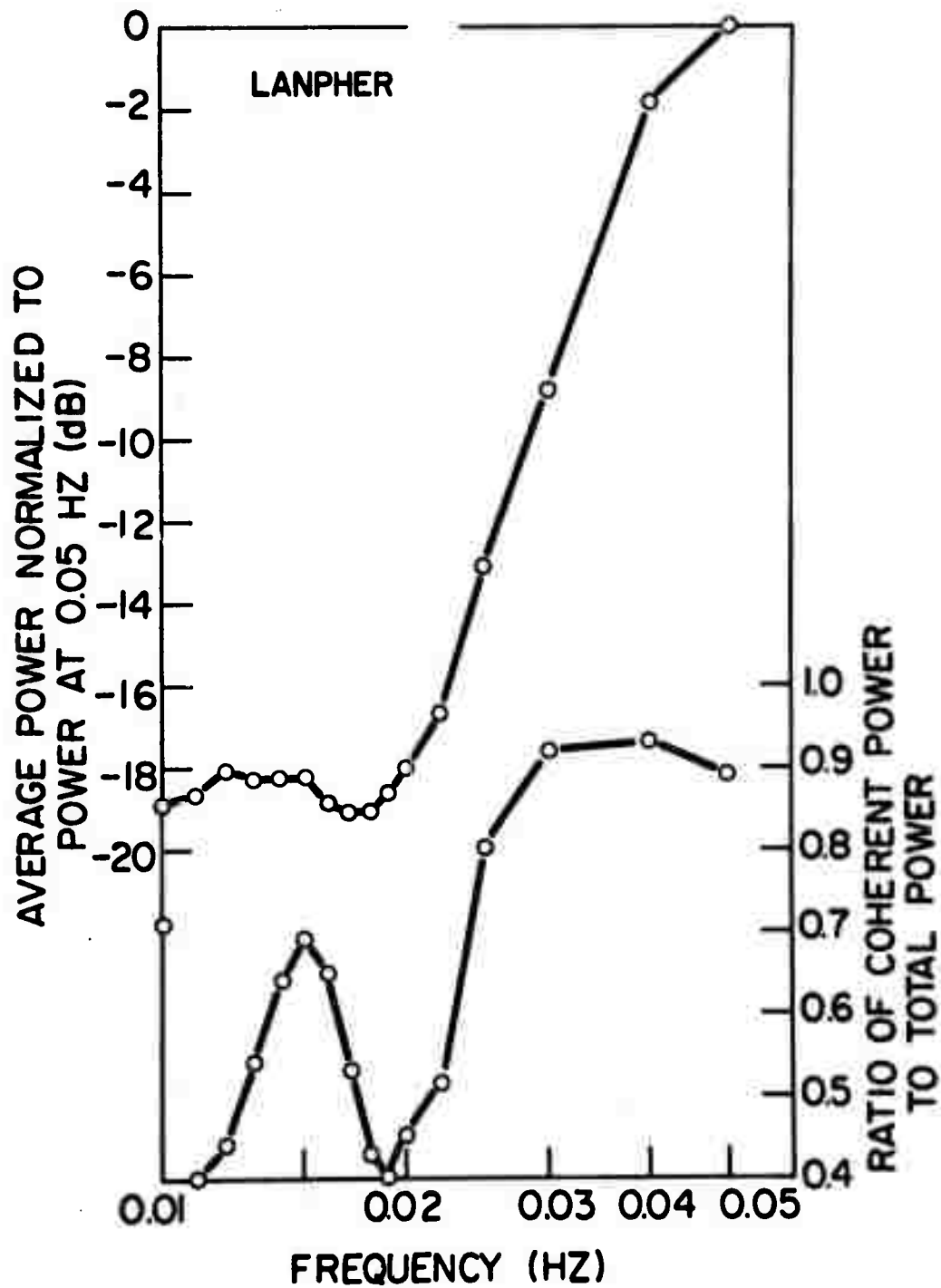


Figure 2. Average power spectrum of LANPIER recorded at IASA (upper curve and left hand scale), and normalized peak values of wavenumber spectra versus frequency (lower curve and right hand scale).

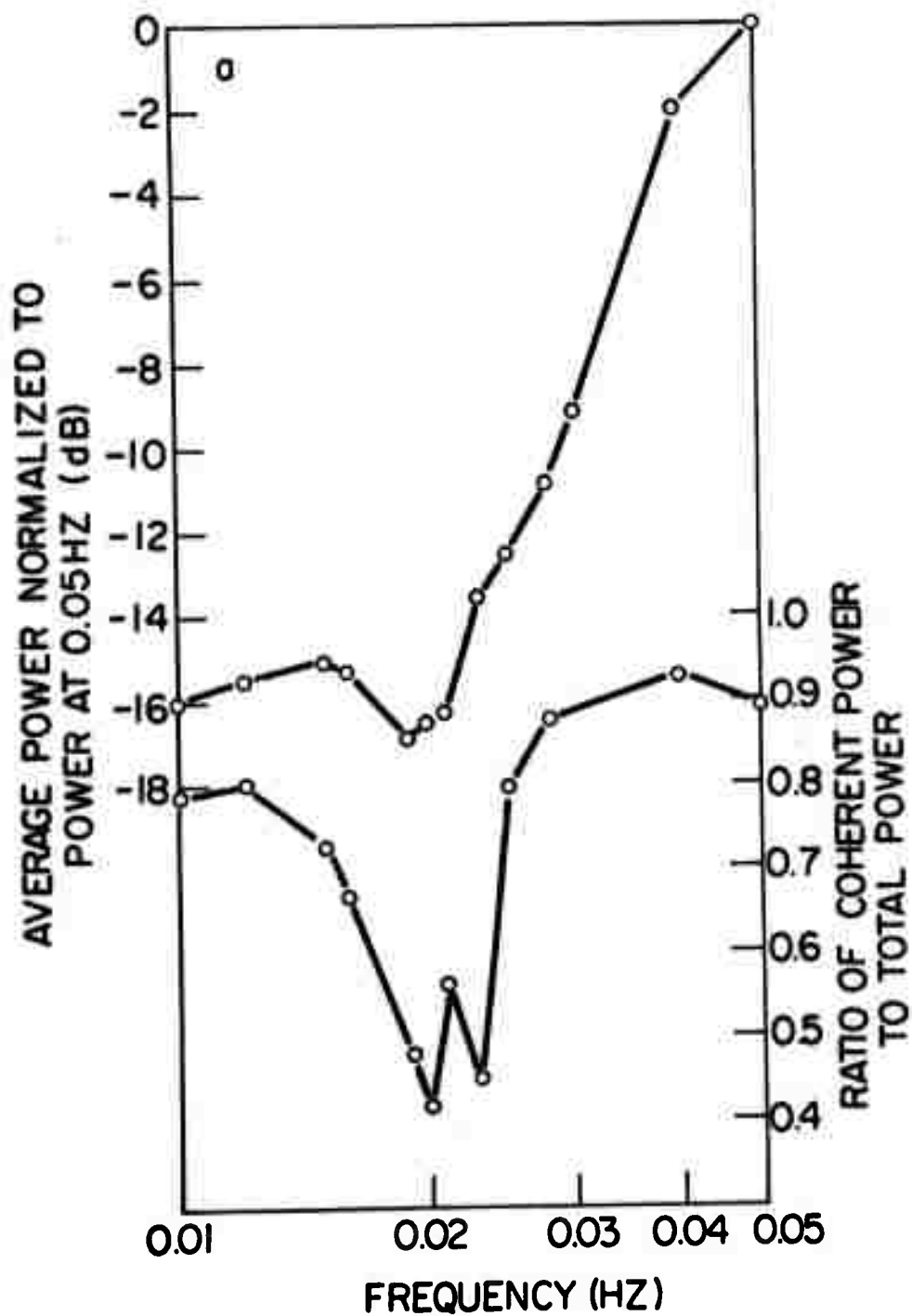


Figure 3a. Average power spectra of SLED recorded at LASA (upper curve and left hand scale), and normalized peak values of wavenumber spectra versus frequency (lower curve and right hand scale).

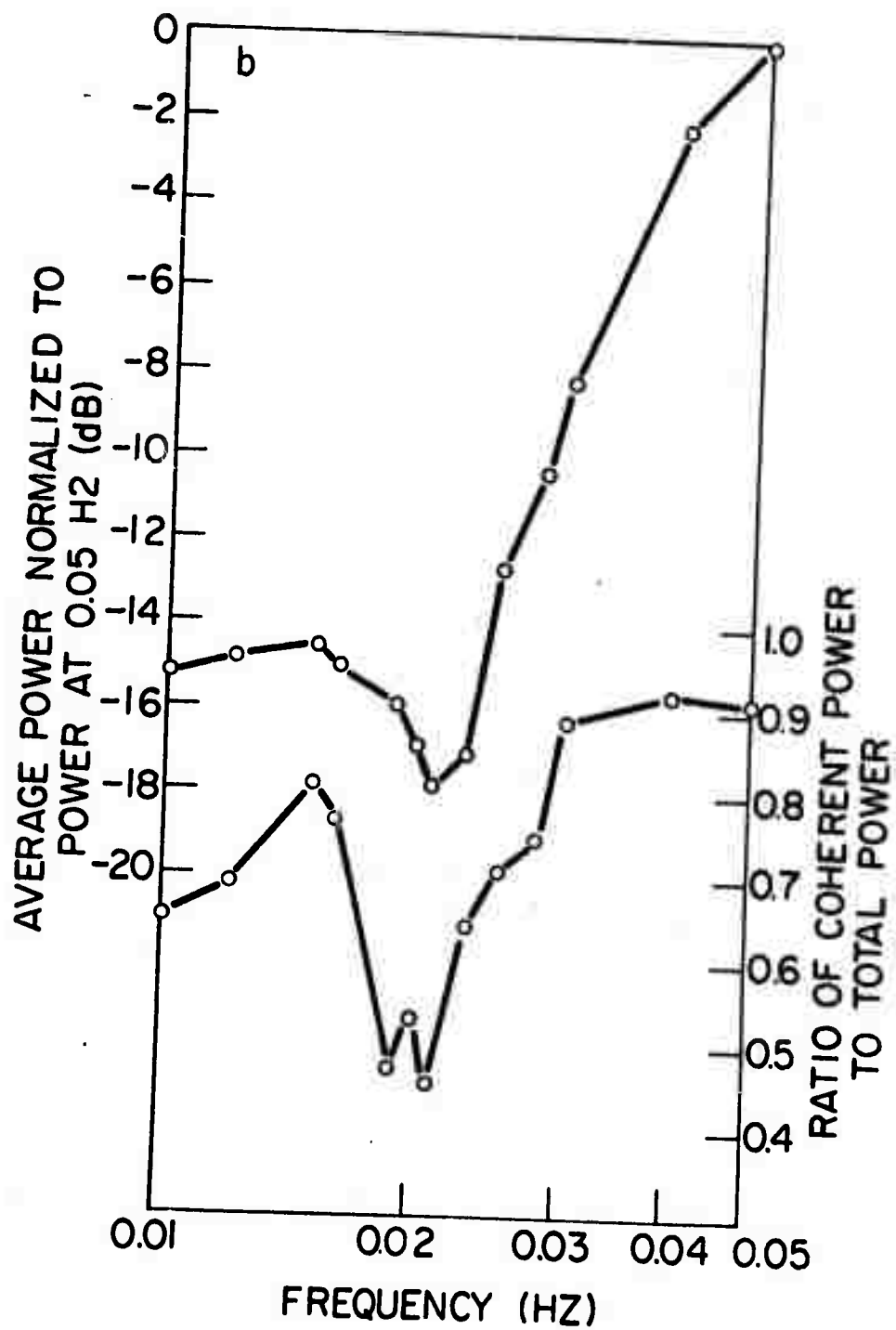


Figure 3b. Average power spectra of ZAZA recorded at LASA (upper curve and left hand scale), and normalized peak values of wavenumber spectra versus frequency (lower curve and right hand scale).

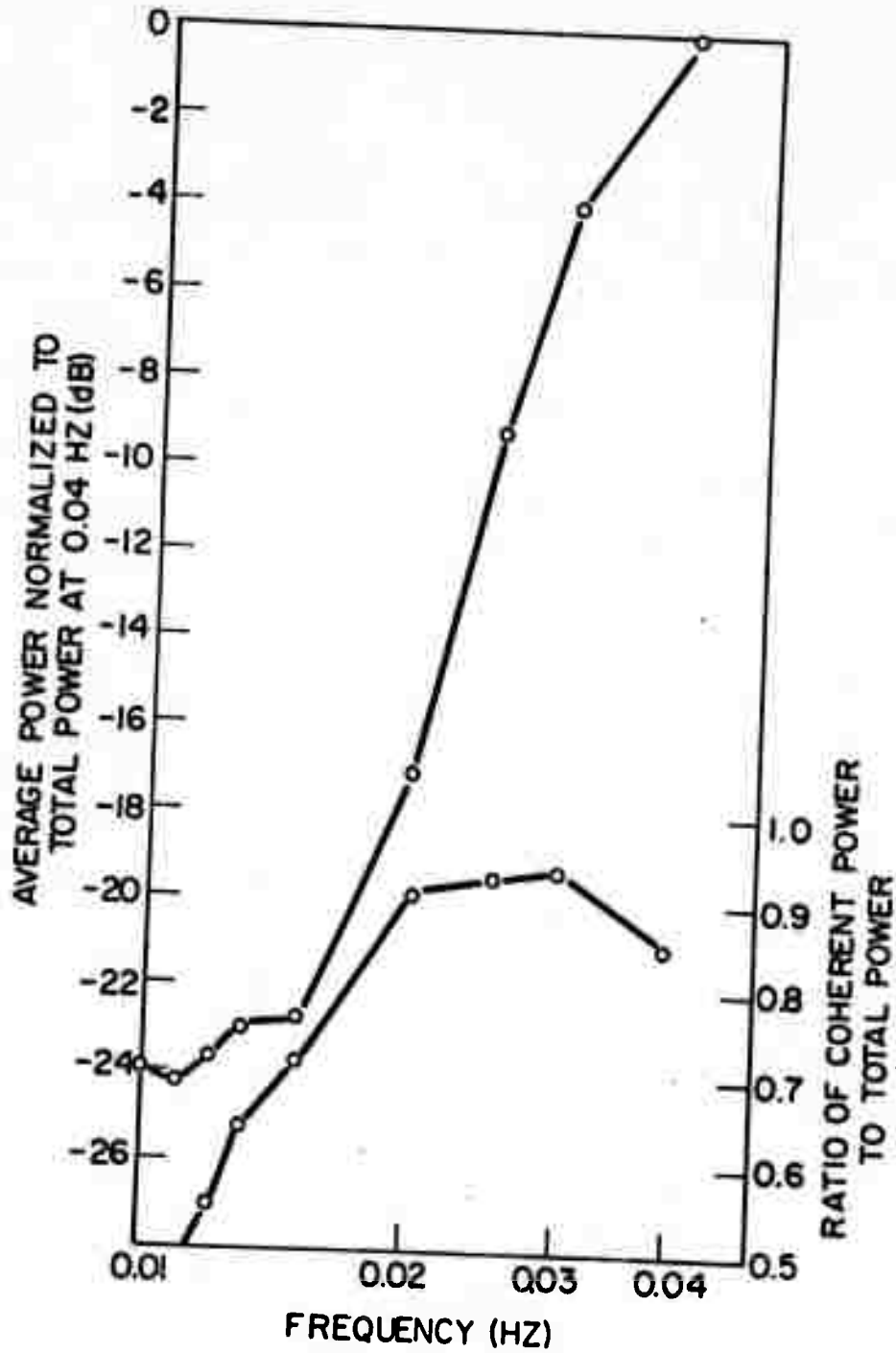


Figure 4. Average power spectrum of earthquake from Baja California recorded at LASA (upper curve and left hand scale), and normalized peak values of wavenumber spectra versus frequency (lower curve and right hand scale).

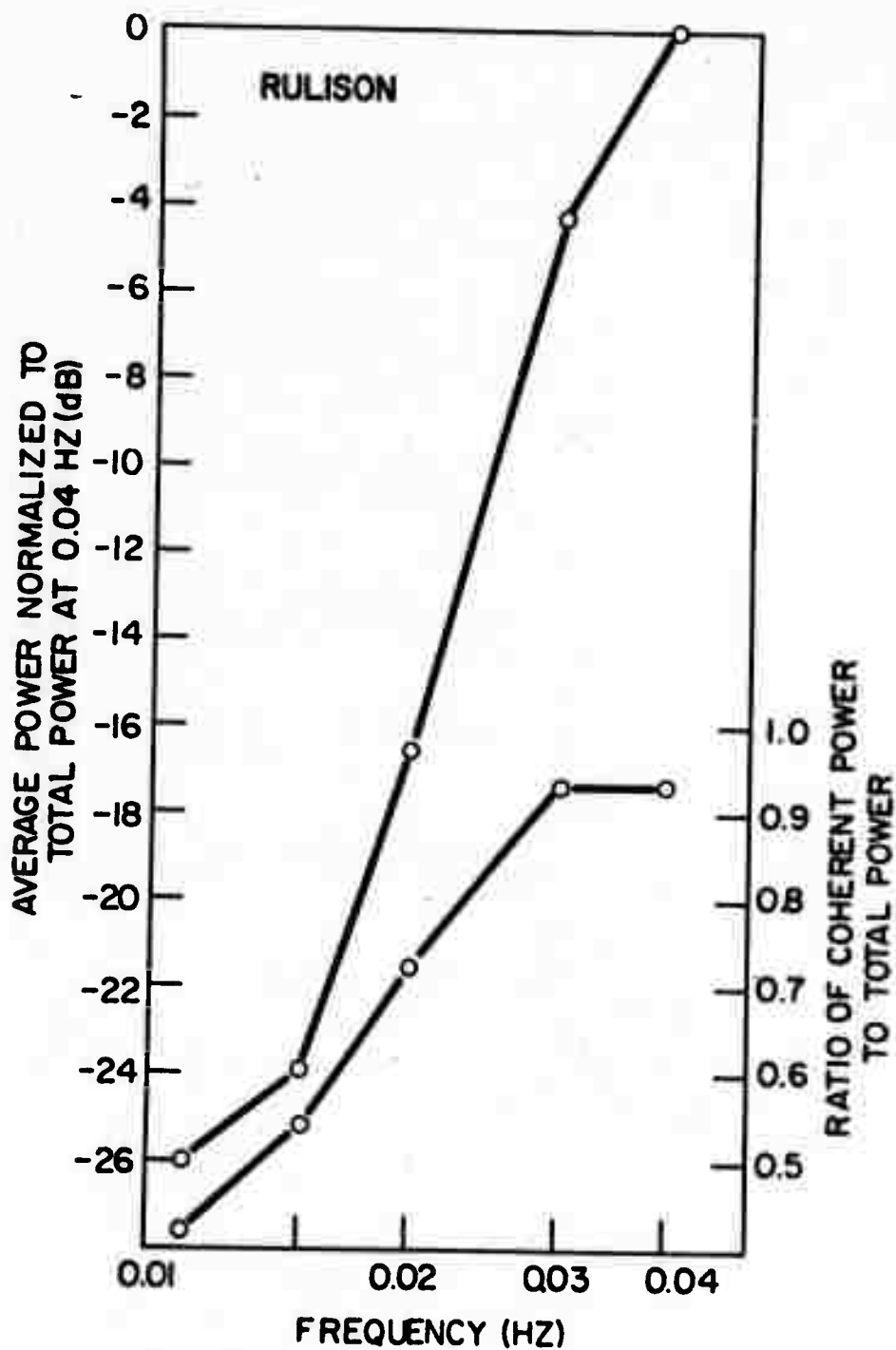


Figure 5. Average power spectrum of RULISON recorded at LASA (upper curve and left hand scale), and normalized peak values of wavenumber spectra versus frequency (lower curve and right hand scale).

### III.2 Multipathing of Rayleigh Waves Generated by Milrow by Harry Mack

#### Abstract

Frequency wavenumber analysis of Rayleigh waves generated by MILROW shows that multipathing occurs between the source and LASA in the period range 20-25 seconds. No multipathing is detected at longer periods.

The underground nuclear explosion MILROW was detonated on October 2, 1969 in the Aleutian Islands. The body wave magnitude ( $m_b$ ) was 6.5 and Rayleigh waves were well recorded at LASA. Frequency-wavenumber analysis of the Rayleigh wavetrain showed that significant mutipathing occurred at periods in the range 20-25 seconds but none was observed at longer periods.

Figure 1 is a composite of three plots. The upper curve shows the peak wavenumber spectral value versus frequency. The coherency remains high and almost flat from 0.06 Hz to about 0.02 Hz. The values then decrease rapidly towards the lower frequencies. The triangle shows the peak wavenumber spectral value at 0.05 Hz for an arrival which came approximately five minutes after the original wavetrain.

The middle curve shows how the back azimuth of arrival varied with frequency. The angle increases with decreasing

period to an asymptotic value of  $306^\circ$  which is close to the true back azimuth. The triangle indicates that the later arrival had back azimuth of  $321^\circ$ . The value of  $300^\circ$  at 0.06 Hz is difficult to explain except that this value may be the result of averaging over more than one direction of arrival.

The bottom curve shows the phase velocity dispersion curve. The velocity increases with period in an expected manner and then low values appear as the signal disappears at the lower frequencies. This phenomenon is the result of spectral leakage.

Figure 2 shows the wavenumber spectrum at 0.05 Hz at the two time periods indicated on the figure. The main arrival at this frequency is followed by a later arrival five minutes afterwards at a higher angle. Both phase velocities are the same and this figure illustrates a case of multipathing.

In conclusion, the above results indicate that multipathing of Rayleigh waves may not be a problem at periods greater than 40 seconds.

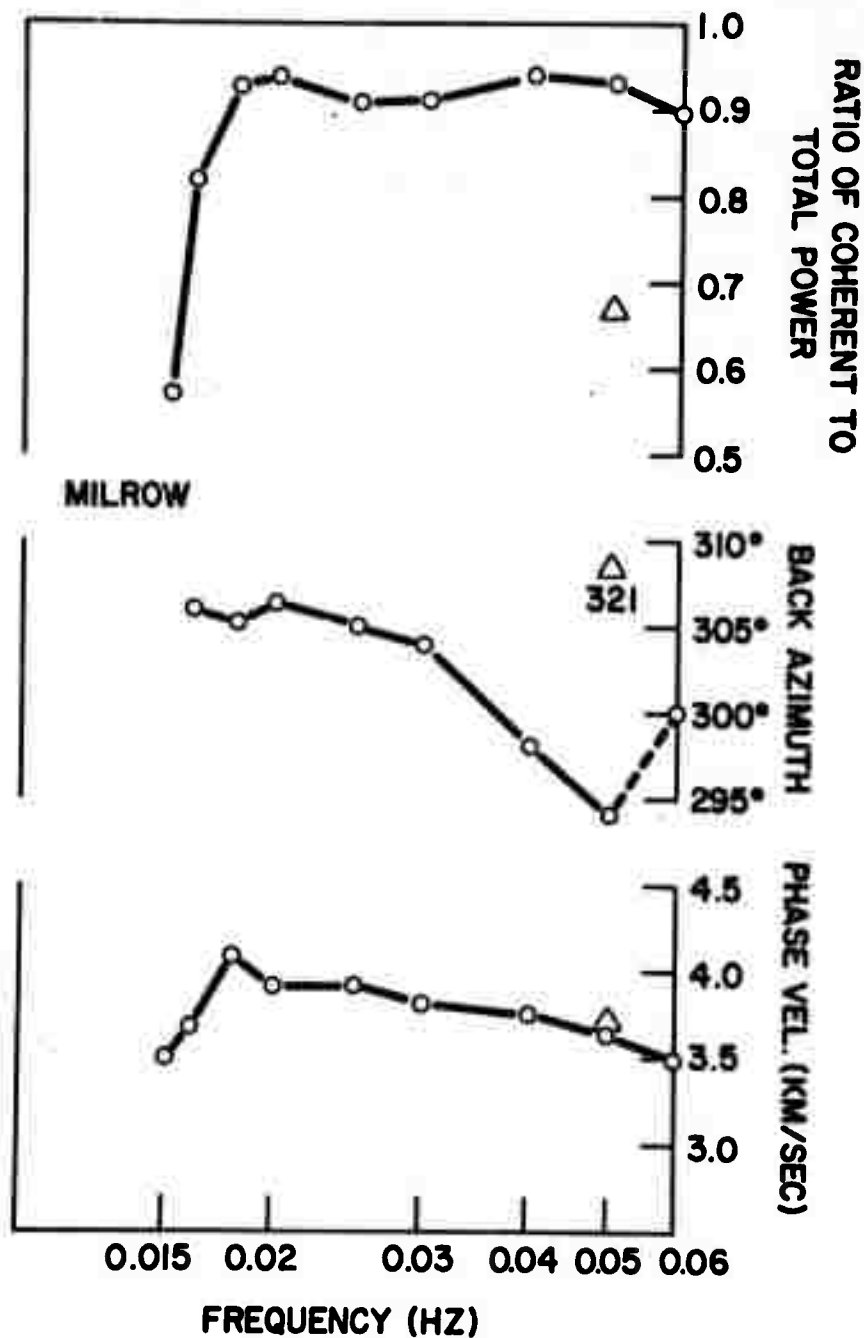


Figure 1. Analysis of Rayleigh waves generated by MILROW recorded at LASA. The top curve is the normalized peak value of the wavenumber spectra versus frequency. The middle curve shows direction of arrival versus frequency. The bottom is the phase velocity dispersion curve. The triangles relate to the later arrival.

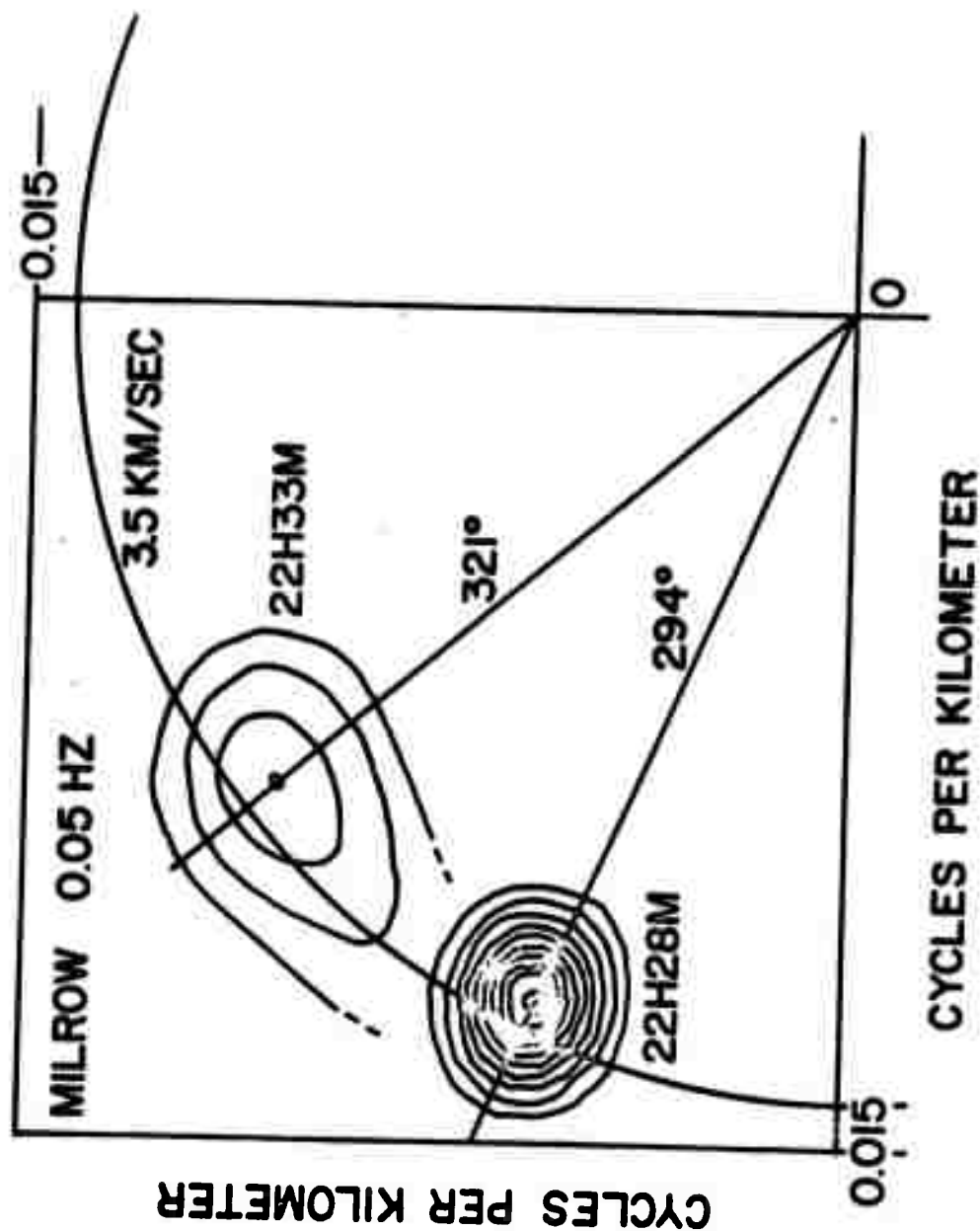


Figure 2. High resolution F-K spectra, at 0.05 Hz, of the Rayleigh wave from MILROW recorded at LASA. The contours (in dB) show the direction and velocity of two separate arrivals at the times shown, illustrating the effects of multipathing.

IV.

SOURCE PROPERTIES OF EARTHQUAKES

- IV.1 A Two-Dimensional Moving Dislocation Model for a Strike-Slip Fault by D. M. Boore, K. Aki, and T. Todd (Abstract)

For a propagating, vertical, strike-slip fault whose breakage extends to the Earth's surface, previous studies by Aki (1968) and Haskell (1969) have suggested that the near-field motions may be similar to those from uniformly-gliding-edge dislocations. The theory of these dislocations in uniform motion leads to a simple, convenient relation between the perpendicular and parallel components of motion at the fault's surface. A number of examples are considered in order to illustrate this relation between the horizontal components. In general, step-function-like parallel motions result in pulse-like perpendicular displacements. For a given parallel displacement, the amplitude of the pulse depends in a concise manner on ratios of the rupture to shear-wave velocity, and on shear- to compressional-wave velocity. Increasing either of these ratios leads to an increased pulse-amplitude. The dislocation model is applied to the near-field observations of the Parkfield earthquake. The resulting estimate of the total fault offset is within the range of those based on the more detailed models of Aki (1968) and Haskell (1969).

IV.2 Focal Depths of the 1966 Parkfield, California,  
Earthquake by William H. Bakun

Abstract

Differences in arrival times of seismic phases at Berkeley California (BRK),  $\Delta = 270$  km, for the 0408 GMT June 28 ( $M = 5.1$ ), 0426 GMT June 28 ( $M = 5.5$ ), and 1953 GMT June 29 ( $M = 5.0$ ) 1966 Parkfield, California, earthquakes imply that focal depths for these three largest events of the 1966 Parkfield sequence increased with time through the sequence. The data available are not sufficient to determine whether the observed secondary arrivals at BRK result from a slower propagation path or are part of a complicated source-time function.

The 1966 Parkfield, California earthquake sequence occurred on the San Andreas fault in central California, approximately equidistant from San Francisco and Los Angeles. The largest earthquake in the sequence, at 0426 GMT on June 28, 1966, had a Wood-Anderson magnitude of 5.5. Surface fracture (Brown and Vedder, 1967) along a 38 km segment of the San Andreas fault zone in the epicentral region accompanied the sequence. An important aspect of the Parkfield earthquakes is the wealth of near-field seismic data available to model the earthquake source and to test techniques of estimating earthquake source parameters from far-field seismic data. Consequently the 1966 Parkfield sequence is unique -- at least among magnitude 5.5 sequences -- in the quantity of research that has been reported concerning its focal mechanism and source parameters (Aki, 1967; Eaton, 1967; Filson and McEvilly, 1967; McEvilly et al., 1967; Aki, 1968; Smith and Wyss, 1968; Wu, 1968; Wyss and Brune, 1968; Haskell, 1969; Scholz et al., 1969; Boore et al., 1970; Eaton et al., 1970).

Eaton et al., (1970) reported that 95% of the Parkfield aftershocks considered in their study had focal depths between 1 and 12 km, and none were deeper than 15 km. Available focal depths for large aftershocks ( $M \geq 2.0$ ) in the sequence range from 1.6 to 12.2 km with an average depth near 5 km (McEvilly et al., 1967). Although focal depths are available for some of the aftershocks, near data are not sufficient to assign focal depths to the 3 largest events (Table 1) in the sequence. The USCGS lists focal depths of 5, 4, and 5 km for the 0408, 0426, and 1953 GMT Parkfield events respectively (USCGS Earthquake Data Report PDE #45-66). The relatively large standard errors assigned to the focal depths ( $\sim 6$  km) by the USCGS indicate significant scatter in the data. Using Love and Rayleigh wave spectral amplitudes,

Tsai and Aki (1970) estimated depths of 7, 4 and 9 km respectively for these 3 events. In this report seismograms written at the University of California seismographic station BRK ( $\Delta = 270\text{km}$ ) are interpreted to imply that focal depths for these 3 Parkfield events increased with time through the sequence. (It should be stressed that this conclusion regarding focal depth is applicable only to these 3 largest Parkfield events and not to the sequence as a whole.) It is hoped that these data will serve as a useful constraint to discussions of the source parameters of the Parkfield earthquakes.

The seismographic station BRK ( $37^{\circ}52.4'$  N,  $122^{\circ}15.6'$  W, elev. = 81 m) is located in the Havilland Hall vault on the Berkeley campus of the University of California. The broad band 3-component system is described in detail by Rodgers et al., (1965). Seismograms written at BRK for the 3 largest 1966 Parkfield earthquakes are shown in Figure 1. The traces are aligned at the trough of the first arrival, labeled  $P_n$ . The second arrival, labeled  $P_1$ , is clearly visible on each of the traces. The central point to be taken from Figure 1 is that the  $P_1 - P_n$  time difference increases through the sequence for these 3 events. The absolute  $P_1 - P_n$  time difference depends on whether the time picks are read from the breaks or peaks or troughs of the traces. The  $P_1 - P_n$  time differences are estimated to be 2.9 sec (0408 GMT), 3.3 sec (0426 GMT) and 3.5 sec (1953 GMT) with an uncertainty of about 0.1 - 0.2 sec.

The 3 Parkfield events shown have essentially identical epicenters -- the difference in the epicentral coordinates listed in Table 1 is due to the reading accuracy ( $\pm 0.1$  sec) used in their location. The epicentral distance to BRK is about 270 km. Eaton (1967) determined an average rupture velocity of 2.2 km/sec to the southeast along the San Andreas fault for the 0426 GMT event. Filson and McEvilly (1967) found

a rupture velocity of 2.2 km/sec and a fault length of 30 km to be consistent with Love wave spectral amplitudes at BRK for the 0426 GT event. Similarity in the shape of the Love wave spectral amplitudes at BRK for the 0408 GT and 1953 GT events and 2 smaller 1966 Parkfield earthquakes suggested source dimensions less than 10 km for these events (Filson and McEvilly, 1967).

The fact that the  $P_1$  phase in Figure 1 is prominent for each of these 3 apparently quite different Parkfield earthquake sources indicates 1) that the  $P_1$  phase is a secondary crustal arrival, independent of the source-time function or 2) that  $P_1$  is a source phase, common to the 3 Parkfield earthquakes, possibly the "breakout phase" predicted by Savage (1965) and Burridge and Halliday (1971). It is unfortunate that the seismic data necessary to resolve this question are not available. Seismograph stations at near and regional distances in California were generally saturated by the first P-wave arrivals from these 3 events. Records from Wood-Anderson seismographs operated by the University of California, Berkeley, at Berkeley and Mount Hamilton, and by the California Institute of Technology at Cottonwood, Pasadena, Santa Barbara and Tinemaha are not saturated but the horizontal Wood-Anderson instruments are not suited for recording crustal P-wave arrivals. (For example, the  $P_1$  phase recorded on the broad-band vertical instrument at Berkeley shown in Figure 1 is not evident on the Wood-Anderson records written at Berkeley). At teleseismic distances, the P-waves from these Parkfield events are emergent so that little information concerning secondary arrivals in the P-wave train can be obtained from seismograms written at teleseismic distances. It should be noted that the standard deviations of P-wave arrival times for these events reported in the Bulletin of the Interna-

tional Seismological Centre are unusually large for magnitude 5 earthquakes. One explanation of these large deviations is that stations reported P-wave readings from different phases of complicated sources. Such an explanation would support the source phase hypothesis for  $P_1$ .

In this report the  $P_1$  phase is considered first to be a secondary crustal arrival, and second as a source phase. In each case the result that the focal depths for these 3 largest Parkfield events increased with time through the sequence is obtained.

### $P_1$ - A Secondary Crustal Arrival

To interpret the  $P_1 - P_n$  time differences in terms of different focal depths it is convenient to assume ray paths through the crust and upper mantle for the  $P_n$  and  $P_1$  phases.  $P_n$  is assumed to be the arrival of a head wave propagating along the Moho and  $P_1$  is a phase propagating within the crust. If one assumes a  $P_g$  velocity of 6 km/sec and the origin times given in Table 1, the  $P_g$  phase (direct wave) would arrive at BRK about 8 sec after the  $P_n$  arrival. A sharp arrival near this time is clearly evident on the 1953 GMT trace and can be seen for the other events as well. In Figure 2 a diagram of one of the possible ray paths of the  $P_1$  phase is shown. In this case,  $P_1$  is assumed to be the head wave arrival from a crustal interface at a depth of 15 km. Assuming the crustal model and ray paths shown in Figure 2,  $P_1 - P_n$  time differences, computed for focal depths ranging from 2 to 15 km, increase with focal depth. This result -- that the  $P_1 - P_n$  time difference increases with focal depth -- is not affected by variations in the assumed crustal model. As an example the  $P_1 - P_n$  time differences for focal depths of 2 km and 15 km versus the compressional velocity in the bottom layer of the crustal model (6.8 km/sec in Figure 2) are shown in Figure 3. While the sense of proportionality between the  $P_1 - P_n$  time difference and focal depth remains the same, it is clear that absolute focal depth and even absolute focal depth difference is strongly dependent on the assumed crustal model. Since the crustal structure in central California is certainly more complicated than the model assumed in these calculations, precise statements concerning the focal depths for the 3 largest Parkfield events from the  $P_1 - P_n$  data presented in Figure 1 are not justified.

The  $P_1 - P_n$  time differences shown in Figure 3 were computed assuming that the  $P_n$  and  $P_1$  phases were head wave arrivals propagating along the Moho and along an intermediate crustal interface respectively. Similar  $P_1 - P_n$  time difference analyses for other  $P_1$  propagation paths within the crust lead to the same result -- that an increase in focal depth results in an increased  $P_1 - P_n$  time difference. In fact, it is clear that the  $P_1 - P_n$  time difference will increase with focal depth as long as the propagation path of the  $P_1$  phase is confined to the crust and the  $P_n$  phase propagates at or near the top of the mantle at a greater-than-crustal velocity. The conclusion that the focal depths of the 3 Parkfield events listed in Table 1 increased with time in the sequence then is based only on the assumption that  $P_1$  is a crustal phase and  $P_n$  propagates at or near the top of the mantle.

### $P_1$ - A SOURCE EFFECT

Earthquakes on the San Andreas fault appear to be well-suited to test a dynamic model of a shallow focus earthquake source which has been proposed by Burridge and Halliday (1971). Their model consists of a uniform half-space that is prestressed to produce strike-slip movement on a vertical fault plane. Slip is initially inhibited on the non-welded fault surface by static friction which increases with depth. Initial slip results in a stress drop which drives the propagation of the slip upwards and downwards from the focus at the shear velocity  $\beta$ . A "breakout phase" is generated when the upwards propagating slip reaches the free surface.

Burridge and Halliday (1971) have calculated the pulse shapes in the far-field radiation and the residual displacements and stresses on the fault plane for the computationally tractable case where the stress drop on the fault surface decreases quadratically with depth. They show that in this case displacement on the fault surface extends to a certain depth which is independent of the depth of focus. This surprising conclusion is in accord with the well-known observation that earthquake foci on the San Andreas fault do not extend beyond a depth of about 15 km. Burridge and Halliday further show that in the far-field radiation, for take-off angles near the vertical, the "breakout phase" becomes more prominent as the focal depth increases. For example, if the calculations of Burridge and Halliday are scaled so that the depth to which displacement on the fault surface extends is set at 15 km, then the "breakout phase" is larger than the initial motion for focal depths in excess of 4 km.

A possible interpretation of the seismograms shown in Figure 1 is that the  $P_1$  phase is a source effect, the "breakout phase" predicted by Burridge and Halliday. In this interpretation  $P_1$  propagates from the epicenter to the Moho as a P-wave and then as a head wave along the Moho. The  $P_1 - P_n$  time difference is thus due to the delay of  $P_1$  resulting from propagation from the focus to the free surface at the shear velocity and from the free surface down to the depth of focus at the compressional velocity. It is clear that with this interpretation, an increase in focal depth results in an increased  $P_1 - P_n$  time difference and focal depths for the 3 Parkfield events discussed here, would increase from about 7 km for the 0408 GMT event to about 8 km for the 0426 GMT event to about 9 km for the 1953 GMT event.

## DISCUSSION



Tsai and Aki (1970) determined focal depths for the 3 Parkfield events studied here from 10-50 sec Love and Rayleigh wave spectral amplitudes recorded at Albuquerque, New Mexico and Colden, Colorado. Assuming a point source vertical strike-slip dislocation, they found focal depths of 7 km for the 0408 GMT event and 9 km for the 1953 GMT event to be consistent with the observed surface wave spectral amplitudes. Assuming a vertical strike-slip dislocation of 37 km length and a constant rupture velocity of 2.2 km/sec, they found that a focal depth of 4 km best fits the vertical component Rayleigh wave spectral amplitude recorded at Atlanta, Georgia for the 0426 GMT event. Filson and McEvilly (1967) and Wu (1968) have suggested that the 0426 GMT event could have been a series of events closely spaced in time. The variation in rupture velocity resulting from a multiple source would complicate the surface wave spectral amplitudes considerably and possibly introduce a significant error in the focal depth determined for the 0426 GMT event by Tsai and Aki. The  $P_1 - P_n$  time difference data reported here support the focal depths determined by Tsai and Aki in that their estimates of focal depths increase in time through the sequence for the 0408 GMT and 1953 GMT events. The point source dislocation model assumed for these 2 events is in accord with the Love wave spectral amplitude data of Filson and McEvilly (1967). Tsai and Aki's conclusion that the focus of the 0426 GMT event was shallower than the focus of the 0408 GMT event could result from errors introduced by assuming too simple a source dislocation model for the 0426 GMT event. If the dislocation is not constant but varies with depth, then Tsai and Aki's results are more indicative of an average

location depth than the depth of initial rupture. Regardless of the size of the focal depth errors, the result obtained here - that focal depths increased with time for these 3 events -- implies an empirical error of about 50% for focal depths less than 10 km that are determined by the technique proposed by Tsai and Aki (1970).

#### ACKNOWLEDGEMENTS

The suggestions and comments of Dr. Dai Davies and the staff of the Seismic Discrimination Group, Lincoln Laboratory, MIT, are gratefully acknowledged. Dr. Alfredo Eisenberg of the Seismographic Station of the University of California, Berkeley and Dr. Wayne Thatcher of the Seismological Laboratory of the California Institute of Technology are thanked for their assistance in obtaining data pertinent to this report. Drs. Don Tocher and Charles Bufe of the Earthquake Mechanism Laboratory/NOAA reviewed the manuscript. This research was partially supported by the U. S. Air Force under contract No. AF49(638)-1763.



REFERENCES

- Aki, K., "Scaling Law of Seismic Spectrum," J. Geophys. Res. 72, 1217-1231, 1967.
- Aki, K., "Seismic Displacements Near a Fault," J. Geophys. Res. 73, 5359-5376, 1968.
- Boore, D. M., K. Aki and T. Todd, "A Two-Dimensional Moving Dislocation Model for a Strike-Slip Fault (Abstract)," EOS. Trans. AGU 51, 780, 1970.
- Brown, R. and J. Vedder, "Surface tectonic fractures along the San Andreas fault," U.S. Geological Survey Prof. Paper, 579, 2-22, 1967.
- Burridge, R., and G. S. Halliday, "Dynamic Shear Cracks with Friction as Models for Shallow Focus Earthquakes," Geophys. J., in press, 1971.
- Eaton, J. P., "The Parkfield-Cholame, California, Earthquakes of June-August 1966; instrumental seismic studies," U.S. Geol. Survey Prof. Paper, 579, 57-65, 1967.
- Eaton, J. P., M. E. O'Neill, and J. N. Murdock, "Aftershocks of the 1966 Parkfield-Cholame, California, Earthquake: A detailed Study," Bull. Seism. Soc. Am. 60, 1151-1197, 1970.
- Filson, J., and T. V. McEvilly, "Love Wave Spectra and the Mechanism of the 1966 Parkfield Sequence," Bull. Seism. Soc. Am. 57, 1245-1257, 1967.

- Haskell, N. A., "Elastic Displacements in the Near-Field on a Propagating Fault," Bull. Seism. Soc. Am., 59, 865-908, 1969.
- McEvelly, T. V., W. H. Bakun, and K. B. Casaday, "The Parkfield, California, Earthquakes of 1966," Bull. Seism. Soc. Am. 57, 1221-1244, 1967.
- Rodgers, P., W. Marion, R. Sell, and C. Lomnitz, "Magnetic-tape Data Acquisition System," Final Report to the Advanced Research Projects Agency - A Study of Focal Mechanism and Aftershock Characteristics of Small Earthquakes, Seismographic Station, University of California, Berkeley, 15-42, 1965.
- Savage, J. C., "The Stopping Phase on Seismograms," Bull. Seism. Soc. Am. 55, 47-58, 1965.
- Scholz, C. H., M. Wyss, and S. W. Smith, "Seismic and Aseismic Slip on the San Andreas Fault," J. Geophys. Res. 74, 2049-2069, 1969.
- Smith, S. W. and M. Wyss, "Displacement on the San Andreas Fault Subsequent to the 1966 Parkfield Earthquake," Bull. Seism. Soc. Am. 58, 1955-1973, 1968.
- Tsai, Y. B. and K. Aki, "Precise Focal Depth Determination from Amplitude Spectra of Surface Waves," J. Geophys. Res. 75, 5729-5743, 1970.
- Wu, F. T., "Parkfield Earthquake of June 28, 1966: Magnitude and Source Mechanism," Bull. Seism. Soc. Am. 58, 689-709, 1968.
- Wyss, M. and J. N. Brune, "Seismic Moment, Stress, and Source Dimensions of Earthquakes in the California-Nevada Region," J. Geophys. Res. 73, 4681-4694, 1968.

TABLE 1

1966 Parkfield, California earthquakes.

Data are taken from McEvilly et al. (1967)

<u>Date</u>	<u>Origin Time (GMT)</u>	<u>Latitude (N)</u>	<u>Longitude (W)</u>	<u>Magnitude (BRI)</u>
June 28, 1966	04:08:56.2	35°57.6'	120°30.3'	5.1
June 28, 1966	04:26:13.4	35°57.3'	120°29.9'	5.5
June 29, 1966	19:53:25.9	35°56.6'	120°31.5'	5.0

FIGURE CAPTIONS

- Figure 1 BRK VERTICAL seismograms for the (top) 0408 GMT, (middle) 0426 GMT and (bottom) 1953 GMT 1966 Parkfield earthquakes. The traces are aligned at the first trough of the first arrival, labeled  $P_n$ . A dashed vertical line has been drawn through the first trough of the  $P_1$  phase on the middle seismogram to facilitate comparison. Compression is down on the records.
- Figure 2 Diagram (not to scale) of the ray paths assumed for the  $P_n$  and  $P_1$  phases for the computation of the  $P_1 - P_n$  time differences plotted in Figure 3. The crustal model is based on the model proposed for the Parkfield area by Eaton (1967).
- Figure 3  $P_1 - P_n$  time differences for focal depths of 2 km and 15 km vs. compressional velocity at the base of the crust (6.8 km/sec in Figure 2). The assumed  $P_n$  and  $P_1$  ray paths and crustal model shown in Figure 2 were used in the computations. Horizontal arrows indicate the  $P_1 - P_n$  time differences taken from Figure 1.

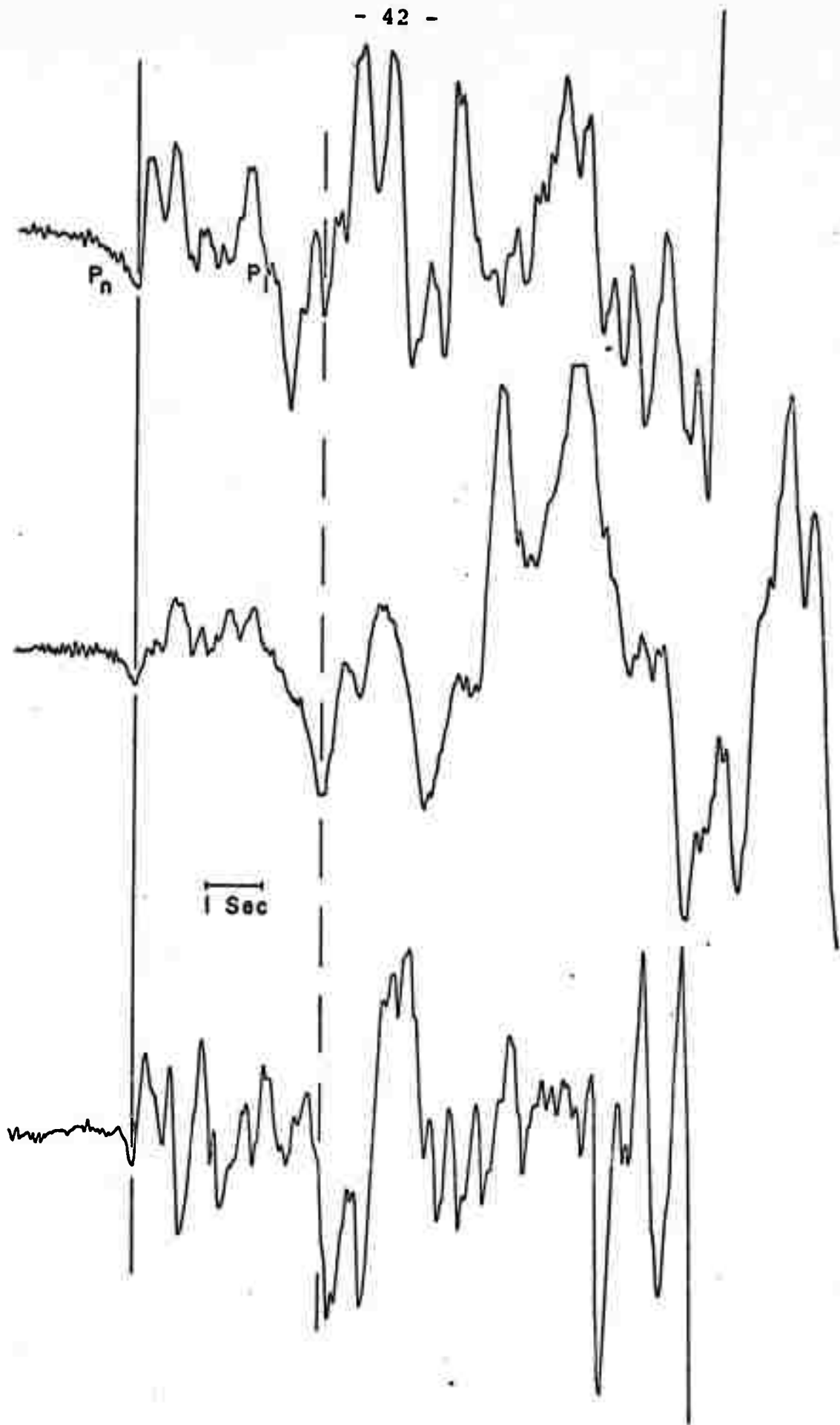
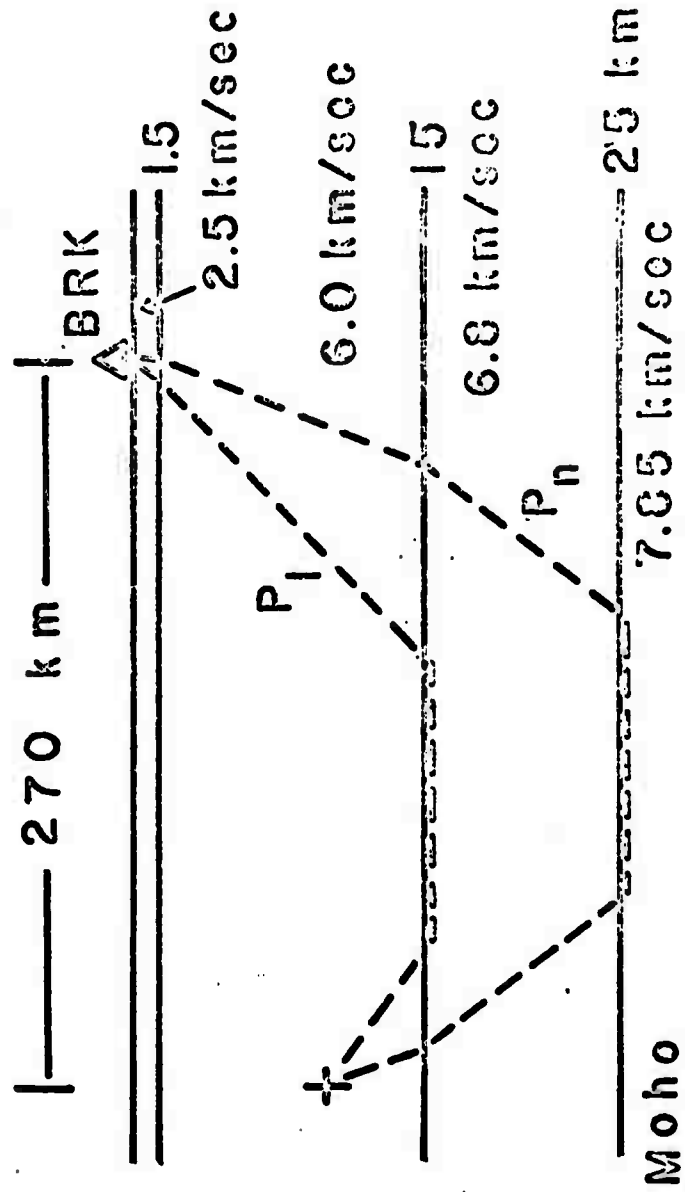


Figure 1



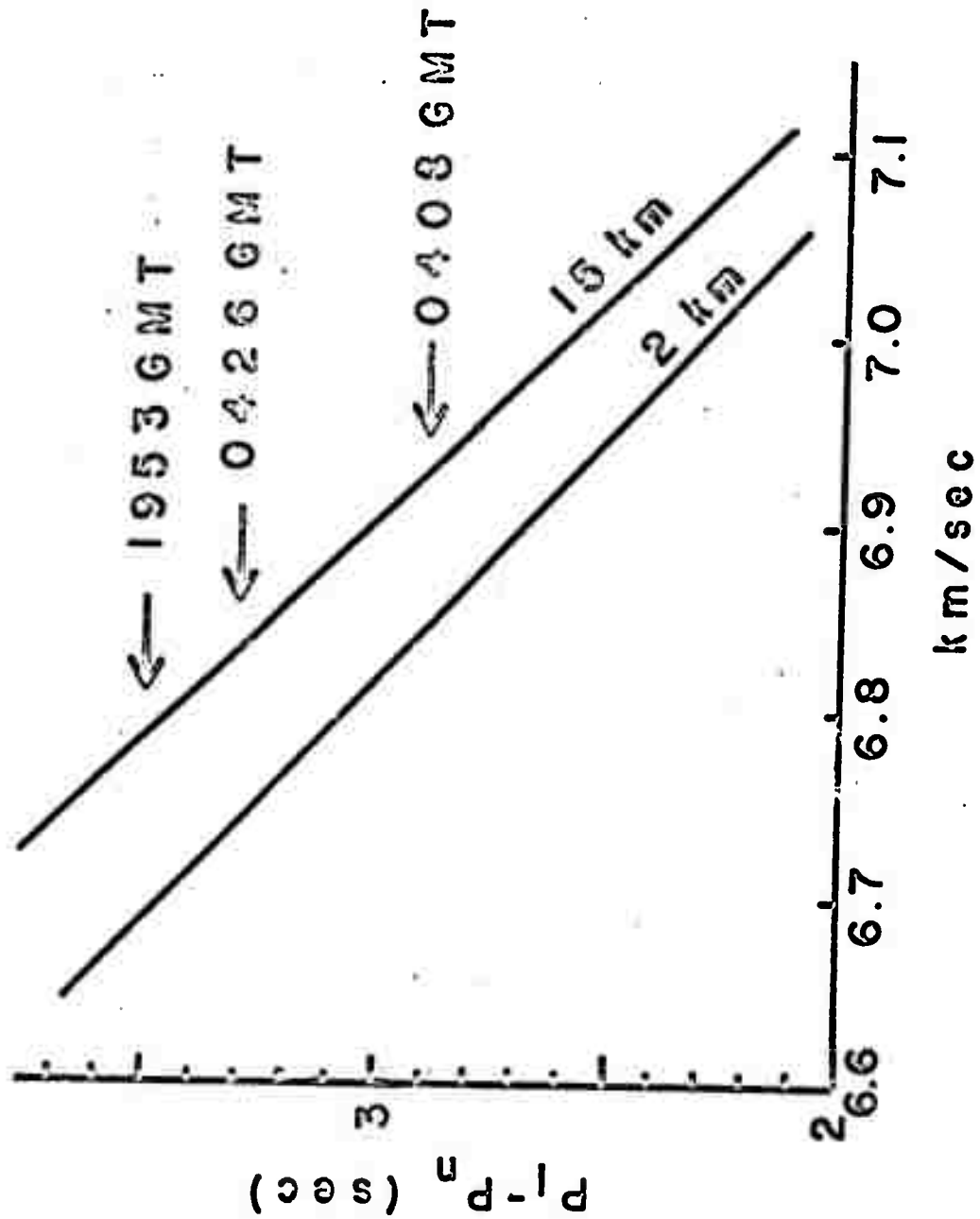


Fig. 10.2

V.

THEORETICAL AND EXPERIMENTAL STUDIES OF BODY-WAVE PROPAGATION

V.1 The Origin of Precursors to Core Waves by E. Husebye and R. Madariaga (Abstract)

The origin of the precursors of the core waves in the range  $105^\circ - 142^\circ$  is studied. Between  $105^\circ$  and  $125^\circ$  a long tail is observed after the P wave diffracted by the core. In the range  $130^\circ \leq \Delta \leq 142^\circ$  we usually observe short-period onsets a few seconds before PKIKP; these are the waves called P(GH). Reflection at a discontinuity in the outer core, near the inner-core boundary, is shown to produce the P(GH) branch. Reflections in the outer core are rejected as a mechanism for the tail of the P diffracted wave. A theoretical study of diffraction of P by the core shows that higher modes of diffracted waves cannot explain the observations of the tail of P diffracted. We conclude, by elimination, that it is due to reflections or multiple paths in the upper mantle.

V.2 Comparison of Two Independent Methods for the Solution of Wave Scattering Problems: Response of a Sedimentary Basin to Vertically Incident SH Waves by D.M. Boore, K.L. Larner and K. Aki (Abstract)

The transient solution to several problems that was obtained

by numerical integration of equations of motion using a finite difference (FD) technique is compared with the complex-frequency solutions obtained by the approximate wave theoretical (AL) method of K. Aki and K.L. Larner. The excellent agreement between the two solutions not only provides a comparative check on the accuracies of the two techniques, but also demonstrates that the interpretation of the AL solution is comparable to the Fourier transform of the transient solution premultiplied by an exponential window. Most of the paper is devoted to a discussion of two models that are relevant to the engineering-seismological study of earthquake motions in soft layers of varying thicknesses. The FD and AL solutions show that lateral reverberations of waves produced by the nonplanar structure form complex interference patterns that are not predicted by the usual flat-layer approximations. In one example, constructive interference enhances the peak amplitude of the transient motion over the center of the basin by a factor of 3 relative to the flat-layer solutions. The results indicate that a realistic appraisal of earthquake hazards in areas underlain by soft surficial layers should include the effect of nonuniformity in the structure.

V.3 Reflected and Head Waves from a Linear Transition Layer in a Fluid Medium by T. Hirasawa and M.J. Berry (Abstract)

Reflected and head waves from a linear transition layer between two homogeneous media are studied in the frequency domain. A point source is located in the upper fluid of lower velocity, and the velocity structure is considered to be continuous throughout.

Exact solutions are derived by numerical evaluation of the contour integrals in the complex wave-number plane. These are compared with approximate solutions obtained by the saddle point method. It was found that the approximate solutions for head and reflected waves beyond the critical distance may be regarded as the asymptotic ones for large values of  $r/2h$ . Similarly, the approximate solutions for reflected waves inside the critical distance are the asymptotic ones for large values of  $H/2h$ , where  $H$  is the sum of vertical distances of the source and a receiver from the transition layer of thickness  $2h$ , and  $r$  is the horizontal distance of a receiver from the source. At high frequencies, the spectral amplitudes of reflected waves inside the critical distance are proportional to  $\omega^{-1}$ , while head-wave amplitudes are proportional to  $\omega^{-2/3}$  ( $\omega$  being the angular frequency).

Numerical calculations also show that contributions from complex poles are significant near the critical distance if

the transition layer is thick. In this region, the amplitude variations of the sum of the reflected and secondary waves are similar to those from a sharp discontinuity, although the maximum amplitude for a wave of narrow-frequency band width occurs at greater distances for thicker transition layers.

V.4 Generalized Ray Theory for a Layered Sphere by F. Gilbert\* and D.V. Helmberger (Abstract)

Pulse propagation in a layered sphere can be investigated, in an approximate way, by what has come to be known as Cagniard's method. Classical methods are used in the analysis through the application of the Debye ray expansion. At this stage Lamb's observation, that the eikonal is linear in the frequency, is employed to bypass the usual methods for evaluation of the inverse transform integrals. The transient response for each Debye ray is obtained directly. It is estimated that the method can be applied to mantle S pulses with periods less than 75 s., and to mantle P pulses with periods less than 40 s. Preliminary results on lateral heterogeneity beneath North America are presented.

\* At the Institute of Geophysics and Planetary Physics, Scripps Institution of Oceanography, University of California San Diego, La Jolla, California 92037.

V.5    Calculated Attenuation of an Underground Explosion  
Wave in the Nearly-Elastic Range by D.J. Andrews and  
S. Shlien.

Abstract

A numerical calculation is presented of a spherically symmetrical wave in granite. Propagation in the range of peak stress below 1 kilobar is calculated, starting from the pulse shape calculated by Butkovich for the Hardhat event at 100 meters from the detonation center. An anelastic material model is used with shear hysteresis, independent of the rate, corresponding to a nominal  $Q$  for P waves of 180. It is found that Fourier components of different frequencies do not attenuate independently, but that energy is transferred from the dominant frequencies around 15 Hertz to frequencies below 3 Hertz.

Observed ground shocks from underground explosions in the close-in region have pulse lengths much shorter than waves observed at teleseismic distances. These wave forms have been matched by numerical calculations in the highly non-linear and irreversible region near the source (Butkovich, 1965). For the Hardhat event, 5 kilotons in granite, Butkovich calculated a peak stress at 100 meters of 1 kilobar with a pulse width at half maximum of 10 millise. Beyond this radius one would expect the granite medium to behave nearly elastically. For spherically symmetric wave propagation in the elastic region a component would appear with wavelength comparable to the radius of the inelastic region (Sharpe, 1938). No transfer of energy to longer wavelengths would occur if the medium behaved elastically.

Of course the close-in waveform consists of Fourier components of all frequencies. Distant waveforms might be explained by propagation and attenuation of each Fourier component independently of the others, as in the case of a linear viscoelastic medium. Then the energy present in low frequencies in the distant waveform is a remnant of the energy present in those components of the close-in waveform.

The mechanism of attenuation in crustal rocks has been reviewed by Knopoff (1964) and by Gordon and Davis (1968). They find that in polycrystalline samples the stress-strain

**Preceding page blank**

path is not reversible, but has a small hysteresis that is nearly independent of strain rate. This effect is not plasticity in the usual sense, for the loading and unloading slopes are only slightly different. The effect probably arises from friction at grain boundaries.

To explain the change of waveform from close-in to distant stations the static hysteresis of crustal rocks should be taken into account. For this type of irreversibility the principle of superposition does not hold, so that different Fourier components will not propagate independently. Since propagation in such a medium is not amenable to analytic solution, a numerical finite difference method must be used. A method of Wilkins (1964), based on direct numerical approximation of first principle equations, is adopted.

A complete prediction calculation of the distant waveform would have to account for the free surface and layers below the surface. Such a calculation would have to be done in two space dimensions with axial symmetry, if not in three dimensions, and would require rather fine zoning to get sufficient accuracy. Such a calculation would require a large amount of computer time.

In this work a spherically symmetric calculation is done. Although it is not a complete prediction calculation,

it shows to what extent the assumption of superposition of independent components is in error.

The material chosen for the calculation is reversible in dilatation and irreversible in shear. Shear stress is plotted against shear strain in Figure 1 for a cycle of loading and unloading. The initial loading slope corresponds to a shear modulus of 0.306 megabar, and the initial unloading is 6 per cent steeper with a shear modulus of 0.326 megabar. If unloading continues until shear stress reverses sign, the modulus goes back to the smaller value, and then again becomes steeper for reverse unloading. A closed stress-strain path is shown in Figure 1, but it need not be closed, depending on the strain history. The 6 per cent irreversibility in shear corresponds to a 3 per cent irreversibility for a P wave, or a nominal Q of 180.

Bulk modulus and shear modulus chosen for the calculation are appropriate to granite with a P wave velocity of 5.4 km/sec. In order to avoid the highly irreversible region very close in, a stress pulse was applied on a virtual surface at a radius of 100 meters. Butkovich's calculated pulse was matched roughly with an initial radial stress of 1 kilobar and an exponential decay with a decay time of 10 millisec. If stress decayed to a finite value (due to gas in the cavity) rather than to zero, low frequency components would be larger. The

finite difference zone size used in the calculation is 80 meters.

A pair of calculations was done; one with a reversible model and one with the irreversible model shown in Figure 1. Waveforms of velocity as a function of time at radii of 0.9, 1.7, 2.5 and 3.3 kilometers were computed and are shown at the distant stations for the reversible case in Figure 2, and for the irreversible case in Figure 3. It is evident that peak velocity is smaller in the irreversible case. There is a break in the slope of the waveform in the irreversible case when the stress deviator reverses sign. This is due to the sudden change of shear modulus in the model and should not be considered realistic. An important feature not evident in Figure 3 is that the integral of the waveform is not zero, but that there is a permanent displacement. The permanent displacement depends on the amount of irreversibility, but not on details of the hysteresis loop.

Calculated velocity waveforms at the 4 stations in each calculation were Fourier analyzed by the Cooley-Tukey algorithm. The time window used for each waveform is 320 milliseconds, so that Fourier amplitudes are found at frequency intervals of 3.12 hertz. Velocity spectra are plotted for the reversible case in Figure 4 and the irreversible case in Figure 5. Amplitudes for the dominant

frequencies of 15 to 20 hertz are smaller for the irreversible case, but amplitudes at very low frequencies are larger. This is because the integrals of the irreversible wave forms are nonzero.

In seismological literature it is customary to measure attenuation in terms of the coefficient  $Q$  given by

$$Q = \frac{2\pi E}{\Delta E} \quad [1]$$

where  $E$  and  $\Delta E$  are the peak energy and energy loss in a single cycle. This definition implicitly assumes that the medium behaves linearly, such that the ration of  $E$  to  $\Delta E$  does not depend upon  $E$  or any other property of the material which is affected by the propagation of a wave. Therefore if a plane wave is propagating through a linear medium, then its amplitude should decay exponentially with distance given by

$$u = u_0 \exp \left( - \frac{\omega r}{2cQ} \right) \quad [2]$$

$Q$  may be a function of frequency. For example, for a Kelvin viscoelastic material  $Q$  is linearly proportional to frequency. In the case of earth, both laboratory

experiments and seismic observations show that  $Q$  is independent of frequency. Thus high-frequency seismic signals decay faster than low-frequency signals in a fixed distance.

To relate the finite difference solution for the non-reversible case to seismic observations,  $Q$  was determined from the amplitude spectrum at the four stations. For a spherically symmetric wave, Blake (1952) showed that without any attenuation geometry requires a harmonic wave to propagate as

$$u = -j (\omega A' / r^2) (1 + j\omega r/c) e^{j(\omega t - kr + \beta)}$$

where  $u$  is velocity,  $r$  radial distance,  $c$  sound speed, and  $A'$  and  $\beta$  constants. Therefore if we include attenuation, then

$$u = \frac{u_0}{r^2} (1 + j\omega r/c) \exp\left(-\frac{\omega r}{2Qc} + j(\omega t - kr + \beta)\right)$$

The attenuation factor,  $1/Q$ , found in this way is plotted for the reversible case in Figure 6. The attenuation is quite close to that expected for the artificial viscosity used. This is a check on the accuracy of the numerical method. The attenuation from artificial viscosity is not significant at frequencies of 15 hertz and

below. If the principle of superposition held, one would expect that  $1/Q$  would be increased at each frequency by  $1/180$  or  $0.0055$  in the irreversible case.

The attenuation factor,  $1/Q$ , for the irreversible case is plotted in Figure 7 as a function of frequency for three pairs of stations. The three curves would be identical if the attenuation were exponential.

Since the curves definitely do not coincide it implies that  $Q$  depends upon the nature of the signal propagating through the medium. For instance, the  $Q$  determined would depend on whether or not the signal is dispersed. Therefore  $Q$  is no longer just an intrinsic property of the medium. Not only does it depend on the frequency for which it was computed but also on the presence or absence of various other frequency components in the signal.

Attenuation at the dominant frequencies of 15-20 hertz is larger than would be expected. At 3 hertz  $1/Q$  is negative and is off the scale of Figure 7. Values of  $1/Q$  at 3 hertz for the three pairs of stations are

$1/Q$	at
-.456	0.9 - 1.7 km
-.129	1.7 - 2.5
-.022	2.5 - 3.3

Different Fourier components are not propagating independently, but energy is being transferred from the dominant components to the 3 Hertz component, the lowest frequency component that can be analyzed with the time window used.

In the work that is in progress at present, the reduced displacement potential is being examined for explosions in a number of rock types. In an elastic material, of course, the reduced displacement potential is invariant as the wave propagates. The small irreversibilities used in numerical calculations have a significant effect on the reduced displacement potential. Recall that displacement in surface waves is proportional to this potential rather than to its derivative as is the case for body waves. Preliminary results indicated that small irreversibilities have a larger effect on surface waves than on body waves.

### References

- Blake, F.G. (1952), Spherical wave propagation in a solid media, J. Accoust. Soc. Am. 24, 211-215.
- Butkovich, T.R. (1965), Calculation of the shock wave from an underground nuclear explosion in granite, J. Geophys. Res. 70, 885-892.
- Gordon, R.B. and L.A. Davies (1968), Velocity and attenuation of seismic waves in imperfectly elastic rock, J. Geophys. Res. 73, 3917-3935.
- Knopoff, L. (1964), Q, Reviews of Geophys. 2, 625-657.
- Sharpe, J.A. (1942), The production of elastic waves by explosion pressures. I. Theory and empirical field observations, Geophysics 7, 144-154.
- Wilkins, M.L. (1964), Calculation of elastic plastic flow, Methods in Computation of Physics Vol. 3, Alder, Fernbach, Rotenberg, Ed.

Figure Captions

- FIGURE 1 Shear stress versus shear strain for an irreversible medium.
- FIGURE 2 Computed radial particle velocity as a function of time for a reversible medium at distances of 2.5 and 3.3 kilometers from a 5 kton explosion.
- FIGURE 3 Computed radial particle velocity as a function of time for an irreversible medium at distances of 2.5 and 3.3 kilometers from a kton explosion.
- FIGURE 4 Square root of energy spectra of radial particle velocity for a reversible medium computed at four distances. Units of spectra are in cm/sec - millisec.
- FIGURE 5 Square root of energy spectra of radial particle velocity for an irreversible medium computed at four distances. Units of spectra are in cm/sec - millisec.
- FIGURE 6  $Q^{-1}$  versus frequency for a reversible medium computed at 3 pairs of adjacent stations using equation [1].
- FIGURE 7  $Q^{-1}$  versus frequency for an irreversible medium computed at 3 pairs of adjacent stations using equation [1].

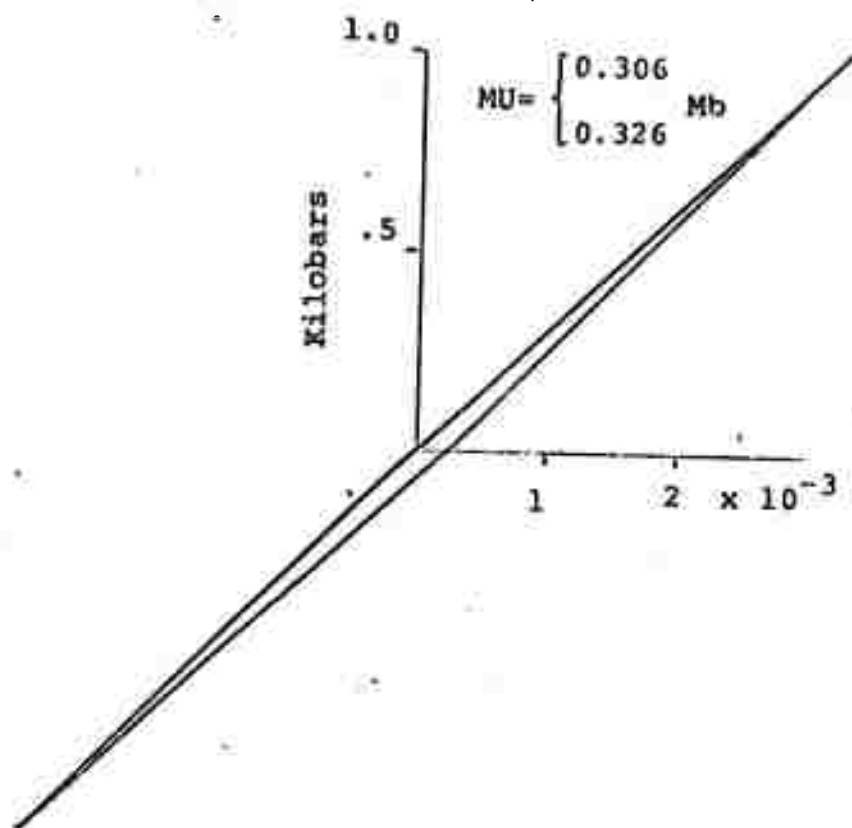
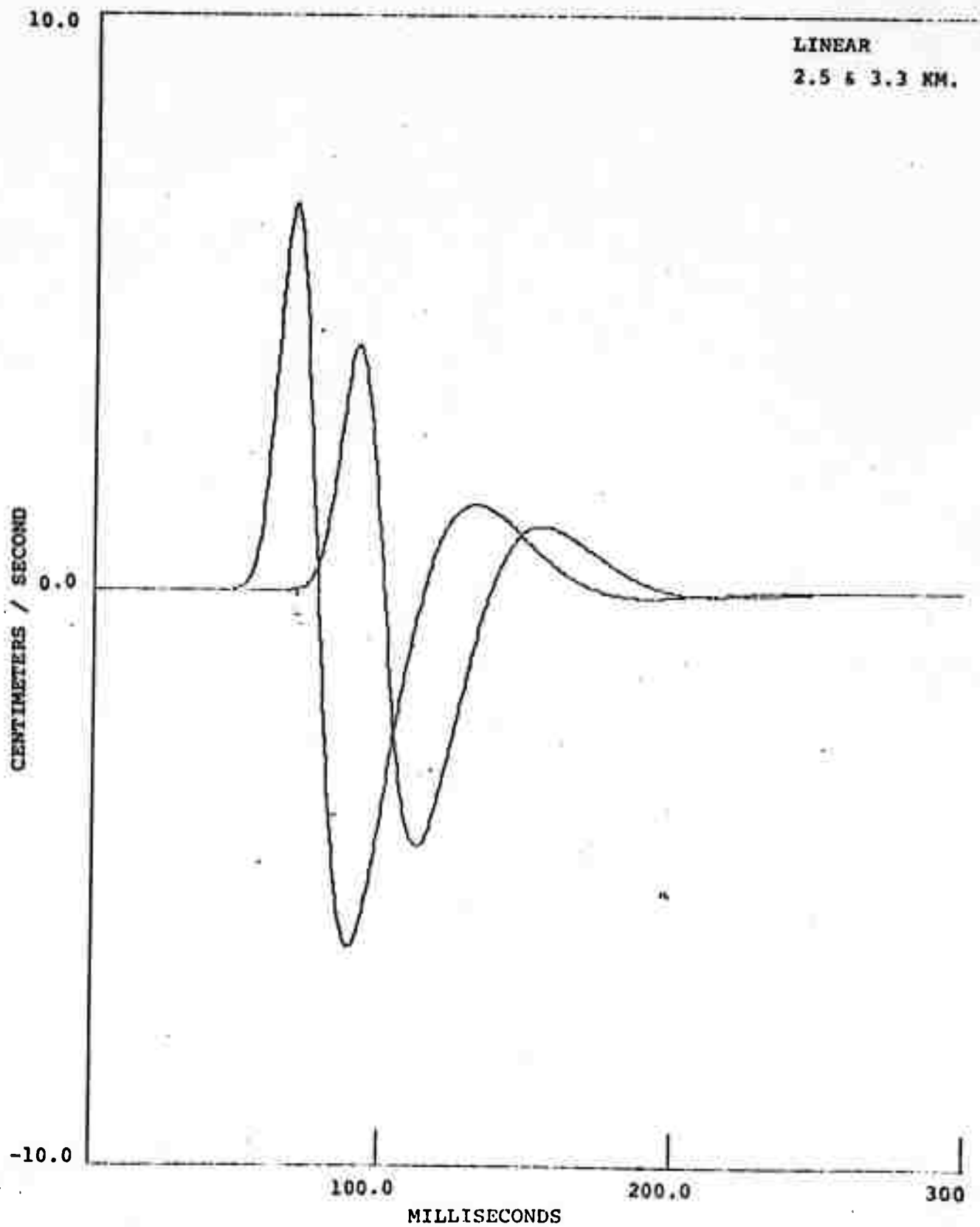
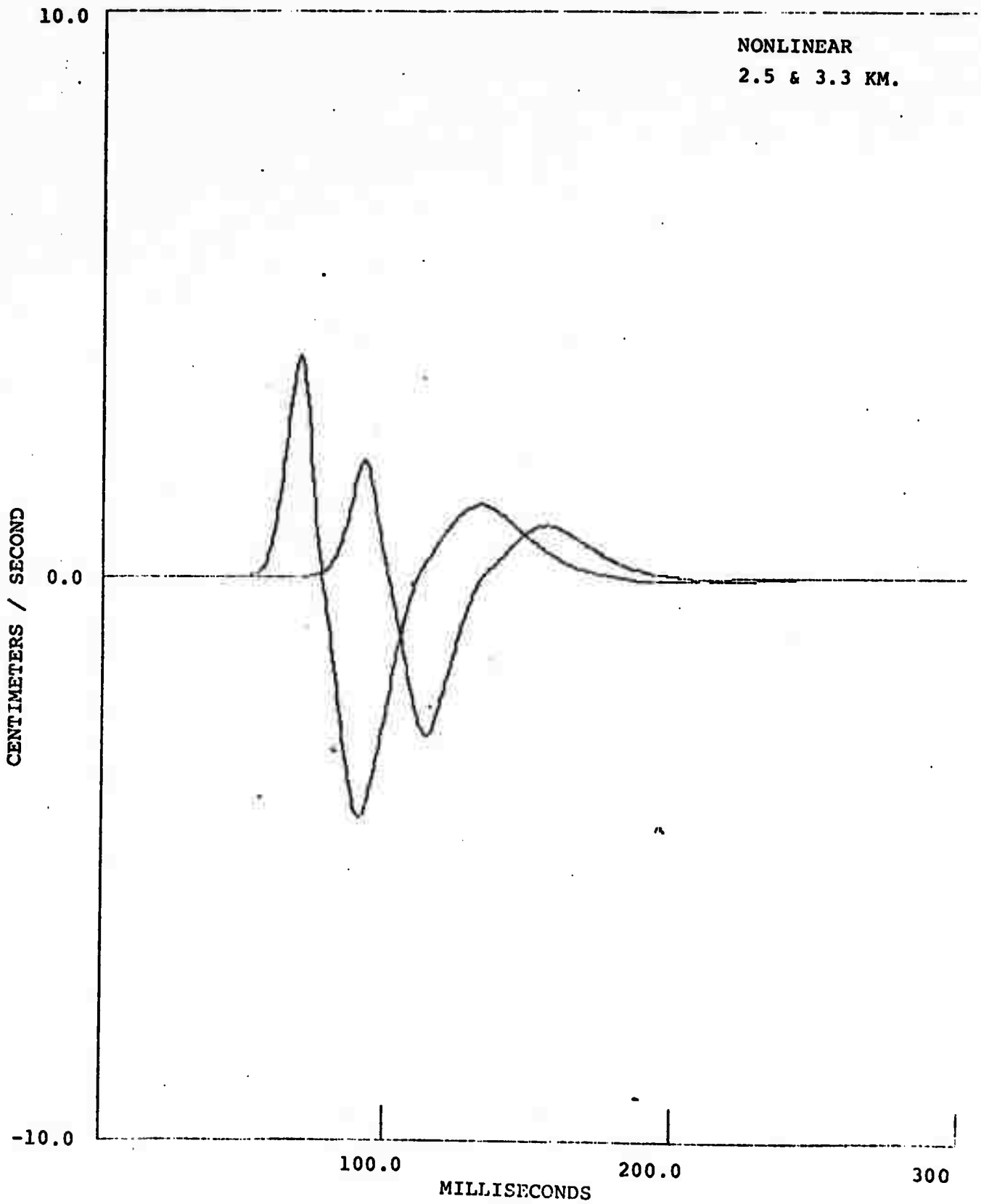
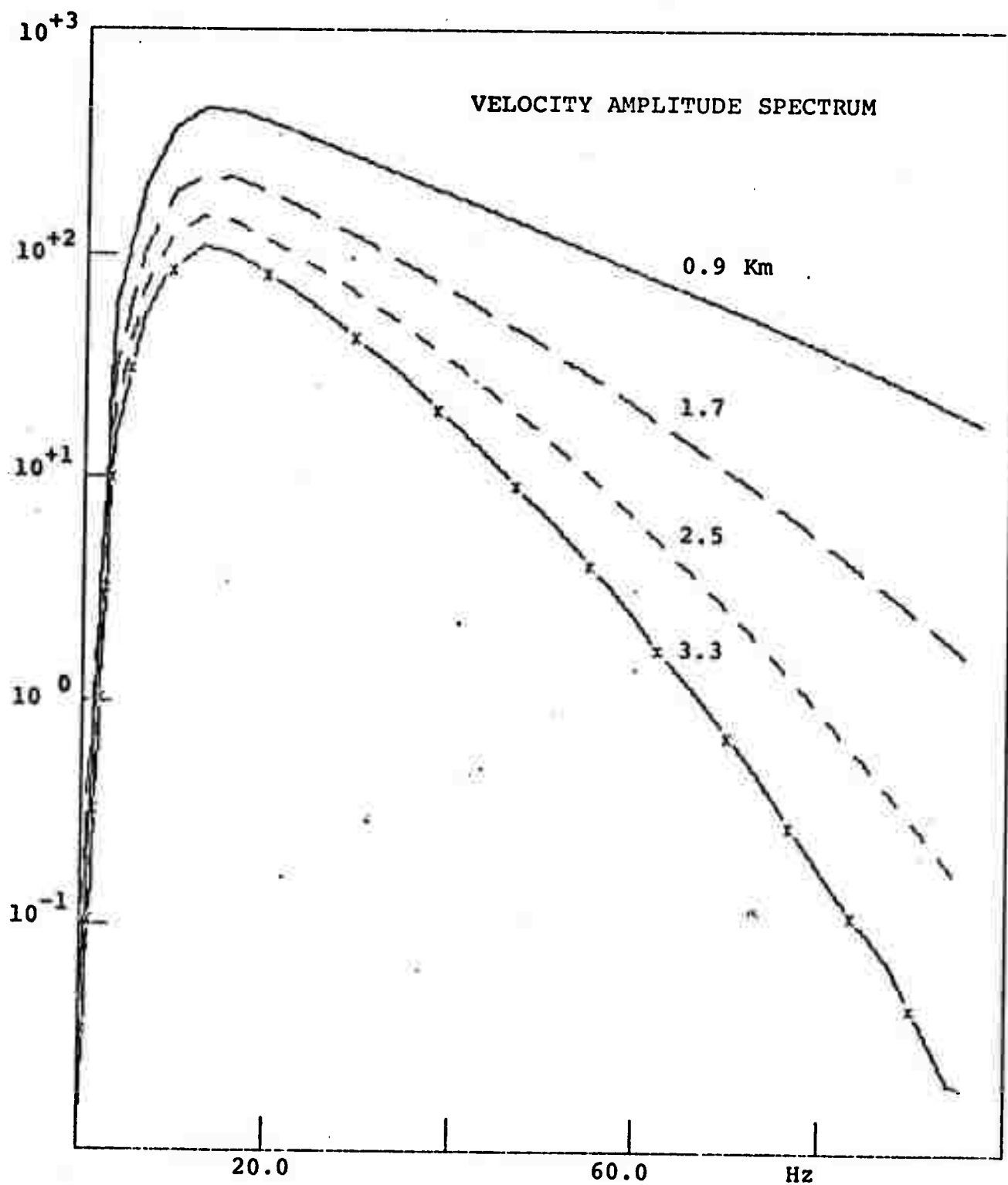


Fig. 2







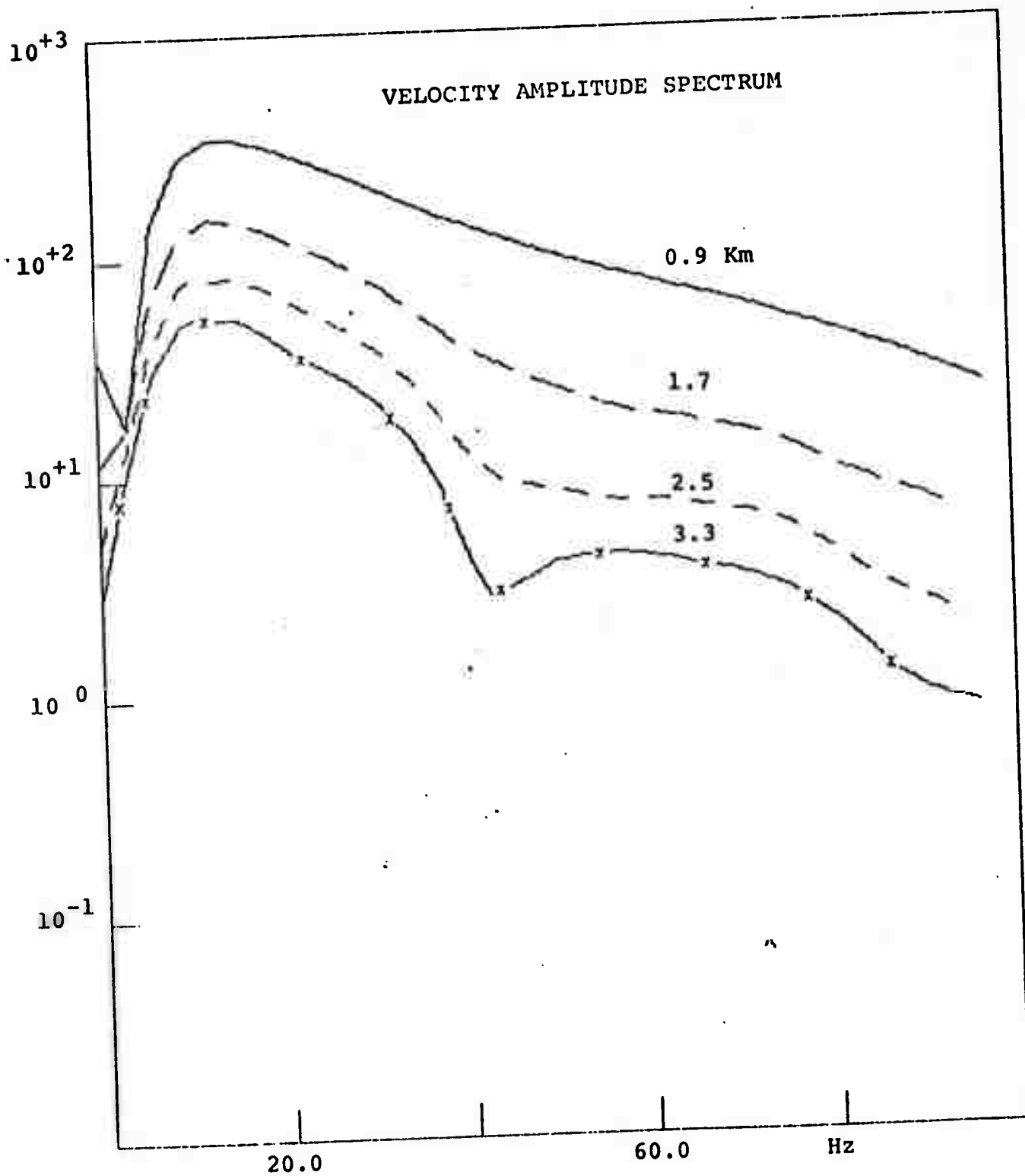
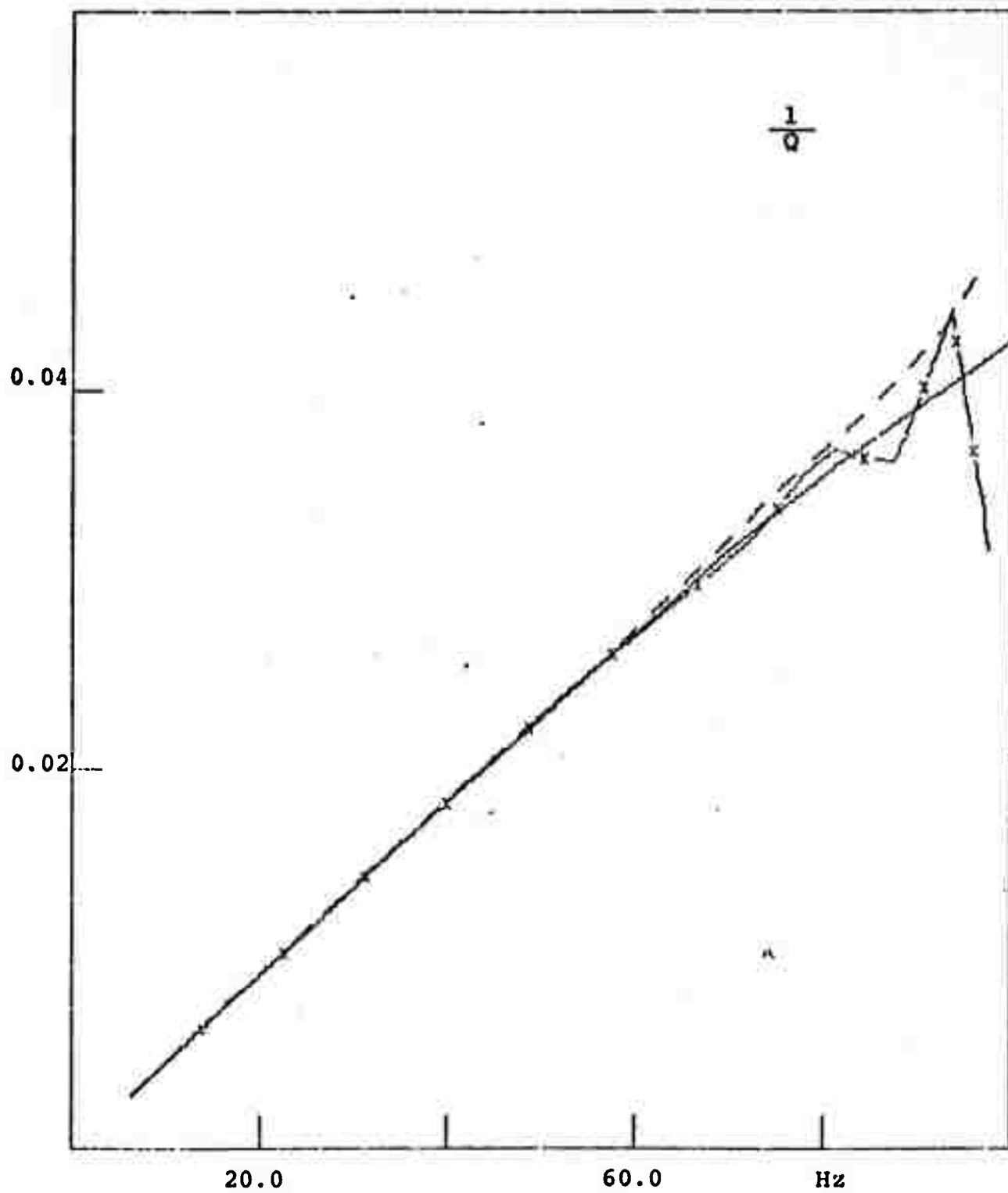
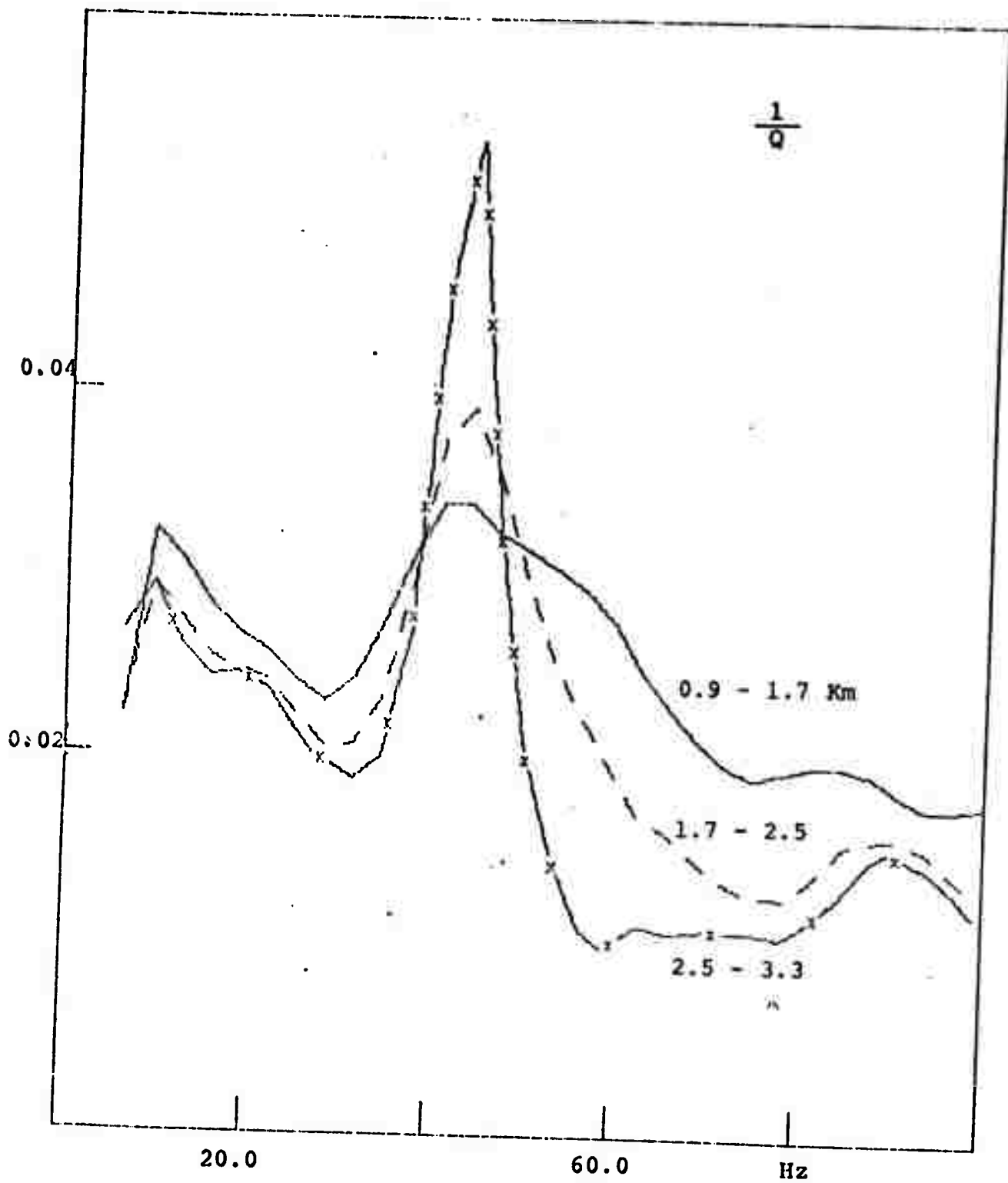


Fig.





VI.

STRUCTURE AND DYNAMICS OF THE CRUST AND UPPER MANTLE

VI.1 Temperature Field and Geophysical Effects of a Down-going Slab by M.N. Toksöz, J.W. Minear and B.R. Julian (Abstract)

The factors affecting the thermal behavior of a lithospheric slab descending into the mantle are so numerous and complicated that only numerical methods can accurately account for them. A series of finite-difference calculations of the temperature field, including the effects of viscous dissipation, adiabatic compression, phase changes and radioactive heat generation are carried out, and the relative effects of different parameters are investigated. An analysis of the stability and convergence of the numerical method indicates that the errors are small and can be reduced to any desired level by varying the grid size and the time steps. At a crustal spreading rate of 8 cm/yr, with all heat sources, the slab reaches thermal equilibrium with the surrounding mantle at a depth of about 650 km. Among observable geophysical quantities, seismic travel times and amplitudes provide the most information about the slab. Surface heat flow is sensitive to subsurface conditions that are at relatively shallow depths, and gravity anomalies are broad and are masked by crustal effects. Three dimensional calculations predict strong bending of seismic

rays near slabs, which causes strong focusing and produces shadow zones. Analysis of travel-time data for the Tonga-Fiji region indicates that waves propagating down the slab from shallow events are advanced by about 4 sec. Observations and theoretical travel-time anomalies based on calculated temperature fields are in general agreement.

VI.2 Upper Mantle Structure of Midwestern United States by D. Helmberger and R.A. Wiggins (Abstract)

Body-wave observations from nuclear events at the Nevada Test Site and several earthquakes near the western edge of the United States have been used to construct a model of the upper mantle along profiles extending toward the Great Lakes. The Cagniard-de Hoop technique for computing synthetic seismograms for laterally homogeneous earth models was used to fit both the amplitudes and travel times of the observations. The model obtained exhibits a prominent low-velocity zone, sharp discontinuities of velocity at about 430 and 660 km, and a discontinuity in the slope of the velocity at about 550 km.

VI.3 Crustal Structure beneath LASA from Long-Period P-Wave Spectra by W.H. Bakun

Abstract

Long-period transfer-function ratios from events in South America, Fiji-Tonga, and Japan recorded at the LASA subarray centers are interpreted in terms of Haskell-Thomson theory. The transfer-function ratio data provide a three-dimensional model for the crustal structure beneath LASA. The proposed structure can be characterized by two trends: (1) crustal thinning from the northeast to the southwest across the array and (2) a synclinal structure in the southwest quadrant of the array with axis plunging toward the northeast.

The response of a crustal model of parallel plane layers of homogeneous isotropic material to an incident P-wave (Haskell, 1962) was utilized by Phinney (1964) to define the crustal transfer-function ratio  $T_p(\omega) = W_o(\omega)/U_o(\omega)$ .  $W_o(\omega)$  and  $U_o(\omega)$  are the spectra of the vertical and horizontal components of displacement at the free surface respectively.  $T_p(\omega)$  is independent of the spectrum of the incident P-wave and depends only on the angular frequency  $\omega$  and the apparent velocity  $c_p$ . The position of the peaks and troughs in  $T_p(\omega)$  is relatively insensitive to changes in phase velocity and sufficiently sensitive to changes in the crustal model parameters to be useful in discriminating between competing crustal models. Phinney proposed that appropriate models for the crust and upper mantle beneath a recording station could be selected by matching  $T_p(\omega)$  for a suite of crustal models to experimental transfer-function ratios computed from the Fourier analysis of observed displacements or velocities of P-waves from

---

\*Now at Earthquake Mechanism Laboratory/NOAA, 390 Main Street, San Francisco, California.

distant earthquakes. Ichikawa and Basham (1965), Utsu (1966); Ellis and Basham (1968), Fernandez and Careaga (1968), Hasegawa (1969), Kurita (1969), and Bakun (1970, 1971) have utilized the transfer-function ratio to investigate crustal structure.

Chiburis (1966) reported station travel-time residuals as large as  $\pm 1$  sec within the 200 km diameter of LASA. Seismic studies (Steinhart and Meyer, 1961; Borchardt and Roller, 1967; Greenfield and Sheppard, 1969; Glover and Alexander, 1969; Iyer et al., 1970; Lerner, 1970; Mack, 1970; and Engdahl and Felix, 1971) have confirmed the existence of marked lateral variations in structure beneath LASA. While the resultant crustal models differ, these studies agree that structure beneath LASA appears to be complex--certainly not well suited for analysis in terms of the plane-layer models assumed in the Haskell-Thomson theory.

In this report, transfer-function ratio data recorded at each LASA subarray center are separated according to the azimuth of P-wave approach in an attempt to isolate the effect of small lateral areas beneath LASA. As a first approximation, it is assumed that these transfer-function ratio data, indicative of sub-LASA structure beneath lateral distance of approximately 50 km, can be interpreted in terms of parallel plane-layered Haskell-Thomson models. The total data imply a three-dimensional structure beneath LASA that incorporates important aspects of the previously published models for LASA.

## DATA

Transfer-function ratios used in this study were obtained from the output of the matched narrow-band three-component long-period seismometers located at the subarray centers of the A, C, D, E, and F rings of LASA. The long-period seismometers at LASA are recorded digitally with a sampling interval of 0.2 seconds. A more complete description of the LASA long-period system has been given by Capon et al., (1969). Ten events (see Table 1) with signal-to-noise ratios  $> 2$  in the 0.05 to 0.15 Hz band were selected from the LASA magnetic tape data library. (Noise spectra were computed for each event from a section of record immediately preceding the P-wave onset.) The event population was limited to events in South America, Fiji-Tonga, and Japan--the only azimuths from LASA for which more than one event with an acceptable signal-to-noise ratio was available. Typical data are shown in Figure 1. A 30-second "modified Hanning taper" window (Bakun, 1971) was applied to the vertical and to the resolved horizontal longitudinal time traces. The Fourier transform moduli of the vertical and longitudinal traces were then divided (e.g., Figure 2) to obtain the transfer-function ratio as suggested by Phinney (1964). Composite transfer-function ratios were then formed for each subarray-azimuth pair. The composite ratio is the mean at each frequency of the transfer-function ratios available. The composite ratios for each subarray-azimuth pair are shown in Figures 3, 4, 5, and 6. The number of events available to define the composite ratio for each subarray-azimuth pair is indicated in parenthesis in Figures 3-6.

### ANALYSIS

The transfer-function ratio samples structure near the recording site on an azimuth toward the source epicenter. The lateral resolution is about a crustal thickness for a window length of 30 seconds (Bakun, 1970) so that crustal model parameters determined from transfer-function ratios at LASA represent structure averaged over a lateral distance of some 50 km from the subarray center toward the source epicenter. The frequency of the first (lowest frequency) peak in the transfer-function ratio is diagnostic of the vertical P-wave travel time through the crust (Bakun, 1971). With this in mind, the lowest frequency peak in the composite ratios shown in Figures 3-6 has been scored by a vertical line. A question mark adjacent to the vertical line indicates that the composite ratio data for that subarray-azimuth pair is judged to be of poorer quality. Quality is judged to be poor if: (a) only one event is available for the subarray-azimuth pair, (b) the standard deviation of the composite ratio is large, or (c) the resolution of the lowest frequency peak is low.

The periods of the lowest frequency peak of the composite ratios of higher quality (ratios not questioned in Figures 3-6) have been plotted on a map of the LASA array in Figure 7. The periods have been plotted 25 km ( $\sim \frac{1}{2}$  crustal thickness) from the subarray center on the azimuth toward the source epicenter. The contours of the periods in Figure 7 provide a three-dimensional model for the structure beneath LASA.

### DISCUSSION

Bakun (1971) presented a relation between the period of the lowest frequency peak in  $T_p(\omega)$  and the vertical P-wave crustal travel time based on theoretical transfer-function ratios computed for many crustal models. Using the results of that study, P-wave times have been assigned to the contours in Figure 7. Since crustal travel time increases rapidly with period for periods  $> 10$  seconds, the periods plotted in Figure 7 imply lateral differences of about 1 second in the vertical P-wave crustal travel times beneath LASA. For example, assuming a constant crustal compressional velocity of 6.5 km/sec, the travel times in Figure 7 imply an increase in crustal thickness from 29 km in the west to 36 km in the east, corresponding to an average dip of the Moho of about  $5^\circ$ , plunging eastward beneath LASA.

The theoretical effect of a dipping crustal layer on the character of  $T_p(\omega)$  is not significant for dips less than or equal to about  $5^\circ$  (Rogers and Kisslinger, 1970). If velocities beneath LASA are greater in the eastern sector than in the west (Glover and Alexander, 1969), the average dip on the Moho beneath LASA would tend to be greater than  $5^\circ$ . On the other hand, all but three of the periods plotted in Figure 7 result from updip approach. Since updip approach would increase the estimated vertical crustal travel times, or periods in Figure 7, the net effect of the dip implied by these data would be to accentuate the lateral variations shown.

The structure beneath LASA shown in Figure 7 is characterized by two trends: (1) crustal thinning from the northeast to the southwest across the array and (2) a synclinal structure in the southwest quadrant of the array with axis plunging to the northeast. It is interesting to

compare this structure obtained from transfer-function ratio data with previously published LASA models. The data presented here tend to confirm Glover and Alexander's (1969) conclusion that the maximum lateral change in structure beneath LASA is in a northeast-southwest direction, with greater crustal thickness in the eastern sector of LASA. On the other hand, a northwest-southeast profile through subarray A0 would result in a two-dimensional model similar in shape to that proposed by Greenfield and Sheppard (1969), but displaced some 50 km to the southeast. Iyer et al. (1970) and Larner (1970) proposed shallower LASA crustal models similar in shape to the model of Greenfield and Sheppard.

The major point of difference between the model proposed here and the previously published crustal models for LASA lies in the scale of the structure. Assuming reasonable crustal velocities, the P-wave travel times of 4.5-5.5 seconds proposed here imply sub-LASA crustal thicknesses of 30-40 km--significantly less than LASA crustal thicknesses published in previous studies. If the periods of the lowest frequency peak of the  $T_p(\omega)$  data were greater than 20 seconds, the second (higher frequency) peak in  $T_p(\omega)$  would be erroneously taken for the desired lowest frequency peak in this analysis. Such a misidentification would result in a significant underestimation of the sub-LASA crustal times.

It should be pointed out however that crustal thickness beneath LASA is a poorly determined parameter. Seismic refraction surveys (Steinhart and Meyer, 1961; Borchardt and Roller, 1967) indicate crustal thicknesses of 47-52 km beneath LASA. Using station travel-time residuals, Greenfield and Sheppard (1969) proposed a model for LASA with total crustal thickness of 58 to 70 km. Larner (1970) found that structure similar in shape to that of Greenfield and Sheppard (1969) adequately explained observed

scattering of short-period P-waves at LASA. However, Lerner's analysis indicates an upper bound of  $48 \pm 5$  km for the average thickness of the LASA crust. Iyer et al. (1970) found evidence for crustal thicknesses of 41 to 55 km beneath LASA.

It is somewhat surprising that a reasonably self-consistent picture of the complicated structure beneath LASA can be obtained using parallel plane-layered theory. It should be noted that only 19 of the 51 composite ratios shown in Figures 3-6 were considered reliable enough for use in constructing the structural contours in Figure 7. (Identical structural contours-- with several inconsistent data points--result if all 51 composite ratios are used in the analysis.) The 19 ratios used here are themselves not totally reliable--e.g., the period of the lowest frequency peak in  $T_p(\omega)$  for individual events in the same subarray-azimuth pair may vary. The vertical and lateral resolution, both on the order of a crustal thickness, of the transfer-function ratio data used here and also the process of forming composite ratios have the effect of smoothing out more rapid variations in structure that may be resolved by short-period data.

Scatter in the periods shown in Figure 7 is most apparent between the D and E rings near the E4 subarray, indicating rapid lateral variation in structure. It is perhaps only coincidence that this portion of LASA lies atop Porcupine Dome, the most significant geological feature in the LASA area (King, 1961).

#### ACKNOWLEDGMENTS

The author wishes to thank the staff of the Seismic Discrimination Group, Lincoln Laboratory, M.I.T., for their interest and comments during the course of this research. Access to the data and facilities of Lincoln Laboratory during the course of this research are gratefully acknowledged. Professors Lane R. Johnson and Thomas V. McDevilly of the University of California, Berkeley; Dr. Don Tocher of the Earthquake Mechanism Laboratory/NOAA; and Professor M. Nafi Toksoz of M.I.T. critically reviewed the manuscript. This research was supported by the U.S. Air Force under contract no. AF49(638)-1763.



# REFERENCES

- Bakun, W. H., Body wave spectra and crustal structure: An application to the San Francisco Bay region, Ph.D. thesis, University of California, Berkeley, 1970.
- Bakun, W. H., Crustal model parameters from P-wave spectra, Bull. Seism. Soc. Am., 61, 913-935, 1971.
- Borcherdt, C. A., and J. C. Roller, Preliminary interpretation of a seismic-refraction profile across the large aperture seismic array, Montana, Open File Report, U.S. Geological Survey, Menlo Park, California, 1967.
- Capon, J., R. J. Greenfield, and R. T. Lacoss, Long-period signal processing results for the Large Aperture Seismic Array, Geophysics, 34, 305-329, 1969.
- Chiburis, E. F., LASA travel-time anomalies for various epicentral regions, Seismic Data Lab. Rep. 159, Earth Sciences, Teledyne, Alexandria, Virginia, 1966.
- Ellis, R. M., and P. W. Basham, Crustal characteristics from short period P waves, Bull. Seism. Soc. Am., 58, 1681-1700, 1968.
- Engdahl, E. R., and C. P. Felix, Nature of travel-time anomalies at Lasca, J. Geophys. Res., 76, 2706-2715, 1971.
- Fernandez, L. M., and J. Careaga, The thickness of the crust in central United States and La Paz, Bolivia, from the spectrum of longitudinal seismic waves, Bull. Seism. Soc. Am., 58, 711-741, 1968.
- Glover, P., and S. S. Alexander, Lateral variations in crustal structure beneath the Montana LASA, J. Geophys. Res., 74, 505-531, 1969.
- Greenfield, R. J. and R. M. Sheppard, The Moho variations under the LASA and their effect on  $dT/da$  measurements, Bull. Seism. Soc. Am., 59, 409-420, 1969.
- Hasegawa, H. S. A study of the effects of the Yellowstone crustal structure upon the P-coda of teleseismic events, Geophys. J., 18, 159-175, 1969.
- Ichikawa, M., and P. W. Basham, Variations in short-period records from Canadian seismograph stations, Can. J. Earth Sci., 2, 510-542, 1965.
- Iyer, H. M., A. R. Jackson, J. H. Healy, and T. E. Landers, LASA anomalies and their relations to crust and upper-mantle structure, Open File Report, U.S. Geological Survey, Menlo Park, California, 1970.

- King, P. B., (ed), Tectonic map of the United States: U.S. Geological Survey and American Association of Petroleum Geologists, 1961.
- Kurita, T., Crustal and upper mantle structure in Japan from amplitude and phase spectra of long-period P-waves. Part 1. Central mountain area, J. Phys. Earth, 17, 13-41, 1969.
- Larner, K. L., Near receiver scattering of teleseismic body waves in layered crust-mantle models having irregular interfaces, Ph.D. thesis, Massachusetts Institute of Technology, Cambridge, 1970.
- Mack, H., Nature of short period P-wave signal variations at LASA, J. Geophys. Res., 74, 3161-3170, 1969.
- Phinney, R. A., Structure of the earth's crust from spectral behavior of long-period body waves, J. Geophys. Res., 69, 2997-3017, 1964.
- Rogers, A., and C. Kisslinger, The effect of a dipping layer on P wave transmission (abstract), Earthquake Notes, 41, 31, 1970.
- Steinhart, J. S., and R. P. Meyer, Explosion studies of continental structure, Publ. 622, Carnegie Inst., Washington, 1961.
- Utsu, T., Variations in spectra of P waves recorded at Canadian arctic seismograph stations, Can. J. Earth Sci., 3, 597-621, 1966.



Table 1. Events studied

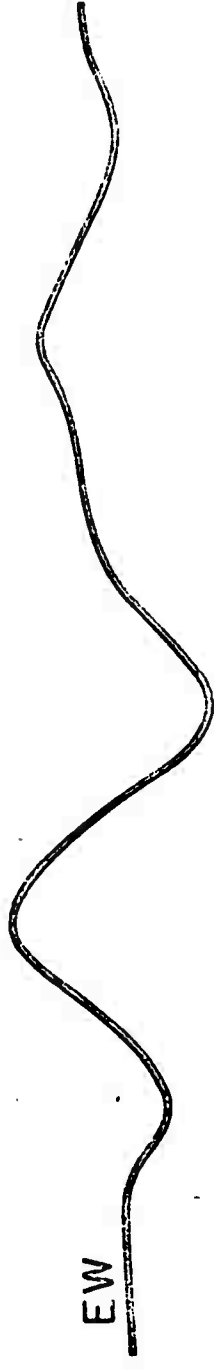
#	Date	Origin Time <sup>1</sup> (GMT)	Epical Coords <sup>1</sup>	Focal Depth	Magn.	Azimuth from center of subarray A0	Distance from center of subarray A0	Angle of Incidence
1	15 Feb 67	16-11-11.8	9.0°S, 71.3°W (Peru-Brazil Border)	597km	6.2	140.8°	63.6°	27.1
2	27 Dec 67	09-17-55.7	21.2°S, 68.3°W (Chile-Bolivia Border)	135	6.4	143.7	75.8	23.
3	19 June 68	08-13-35.0	5.6°S, 77.2°W (No. Peru)	28	6.4	145.3	58.1	39
4	28 Sept 68	13-53-35.3	13.2°S, 76.4°W (Coast of Peru)	70	6.0	147.8	65.3	27.5
5	11 Mar 68	08-26-32.8	16.2°S, 173.9°W (Tonga Is.)	112	6.0	242.9	87.1	20.3
6	19 Jan 67	12-40-12.6	14.8°S, 178.8°W (Fiji Is.)	18	6.6	247.4	89.1	19.9 <sup>2</sup>
7	12 June 68	13-41-50.7	39.5°N, 142.7°E (Honshu Is., Japan)	44	6.0	311.5	74.5	24.5
8	3 Aug 68	04-54-32.7	25.6°N, 128.5°E (Ryukyu Is.)	19	6.4	312.4	92.7	19.3
9	14 May 68	14-05-06.0	29.9°N, 129.4°E (Ryukyu Is.)	168	5.9	314.2	88.7	19.9
10	5 Aug 68	16-17-04.8	33.3°N, 132.3°E (Shikoku Is., Japan)	41	6.3	314.2	84.6	21.1

<sup>1</sup>Hypocenter parameters from USCGS PDE cards.<sup>2</sup>Angle of incidence at the base of the crust computed from the Jeffreys-Bullen travel time tables with  $P_n = 8.0 \text{ km/sec}$ .

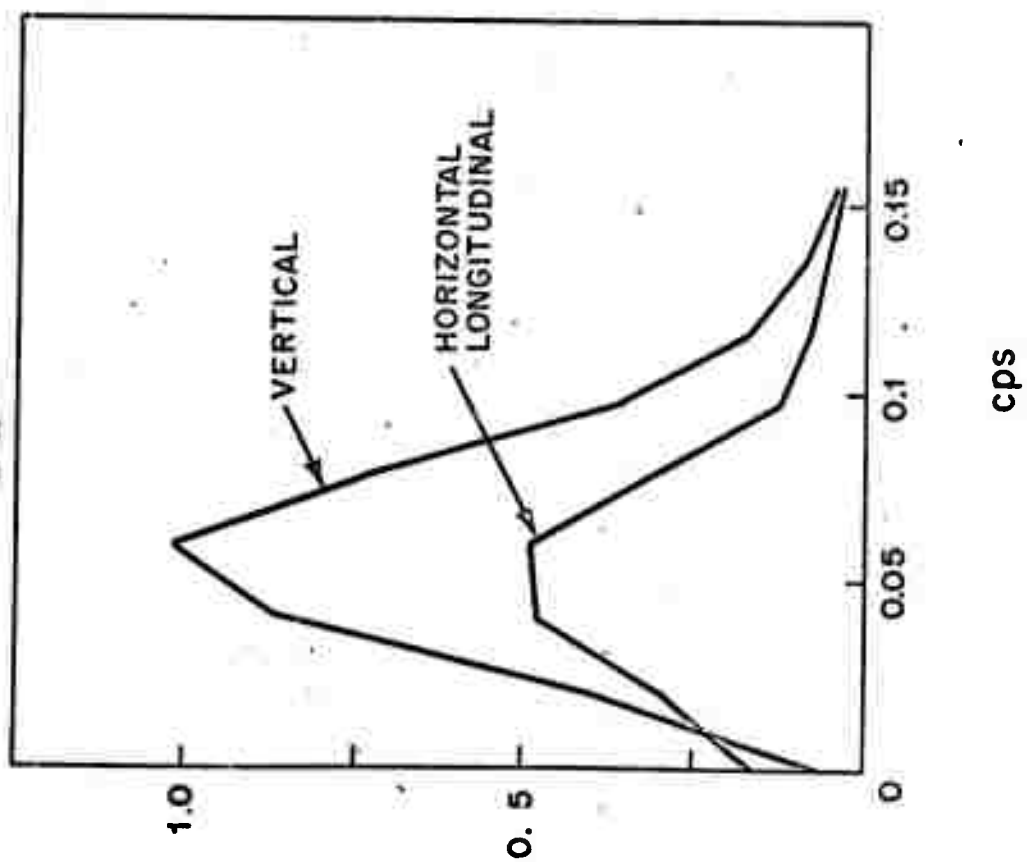
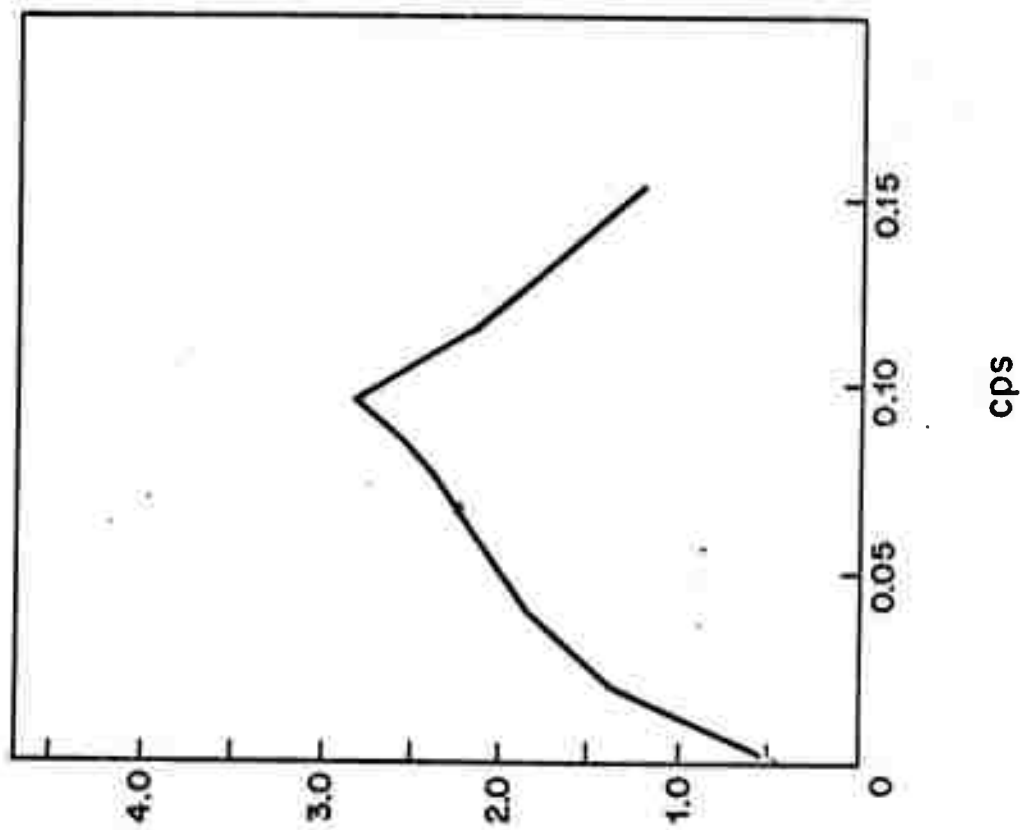
Reproduced from  
best available copy.

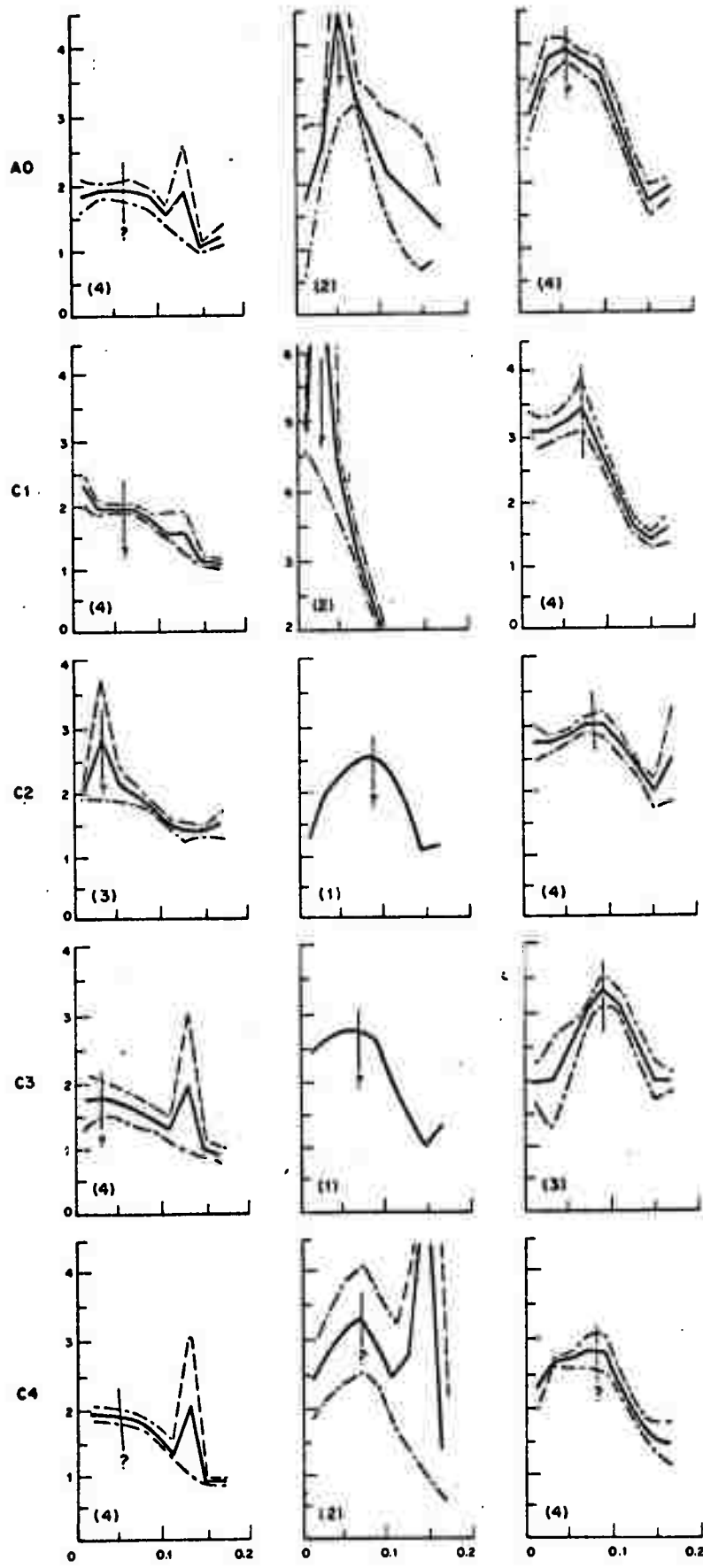
# FIGURE CAPTIONS

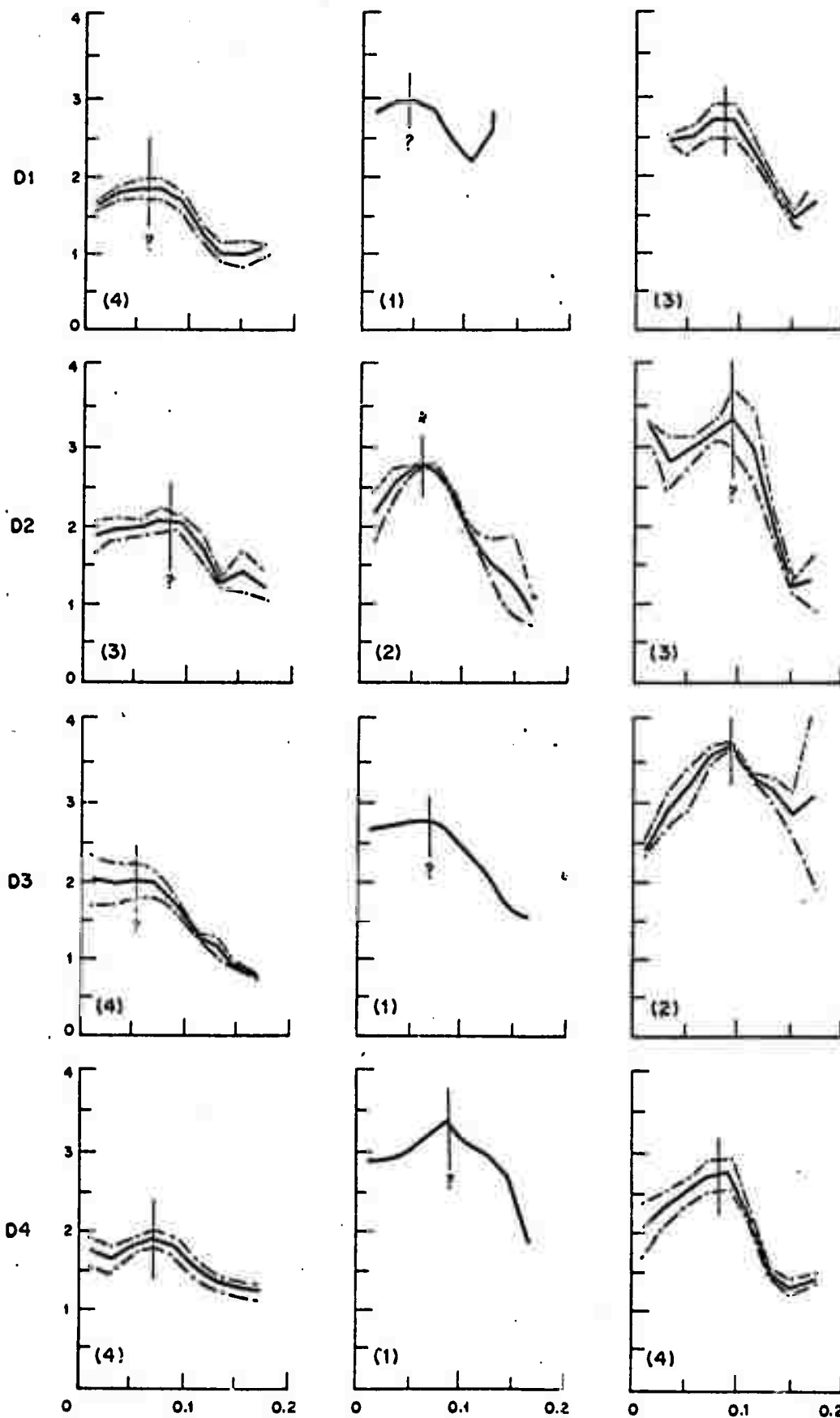
- Figure 1. Vertical (Z), north-south (NS) and east-west (EW) components of the P-wave from the 15 Feb 67 South America event (see Table 1) recorded on the long-period seismometers at the center of subarray F3.
- Figure 2. Moduli (left) of the Fourier transforms of the vertical and resolved horizontal longitudinal components for the event shown in Figure 1. The transform moduli are normalized to the maximum of the vertical spectrum. The transfer function ratio (right) is the vertical spectrum divided by the resolved horizontal longitudinal spectrum.
- Figure 3. Composite transfer function ratios (solid traces) for the subarrays A0, C1, C2, C3, and C4 for the South America events (left column), the Fiji-Tonga events (middle column) and the Japan events (right column) as a function of frequency (Hz). The composite ratio  $\pm$  its standard deviation is indicated by dashed traces.
- Figure 4. Composite transfer function ratios for the D1, D2, D3, and D4 subarrays. See the legend for Figure 3.
- Figure 5. Composite transfer function ratios for the E1, E2, E3, and E4 subarrays. See the legend for Figure 3.
- Figure 6. Composite transfer function ratios for the F1, F2, F3, and F4 subarrays. See the legend for Figure 3.
- Figure 7. Map of the Montana LISA. The periods of the lowest frequency peaks of the composite transfer function ratios (Figures 3-6) are plotted 25 km,  $\sim \frac{1}{2}$  the crustal thickness beneath LISA, from the subarray centers along the azimuth toward the appropriate source epicenter. Contour values are the one-way vertical P-wave crustal travel times determined from the periods of the lowest frequency peaks.

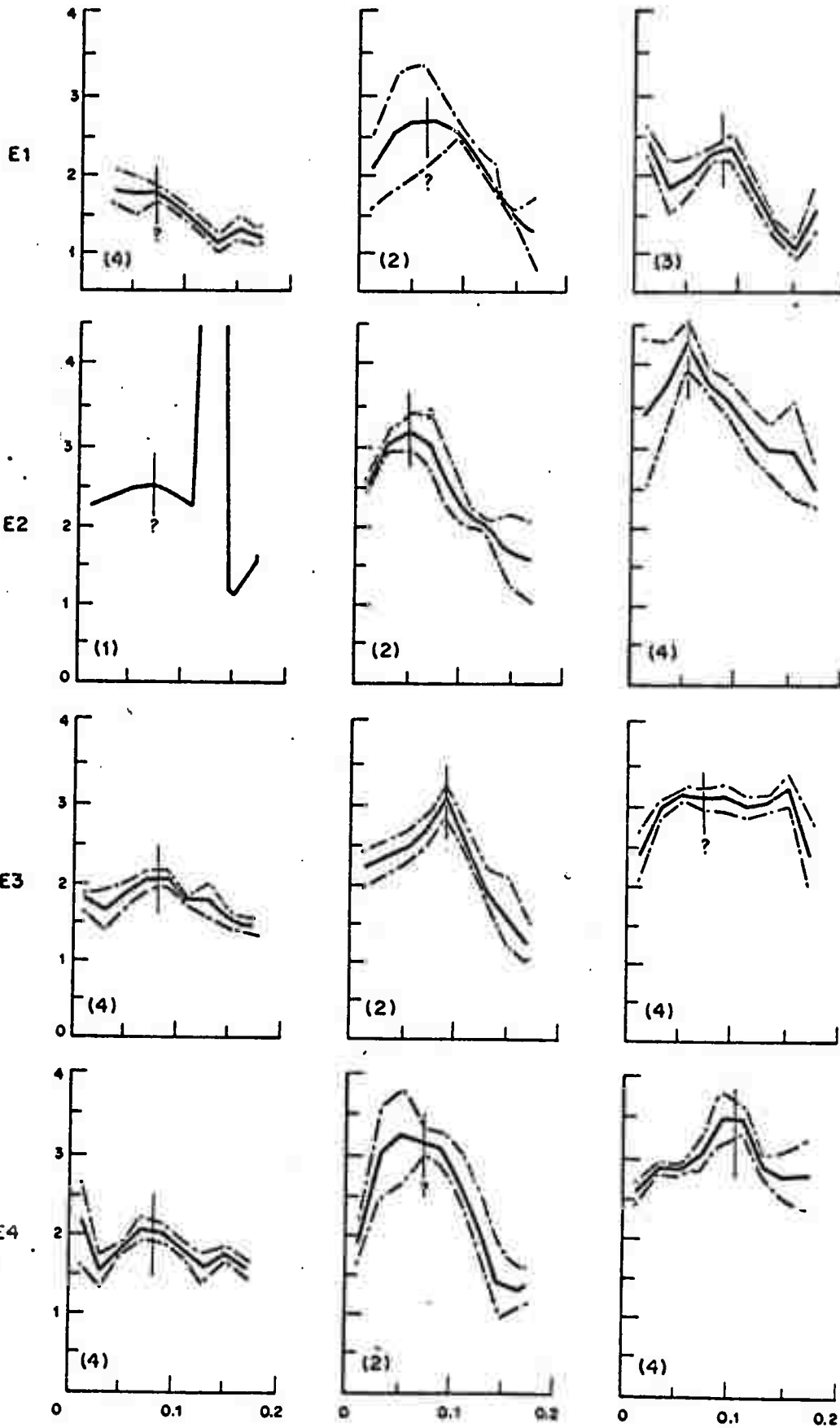


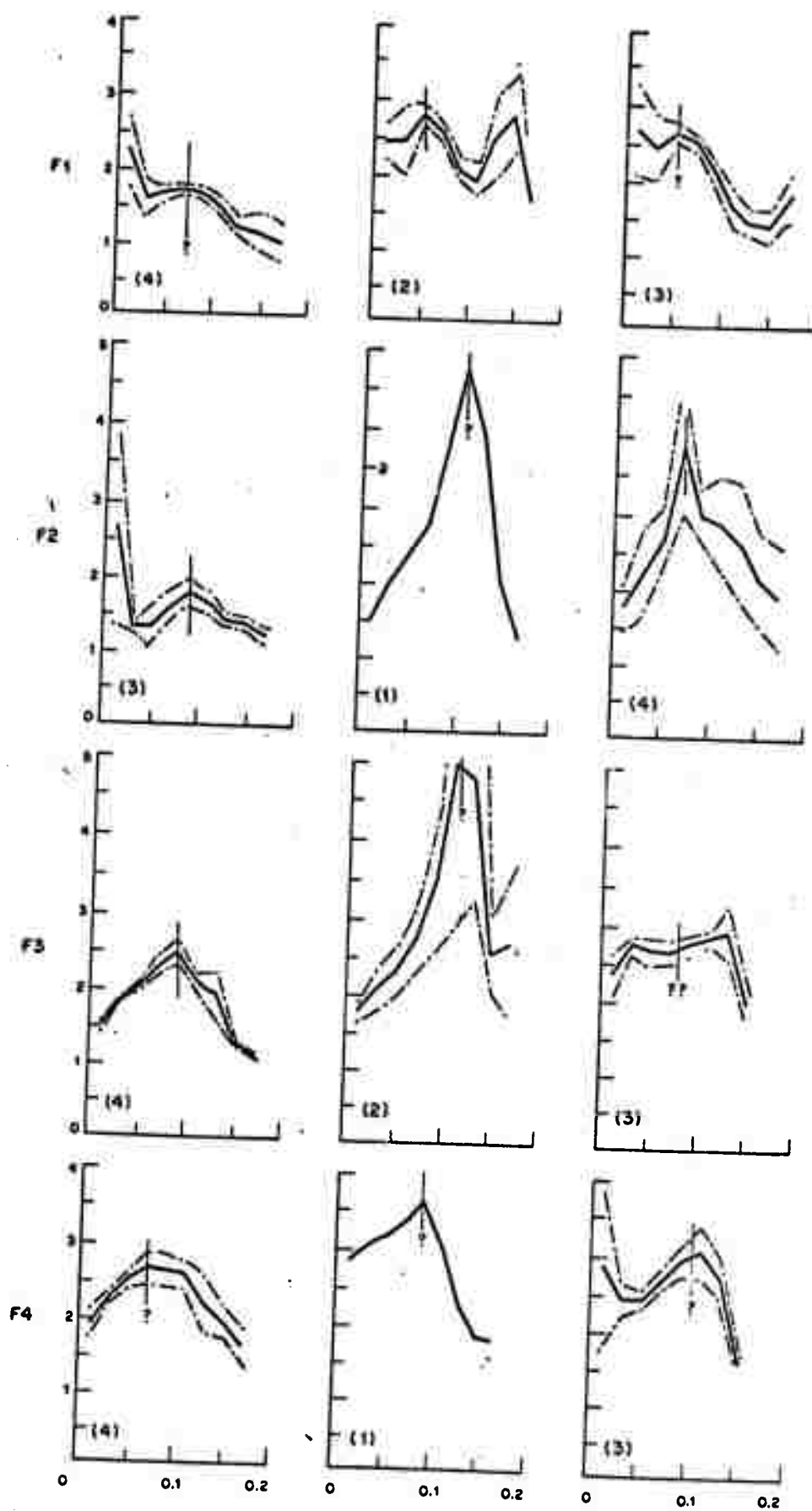
10 sec

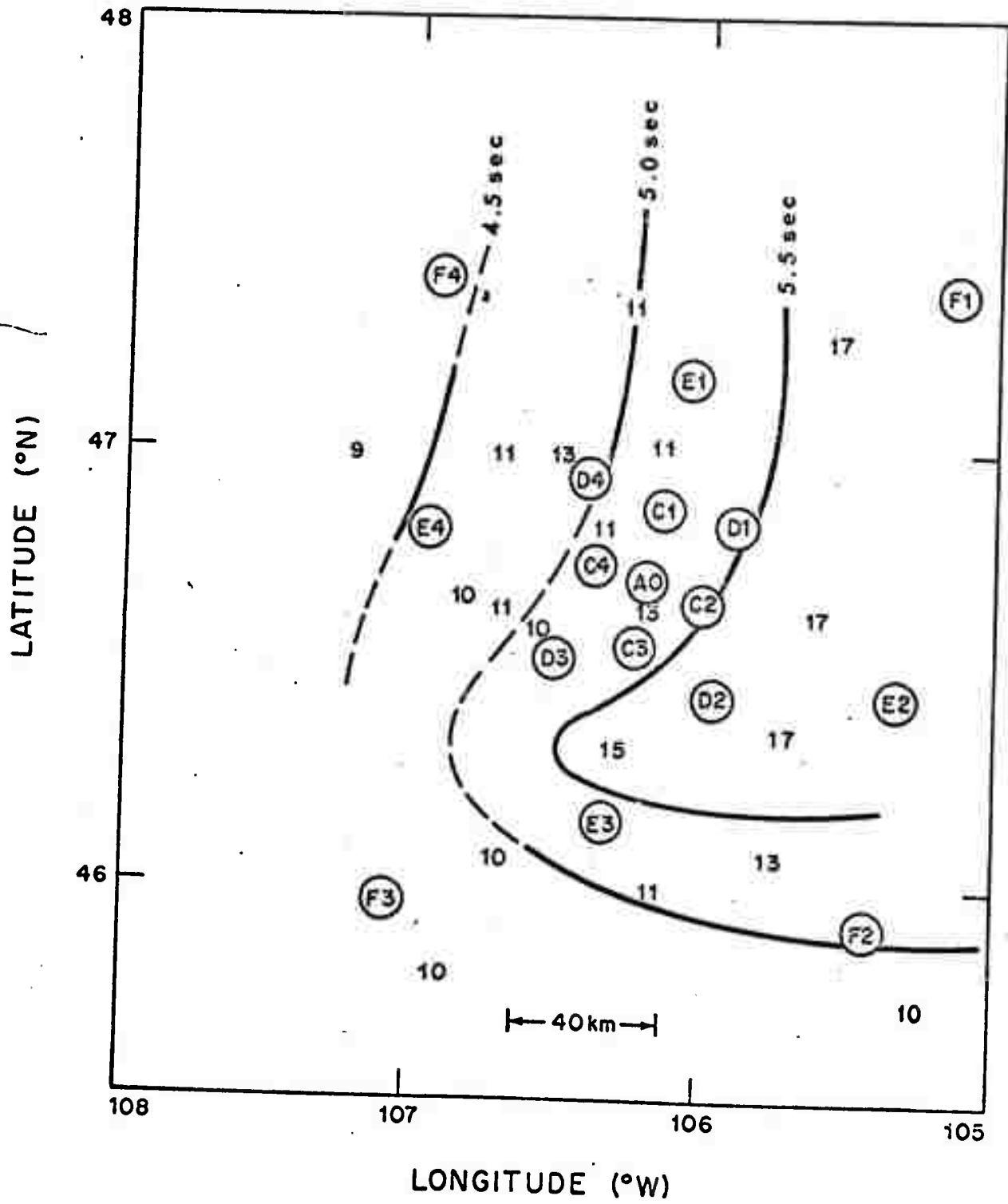












VI.4 Numerical Simulation of Sea-Floor Spreading by  
D.J. Andrews

Abstract

Upper mantle convection, including lithospheric plate motion, is simulated numerically using a two-dimensional time-dependent method that allows large viscosity variations. The numerical operator developed for viscous flow is in self-adjoint form, so that the conjugate gradient iteration method may be used. Convergence is faster than with relaxation methods. The method is applied to sea-floor spreading with the objective of examining the driving mechanism of mid-ocean ridges. In accordance with this objective, deep convection is suppressed in the model. Counterflow below the plates is confined to depths less than 340 km. The model is fit to observed topography at four different ridge locations. It is found that for a spreading velocity of 1.2 cm/yr, the ridge can produce compressive stress in the lithosphere out to a distance of 1600 km. For a spreading velocity of 6 cm/yr this model is clearly excluded, for it requires excessively large stress in the lithosphere. Therefore upwelling material must cross the seismic discontinuity at 400 km depth.

A new method is presented in this paper for the calculation of convection in a fluid with strongly varying viscosity. Time dependent heat flow and viscous mass flow are simulated numerically in two space dimensions. The method is designed for tectonic flow in the earth, so that inertia is neglected. Therefore the Reynolds number is zero and the Prandtl number is infinite.

Numerical calculations of steady state convection with large viscosity variations have been done by Torrance and Turcotte [1971a, 1971b]. They have not included lithospheric plates in their calculations, for extreme viscosity variations reduce the rate of convergence of the solution. With the end in view of calculating problems in plate tectonics, a different approach to the finite difference equations is presented here.

#### Equations to be solved

The flow is assumed to be incompressible, so that velocity components may be derived from a stream function,  $S$ ,

$$u = \frac{\partial S}{\partial y} \tag{1}$$

$$v = - \frac{\partial S}{\partial x} \tag{2}$$

Components of the stress deviator tensor are assumed to be determined by Newtonian viscosity in two dimensional flow,

$$s_{xx} = -s_{yy} = 2\eta \frac{\partial u}{\partial x} \quad (3)$$

$$s_{xy} = \eta \left( \frac{\partial u}{\partial y} + \frac{\partial v}{\partial x} \right) \quad (4)$$

The viscosity,  $\eta$ , need not be constant. Pressure (mean stress) may assume any value needed to produce stress equilibrium. In the absence of inertia each component of force density vanishes

$$\frac{\partial s_{xx}}{\partial x} + \frac{\partial s_{xy}}{\partial y} - \frac{\partial P}{\partial x} = 0 \quad (5)$$

$$\frac{\partial s_{xy}}{\partial x} + \frac{\partial s_{yy}}{\partial y} - \frac{\partial P}{\partial y} + \rho g = 0 \quad (6)$$

We adopt the Boussinesq approximation, that only the variation of density with temperature need be considered, and only in the body force term. A constant thermal expansivity is assumed

$$\rho = \rho_0 (1 - \alpha T) , \quad (7)$$

although this relation could be generalized with no difficulty. Overburden pressure due to a constant density is subtracted from pressure,

$$p = P - \rho_0 g y \quad (8)$$

Then equations (5) and (6) become

$$\frac{\partial s_{xx}}{\partial x} + \frac{\partial s_{xy}}{\partial y} - \frac{\partial p}{\partial x} = 0 \quad (9)$$

$$\frac{\partial s_{xy}}{\partial x} + \frac{\partial s_{yy}}{\partial y} - \frac{\partial p}{\partial y} - \rho_0 g \alpha T = 0 \quad (10)$$

where all terms have about the same order of magnitude. Pressure may be eliminated by taking the curl of force density. The single equation that results, expressed in terms of the stream function, is

$$\begin{aligned} & \frac{\partial^2}{\partial x \partial y} \left[ 4\eta \frac{\partial^2 S}{\partial x \partial y} \right] + \left( \frac{\partial^2}{\partial y^2} - \frac{\partial^2}{\partial x^2} \right) \\ & \left[ \eta \left( \frac{\partial^2}{\partial y^2} - \frac{\partial^2}{\partial x^2} \right) S \right] \\ & - \frac{\partial}{\partial x} (\rho_0 g \alpha T) = 0 \end{aligned} \quad (11)$$

For a fixed temperature field, mass flow will be steady. Time dependence of the solution arises from time-dependence of temperature. At each instant of time the finite difference approximation of this elliptic equation is solved by an iterative procedure.

Relaxation methods for solution of systems of linear equations can be put upon a rigorous basis only for symmetric matrices [Varga, 1962], although such methods have been used more generally. In the hope of handling extreme viscosity variations, the present work will be kept as well-founded as possible.

The differential operator appearing in equation (11) is self-adjoint and can be derived from a variational principle of minimum viscous dissipation. If a finite difference analogue of this operator is formulated from a variational principle, then one has increased confidence that an iterative relaxation procedure will converge. Also it will be seen that the finite difference operator so derived is a self-adjoint (symmetric) matrix.

The single fourth order equation for stream function might be replaced by a set of coupled equations of lower order in more than one dependent variable. For instance, velocity components might be used rather than stream function as dependent variables. One might expect a variational principle to hold with incompressibility imposed as a

subsidiary condition. However, a divergence expression cannot be used as a subsidiary condition in a variational problem [Courant and Hilbert, 1953]. Alternatively, a coupled pair of equations could be used for vorticity and stream function. One would like to use a relaxation procedure for each equation of the pair [Burggraf, 1966], but in the case of variable viscosity the differential operators of the separate equations cannot be derived from variational principles. Vorticity has lost its usefulness as an auxiliary variable. Therefore it is desirable to work with the single equation of fourth order for the stream function.

However, there is a disadvantage to using a relaxation procedure with a fourth order equation. By dimensional arguments one would expect the number of iterations required for each component of the error to decay to be proportional to the fourth power of its wavelength. Then the number of iterations required would go as the fourth power of the number of finite difference zones in one space dimension, rather than the square as for second order equations. Fortunately, with the symmetric matrix equation formulated here, one can use the conjugate gradient method, that ideally gives an exact solution after a number of iterations proportional to the square of the number of zones in one dimension.

The equation used for evolution of the temperature field in time is

$$\begin{aligned} \frac{\partial T}{\partial t} = & -u \frac{\partial T}{\partial x} - v \frac{\partial T}{\partial y} + \frac{1}{\rho C_p} \left[ \frac{\partial}{\partial x} \left( K \frac{\partial T}{\partial x} \right) \right. \\ & + \frac{\partial}{\partial y} \left( K \frac{\partial T}{\partial y} \right) + 4\eta \left( \frac{\partial^2 S}{\partial x \partial y} \right)^2 \\ & + \eta \left( \frac{\partial^2 S}{\partial y^2} - \frac{\partial^2 S}{\partial x^2} \right)^2 \\ & \left. + \nu \rho_0 g \alpha T + H \right] \end{aligned} \quad (12)$$

where  $K$  is thermal conductivity and  $H$  is the rate of heat generation per unit volume. The terms on the right side account for advection of heat by mass transport, thermal conduction, viscous dissipation, adiabatic temperature change with depth, and radioactive heat generation.

### Finite Difference Equations

In describing the finite difference equations, intersections of grid lines will be called grid points and mesh spaces between grid lines will be called zones or zone interiors. Grid lines are parallel to the  $x$  and  $y$  coordinate

axes. The stream function is defined at grid points. Then the stress deviator

$$s_{xx} = 2\eta \frac{\partial^2 S}{\partial x \partial y}$$

is most naturally defined by a finite difference expression centered in a zone interior

$$\begin{aligned} (s_{xx})_{i-\frac{1}{2},j-\frac{1}{2}} = & 2\eta_{i-\frac{1}{2},j-\frac{1}{2}} (S_{i,j} - S_{i-1,j} \\ & + S_{i-1,j-1} - S_{i,j-1}) / \Delta x \Delta y \end{aligned} \quad (13)$$

where subscripts are column number and row number in the grid.

The stress component

$$s_{xy} = \eta \left( \frac{\partial^2 S}{\partial y^2} - \frac{\partial^2 S}{\partial x^2} \right)$$

is most naturally defined by a finite difference expression centered at a grid point. For the case of square zones of uniform size the expression is

$$\begin{aligned} (s_{xy})_{i,j} = & \eta_{i,j} (S_{i,j+1} + S_{i,j-1} \\ & - S_{i+1,j} - S_{i-1,j}) / (\Delta x)^2 \end{aligned} \quad (14)$$

Of course, strain rates are given by the same expressions divided by  $2\eta$ .

The finite difference expressions for strain rates may be multiplied by finite difference expressions for stress deviators and summed to get an expression for shear dissipation. In the continuous case the differential operator

$$\frac{\partial^2}{\partial x \partial y} \left[ 4\eta \frac{\partial^2 S}{\partial x \partial y} \right] + \left( \frac{\partial^2}{\partial y^2} - \frac{\partial^2}{\partial x^2} \right) \left[ \eta \left( -\frac{\partial^2}{\partial y^2} - \frac{\partial^2}{\partial x^2} \right) S \right]$$

may be found by minimizing the volume integral of shear dissipation. We will form a finite difference analogue of this differential operator by minimizing our finite difference expression for shear dissipation. The value of the stream function at a particular grid point enters into expressions for shear dissipation at the four neighboring grid points and four neighboring zone interiors. The sum of these terms is minimized with respect to the stream function at the central grid point when the following equation is satisfied.

$$\begin{aligned}
 & 4\eta_a (s_{NE} - s_N + s_O - s_E) \\
 & - 4\eta_b (s_N - s_{NW} + s_W - s_O) \\
 & + 4\eta_c (s_O - s_W + s_{SW} - s_S) \\
 & - 4\eta_d (s_E - s_O + s_S - s_{SE}) \\
 & + \eta_N (s_{NN} + s_O - s_{NE} - s_{NW}) \\
 & + \eta_S (s_O + s_{SS} - s_{SE} - s_{SW}) \\
 & - \eta_E (s_{NE} + s_{SE} - s_{EE} - s_O) \\
 & - \eta_W (s_{NW} + s_{SW} - s_O - s_{WW}) = 0
 \end{aligned} \tag{15}$$

where subscripts indicate positions shown in Figure 1. It is assumed that the zones are square and uniform in size. More generally there will be a term on the right-hand side arising from buoyant body force.

This finite difference analogue of the differential operator not only satisfies a finite difference variational principle precisely, but also gives a solution that precisely satisfies analogues of the stress equilibrium equations (9) and (10) with stress components defined by equations (13) and

(14). Viscosity may be defined arbitrarily at each grid point and zone interior. Moreover, the self-adjoint property of the differential operator is preserved, for the matrix relating values of stream function at different grid points is symmetric. This may be seen more readily if the expression is rearranged as follows,

$$\begin{aligned}
 & [4(\eta_a + \eta_b + \eta_c + \eta_d) + \eta_E + \eta_N + \eta_W + \eta_S] S_O \\
 & - 4(\eta_d + \eta_a) S_E - 4(\eta_a + \eta_b) S_N \\
 & - 4(\eta_b + \eta_c) S_W - 4(\eta_c + \eta_d) S_S \\
 & + (4\eta_a - \eta_E - \eta_N) S_{NE} + (4\eta_b - \eta_N - \eta_W) S_{NW} \\
 & + (4\eta_c - \eta_W - \eta_S) S_{SW} + (4\eta_d - \eta_S - \eta_E) S_{SE} \\
 & + \eta_E S_{EE} + \eta_N S_{NN} + \eta_W S_{WW} + \eta_S S_{SS} \\
 & = - (\rho_o g \alpha)_O (T_a - T_b - T_c + T_d) (\Delta x)^3 / 2 \quad (16)
 \end{aligned}$$

Here the buoyant term has been written on the right hand side. A system of such equations is to be solved, one equation for each grid point, with the diagram of Figure 1 shifted so that it is centered on each point. The matrix

element linking  $S_E$  to  $S_O$  is  $-4(\eta_d + \eta_a)$ . If the diagram is shifted to the right one zone, one can see that the matrix element linking the same two values (now called  $S_O$  and  $S_W$ ) is  $-4(\eta_b + \eta_c)$ , which is the same. One may examine the other terms in the same way to show that the matrix is symmetric.

We have chosen to define temperature in zone interiors, that is, at points staggered with respect to points where the stream function is defined. In formulating a finite difference analogue of equation (12) the advection terms must be considered carefully. In a mantle convection problem the advection terms will be several times larger than the conduction terms, so it is important that no anomalous diffusion is introduced by the finite difference approximation.

If a system of implicit finite difference equations were used for temperature, the advection terms would contribute antisymmetric components to the matrix operator. Alternating direction implicit (ADI) methods, as well as relaxation methods, are well-founded only for symmetric matrices. Although numerical methods are commonly used successfully in situations that cannot be rigorously defended, a more conservative approach will be used here. Explicit finite difference expressions will be used for the advection terms. To insure stability the time step must be

less than the time for a fluid particle to cross one zone. For a zone size of 10 or 20 kilometers and a fluid velocity of a few centimeters per year, the stability criterion imposed by explicit conduction terms is no more stringent than this advection criterion. Therefore the entire finite difference approximation to equation (12) will be explicit.

In the following equations the superscript  $o$  for old indicates a value from the previous time step, the superscript  $n$  for new indicates a value updated to the current step in time, and  $h$  indicates a value half-way through the time step. To calculate the advection terms temperatures are first defined on faces between zones half-way through the time step,

$$T_A^h = (T_0^o + T_1^o)/2 + u_A^o(T_1^o - T_0^o)\Delta t/(2\Delta x) \quad (17)$$

$$T_B^h = (T_0^o + T_2^o)/2 + v_B^o(T_2^o - T_0^o)\Delta t/(2\Delta y) \quad (18)$$

where subscripts indicate positions in Figure 2. Then an updated temperature due to advection is found by an equation in conservation form

$$T_0^n = T_0^o - (u_A^o T_A^h - u_C^o T_C^h)\Delta t/\Delta x \\ - (u_B^o T_B^h - u_D^o T_D^h)\Delta t/\Delta x \quad (19)$$

This procedure is accurate to second order. For a uniform velocity field there is second order dispersion and fourth order diffusion of temperature, as for the Lax-Wendroff procedure.

Finite difference approximations to the remaining terms of equation (12) are not novel and will not be listed here.

After temperature is advanced a step in time, new values of viscosity and updated buoyant terms can be evaluated. Then an iteration must be performed to find the stream function appropriate to the new temperature field. A few relaxation iterations suffice to correct short wavelength components. After a long wavelength error has accumulated, the complete conjugate gradient iterative procedure should be performed.

#### The Method of Conjugate Gradients

The solution of the system of equations for the stream function over a two-dimensional grid will be discussed in this section as if the unknown values were re-ordered into a vector s of length N. Then the system of equations to be solved is represented by the matrix equation

$$\underline{\underline{K}} \underline{s} = \underline{b} \quad (20)$$

(PRINTER: Single underline in bold face; Double underline in bold face sans serif)

The vector on the right-hand side consists of the buoyant terms and terms containing fixed boundary values. Boundary values proportional to unknown values inside the grid are treated as modifications to some components of the matrix  $\underline{\underline{K}}$ . The matrix  $\underline{\underline{K}}$  for the viscous flow equations formulated in the previous section is symmetric, and the boundary conditions that have been used preserve the symmetry. Also, it is physically reasonable that  $\underline{\underline{K}}$  is positive definite, although no proof has been found. It is not necessary to store the entire matrix  $\underline{\underline{K}}$ , since all components relating to a particular component of  $\underline{s}$  can be formed easily from viscosity values in the neighborhood.

Bennett and Cooley [1969] devised a method of solving such a system of equations that does not require that an  $N \times N$  matrix be formed and stored. Their method is based on earlier ideas of Hestenes and Stiefel [1952] and Lanczos [1952]. It is assumed that  $\underline{\underline{K}}$  is symmetric and positive definite. Let  $\underline{s}^i$  be the approximation to the solution in the  $i$ th iteration and let  $\underline{r}^i$  be its residual,

$$\underline{r}^i = \underline{b} - \underline{\underline{K}} \underline{s}^i \quad (21)$$

Also, an auxiliary vector  $\underline{z}^i$  appears in the algorithm.

The initial step of the algorithm is

$$\underline{x}^0 = \underline{r}^0 = \underline{b} - \underline{K} \underline{s}^0 \quad (22)$$

Then the following sequence of equations is executed iteratively,

$$\underline{g}^i = - (\underline{r}^{iT} \underline{z}^i) / (\underline{z}^{iT} \underline{K} \underline{z}^i) \quad (23)$$

$$\underline{s}^{i+1} = \underline{s}^i - \underline{g}^i \underline{z}^i \quad (24)$$

$$\underline{r}^{i+1} = \underline{r}^i + \underline{g}^i \underline{K} \underline{z}^i \quad (25)$$

$$\underline{f}^i = (\underline{r}^{i+1T} \underline{r}^{i+1}) / (\underline{r}^{iT} \underline{r}^i) \quad (26)$$

$$\underline{z}^{i+1} = \underline{r}^{i+1} + \underline{f}^i \underline{z}^i \quad (27)$$

In each iteration four vectors must be stored,  $\underline{s}^i$ ,  $\underline{r}^i$ ,  $\underline{z}^i$ , and  $\underline{K} \underline{z}^i$ .

The reader is referred to Bennett and Cooley [1969] for a proof of the algorithm. Residuals from different iterations are orthogonal

$$\underline{r}^{iT} \underline{r}^j = 0, \quad i \neq j \quad (28)$$

and the vectors  $\underline{z}^i$  are conjugate with respect to  $\underline{K}$ ,

$$\underline{z}^{iT} \underline{K} \underline{z}^j = 0, i \neq j \quad (29)$$

More importantly, the vectors  $\underline{z}^i$  are linearly independent, so that the successive corrections to the stream function,  $g^i \underline{z}^i$ , span the entire  $N$  dimensional space, after  $N$  iterations. Also the coefficient of each correction,  $g^i$ , given by equation (23), minimizes  $\underline{e}^{i+1T} \underline{K} \underline{e}^{i+1}$ , where  $\underline{e}^{i+1}$  is the error  $\underline{s} - \underline{s}^{i+1}$ . Therefore, if there were no round-off error, an exact solution would be reached in  $N$  iterations or less.

To reduce the effect of round-off error it is desirable that the error of the initial approximation have negligible components with large eigenvalues (short wavelengths). This can be accomplished with a few relaxation iterations before beginning the conjugate gradient procedure.

In our viscous flow calculations it has been found that the calculated product  $\underline{z}^{iT} \underline{K} \underline{z}^i$  is always positive, giving support to our conjecture that our  $\underline{K}$  is positive definite. Long wavelength components of the solution converge faster with the conjugate gradient method than with relaxation methods. On an IBM 360 with six significant figures convergence has been satisfactory with viscosity varying by a factor of 1000. With double precision arithmetic larger viscosity contrasts have been used with no difficulty.

### Mid-Ocean Ridge Calculations

The general calculational method of the first part of this paper is used here to investigate a single aspect of plate tectonics, namely the effectiveness of a mid-ocean ridge as a driving mechanism. General considerations of plate motion driven by thermally induced density instabilities have been given by McKenzie [1969]. In discussions of driving mechanisms, attention is commonly focused either on the plates themselves, or on convection cells below the plates.

In the first class of models, lithospheric plates themselves are recognized as an important part of the total mass circulation [Elsasser, 1971], [Jacoby, 1970]. The density contrast between lithosphere and asthenosphere is a driving mechanism. Plates are pushed by ridges and pulled by down-going slabs. Plates are rigid enough compared to the asthenosphere to act as stress guides. They may be decoupled by the asthenosphere from the rest of the mantle.

In the second class of models the mantle below the lithosphere is considered to be convecting, and plates ride passively on the tops of convection cells [Torrance and Turcotte, 1971a, 1971b].

These two classes should not be considered antithetical, for they both may be important aspects of the complete picture. The model considered here belongs to the first

class with attention focused on the lithosphere. However, it must be recognized that convection is taking place through much of the mantle.

A Newtonian fluid of constant viscosity is unstable against convection if the Rayleigh number exceeds a critical value. Recall that the Rayleigh number increases with larger heat flow, smaller conductivity, smaller viscosity, and greater depth of convection cells. Recent determinations of viscosity by Cathles [1971] and of conductivity by Schatz [1971] strongly support mantle-wide convection. Cathles concludes from a comprehensive analysis of glacial uplift data that viscosity does not exceed  $10^{22}$  poise anywhere in the mantle. With Cathles' viscosity, and any reasonable values for other physical parameters, the critical Rayleigh number is exceeded for the mantle as a whole.

Schatz [1971] has determined that the radiative portion of thermal conductivity of olivine is not as important at high temperature as had previously been thought. He concludes that conductivity in the mantle is roughly constant as a function of depth. If heat were transported by conduction alone in the mantle, Schatz's value of conductivity would require temperatures far above the solidus for most of the mantle. Furthermore, with Cathles' viscosity and Schatz's conductivity, convection

may take place with cells only 140 km from top to bottom. Therefore convection is certainly taking place.

In this work we will consider plate movement away from the ridge axis and a counterflow below the plate confined to depths less than 340 km. The objective is to consider this relatively shallow flow and counterflow independently of the deeper circulation that is certainly taking place, and to establish the conditions for which this model is reasonable.

In order to separate effects, it is necessary to artificially inhibit convection below the lithosphere in our model. The initial geotherm used should be stable against convection in the depth considered. To achieve this objective an artificially high conductivity of 0.1 cal/cm-sec-deg is used for temperatures above 1275 °C. In this way the heat flux from the earth's interior is obtained by conduction alone with a small thermal gradient (1 deg/km), about the magnitude to be expected in the case of convection. A realistic conductivity is used for the lithosphere, 0.0075 cal/cm-sec-deg.

A normal surface heat flux of  $1.1 \times 10^{-6}$  cal/cm<sup>2</sup>-sec is assumed and radioactive heat generation of  $1 \times 10^{-14}$  cal/cm<sup>3</sup>-sec is adopted [Sclater and Francheteau, 1970]. The normal geotherm corresponding to these parameters is shown in Figure 3a. It is assumed that radioactivity is

uniform, for no chemical differentiation is accounted for in this model.

The viscosity model used is shown in Figure 1b for the normal geotherm. Values of viscosity for the asthenosphere and mesosphere are taken from Cathles [1971]. The transition from lithosphere to asthenosphere, normally at 80 km, [Press and Kanamori, 1970] is prescribed to take place at 1130 °C. The transition from asthenosphere to mesosphere is fixed at 160 km depth. The lithosphere is treated as a viscous fluid with viscosity much larger than the rest of the mantle. The actual value of viscosity used in the lithosphere is not important in this calculation, if it is large enough to ensure nearly rigid motion.

A closed circulation path is not considered in this work. An artificial lateral boundary is used, on which horizontal input and output velocities are prescribed. From the calculation, stress at the boundary is found. Although it is artificial to separate this region from the rest of the world, stress at the boundary gives a quantitative indication of their mutual interaction for the assumed spreading velocity.

The prescribed velocity profile at the lateral boundary is shown in Figure 3c. This profile was chosen to minimize dissipation for one-dimensional shear flow. This profile is scaled to get whatever plate velocity is desired.

From this velocity profile shear drag at the base of the lithosphere can be found. It is proportional to velocity and is 9 bars for 1.2 cm/yr half spreading rate. The two-dimensional calculations show nearly horizontal flow and smooth variation of stress near the lateral boundary, thus supporting the treatment of flow through this boundary.

A constant thermal expansivity,  $\alpha = 4 \times 10^{-5} \text{ deg}^{-1}$ , is used [Sclater and Francheteau, 1970; Sleep, 1969]. This value affects flow through buoyancy and affects topography by thermal expansion of the lithosphere. Other physical parameters are heat capacity,  $C_p = 0.311 \text{ cal/gm-deg}$ , density,  $\rho_0 = 3.4 \text{ gm/cm}^3$ , and acceleration of gravity,  $g = 990 \text{ cm/sec}^2$ .

Each of the calculations was done with finite difference zone size of 20 km, and with the calculational region extending to a depth of 340 km and a distance of 1000 km from the ridge axis. The ridge axis was treated as a plane of reflection.

### Results

Streamlines and isotherms are shown in Figure 4 for the case of 1.2 cm/yr plate velocity run to steady state. Streamlines within the lithosphere are quite close to being straight and parallel. The velocity of upwelling at the ridge axis is 1.6 cm/yr, greater than the plate velocity

in this case. The flow pattern is not similar for different spreading rates. For a plate velocity of 6.0 cm/yr the upwelling velocity is 2.6 cm/yr. Shear heating far from the ridge in the case of 1.2 cm/yr plate velocity contributes only 1.5% to the normal surface heat flux. Shear heating, of course, is proportional to the square of plate velocity for moderate velocities, and then increases less rapidly since the increased heat flow thins the lithosphere.

The time dependent calculations done represent spreading histories at four different ridge locations. A calculation to steady state was run for 1.2 cm/yr to represent the Mid-Atlantic ridge at 32 N. This spreading rate was averaged from Pitman et al. [1971]. A constant velocity of 1.8 cm/yr was used to represent the Mid-Atlantic ridge at 28 S, [Dickson, 1968; Maxwell, 1969]. A variable spreading rate was used for the Reykjanes ridge of 1.2 cm/yr for 0 to 9 m.y.b.p., 0.4 cm/yr for 9 to 37 m.y.b.p., 1.8 cm/yr for 37 to 50 m.y.b.p., and 1.2 cm/yr earlier [Pitman et al., 1971]. The East Pacific Rise at 43 S is represented by spreading history of 6 cm/yr for 0 to 9 m.y.b.p. and 1.8 cm/yr before that [Pitman, 1968]. According to Pitman's magnetic anomaly map the ridge is spreading asymmetrically. The spreading history used here applies to the east flank.

Surface heat flow found in each of these calculations closely agrees at corresponding ages of ocean floor. Since

observed heat flow data have large scatter, it is reasonable to make one plot applicable to all locations by using age as the independent variable. In Figure 5 calculated heat flow is compared with data from the Pacific [Sclater and Francheteau, 1970]. Calculated heat flow values for the two steady state cases are identical at corresponding ages and are shown as Curve A. Calculated heat flow for the Reykjanes and East Pacific ridges, Curves B and C, deviate from the steady state case much less than the deviation of observed data. The error bars indicate standard deviations of the observations. Since measurements are made preferentially in sediment ponds, the data may be as much as 50% too low [Sclater and Francheteau, 1970]. If there is water circulation through fractures in the ocean floor, a significant part of the total heat flow may not be measured, especially in rough topography near the ridge crest [Lister, 1971]. Therefore it is not unreasonable that the theoretical prediction is at the upper side of the scatter of data.

In the viscous flow calculation the upper boundary is a rigid horizontal plane on which free sliding is allowed. From the calculated stream function, pressure and viscous stress deviators are known throughout the region. The vertical stress component (pressure plus deviator) is not zero at the upper surface. From this component one obtains

mass per unit area lying above this reference plane, and hence elevation of the ocean floor.

In Figures 6 through 9 calculated results for the four ridge locations are compared to observed data. In each case an observed topography is shown [Talwani, 1970], together with calculated topography resulting from viscous stress. Also shown is topography calculated from temperature assuming isostatic compensation at 1.00 km depth.

Comparison with free air gravity measurements is not shown, since the prediction is sensitive to temperature and stress at the artificial lower boundary. The fact that observed mean free air anomalies are near zero may be a sensitive test for later work on the entire mantle circulation. Predicted Bouguer anomalies, dependent primarily on topography, are compared to observed for the Reykjanes [Talwani et al, 1971] and North Atlantic ridges [Talwani et al., 1965].

In the 1.2 and 1.8 cm/yr cases topography calculated from viscous stress and isostatic topography differ only slightly. In this case the cooling slab model of McKenzie [1967] and Sleep [1969] is valid for topography and heat flow. As in that model, one can adjust conductivity and expansivity to fit topography, but it is not possible to fit both topography and mean heat flow with one set of parameters [Sleep, 1969; Sclater and Francheteau, 1970].

In the case of the East Pacific Rise the calculated topography is far from being isostatic.

The effectiveness of a mid-ocean ridge as a driving mechanism is demonstrated in Figure 10, which shows the force transmitted by the lithosphere, acting as a stress guide. The horizontal stress deviator component is integrated through the thickness of the lithosphere, and the result is expressed in terms of the equivalent stress for a thickness of 60 km. Beyond 1000 km reasonable extrapolations are shown. One might ask why the viscous contribution to mean stress, the nonisostatic pressure, is not taken into account in the Figure. In all cases calculated the work done by nonisostatic pressure at the lateral boundary was nearly the same as the work done by the stress deviator there. Therefore the stress deviator is a good indicator of driving mechanism.

Drag on the base of the lithosphere requires that horizontal stress become more tensile with increasing distance from the ridge axis. This explains the positive slope of force with respect to distance far from the ridge. Closer in, where the lithosphere is gradually thickening compressive stress is built up due to the buoyancy of underlying material. For the slow moving ridges this mechanism is an important part of the overall driving mechanism. At a velocity of 1.2 cm/yr, the ridge can

produce compressive stress in the lithosphere out to a distance of 1600 km.

For the East Pacific Rise, however, the horizontal stress deviator in the lithosphere is tensile at all distances, and reaches unrealistically high values within 1000 km. This tensile stress would be high enough to produce continual earthquakes in the interior of the plate. Such earthquakes, of course, are rare. Mendiguren [1971] analyzed the source mechanism of a shock from the middle of the Nazca plate, and found horizontal compressive stress, in contradiction to the prediction of this model for fast spreading.

Therefore the counterflow for fast moving plates cannot be confined to relatively shallow depths, as postulated here. The driving mechanism in these cases certainly must involve upwelling from greater depths, and possibly a convection cell of considerable depth in the mantle. The asthenosphere is not weak enough to decouple plates from flow lower in the mantle.

#### Acknowledgements

The author is grateful to John Minear for calling his attention to the method of conjugate gradients, to Norman Sleep and Larry Cathles for many stimulating discussions and to Jean-Claude de Bremaecker for our mutual

exchange of ideas in this area. Judy Andrews helped with the library search and preparation of figures.

This research was supported by a grant to Professor M. Nafi Toksöz by the Advanced Research Projects Agency and monitored by the Air Force Office of Scientific Research under contract AF49(638)-1763.

# REFERENCES

- Bennett, J.M. and P.C. Cooley, Linear analysis of structures by the method of conjugate gradients, 41 pp., Basser Computing Department, University of Sydney, Technical Report 51, 1969.
- Burggraf, O.R., Analytical and numerical studies of steady separated flows, J. Flu. Mech., 24, 113, 1966.
- Cathles, Lawrence, The viscosity of the earth's mantle, PH.D. thesis, Princeton University, 1971.
- Courant, R. and D. Hilbert, Methods of Mathematical Physics, Vol. I, 561 pp., Interscience, New York, 1953.
- Dickson, G., E. Pitman, and J. Heirtzler, Magnetic anomalies in the south Atlantic and ocean-floor spreading, J. Geophys. Res., 73, 2087, 1968.
- Elsasser, W.M., Sea floor spreading as thermal convection, J. Geophys. Res., 76, 1101, 1971.
- Hestenes, M., and E. Stiefel, Methods of conjugate gradient for solving linear systems, Journal Res. NBS, 49, 409, 1952.
- Jacoby, W.R., Instability in the upper mantle and global plate movements, J. Geophys. Res., 75, 5655, 1970.
- Lanczos, C., Solution of systems of linear equations by minimized iterations, Journal Res. NBS, 49, 33, 1952.

- Lister, C.R.B., On the thermal balance of a mid-ocean ridge, (abstract), Trans. Am. Geophys. Union, 52, 923, 1971.
- McKenzie, D.P., Some remarks on heat flow and gravity anomalies, J. Geophys. Res., 72, 6261, 1967.
- McKenzie, D.P., Speculations on the consequences and causes of plate motions, Geophys. J. R. astr. Soc., 18, 1, 1969.
- Maxwell, E.E., R.P. Von Herzen, K.J. Hsu, J.E. Andrews, T. Saito, S.F. Percival, Jr., E.D. Metow, and R.E. Boyce, Recent deep sea drilling results from the South Atlantic, Science, 168, 1047, 1970.
- Mendiguren, J.A., Focal mechanism of a shock in the middle of the Nazca plate, J. Geophys. Res., 76, 3861, 1971.
- Pitman, W.C. III, E.M. Herron, and J.R. Heirtzler, Magnetic anomalies in the South Pacific Ocean and sea-floor spreading, J. Geophys. Res., 73, 2069, 1968.
- Pitman, W.C. III, M. Talwani, and J.R. Heirtzler, Age of the North Atlantic Ocean from magnetic anomalies, Earth and Planet. Sci. Letters, 11, 195, 1971.
- Press, F., and H. Kanamori, How thick is the lithosphere, (abstract), Trans. Am. Geophys. Union, 51, 363, 1970.
- Schatz, J.F., Thermal conductivity of earth materials at high pressures, Ph.D. thesis, Massachusetts Institute of Technology, 1971.

- Sclater, J.G., and Jean Francheteau, The implications of terrestrial heat flow observation on current tectonic and geochemical models of the crust and upper mantle of the earth, Geophys. J. R. astr. Soc., 20, 509, 1970.
- Sleep, N.H., Sensitivity of heat flow and gravity to the mechanism of sea-floor spreading, J. Geophys. Res., 74, 542, 1969.
- Talwani, M., Gravity, The Sea, Vol. 4, edited by A.E. Maxwell, Interscience, New York, 251, 1970.
- Talwani, M., X. Le Pichon, and M. Ewing, Crustal structure of the mid-ocean ridges, computed model from gravity and seismic refraction data, J. Geophys. Res., 70, 341, 1965.
- Talwani, M., C.C. Windisch, and M.G. Langseth, Jr., Reykjanes ridge crest: a detailed geophysical study, J. Geophys. Res., 76, 473, 1971.
- Torrance, K.E., and D.L. Turcotte, Thermal convection with large viscosity variations, Journal Flu. Mech., 47, 1971a.
- Torrance, K.E. and D.L. Turcotte, Structure of convection cells in the mantle, J. Geophys. Res., 76, 3154, 1971b.
- Varga, R.S., Matrix Iterative Analysis, Prentice-Hall, New York, 1962.

### FIGURE CAPTIONS

- Figure 1. Diagram showing grid locations to which subscripts refer in equations (15) and (16), relative to grid point  $i,j$  (point 0).
- Figure 2. Grid locations to which subscripts refer in equations (17), (18), and (19).
- Figure 3. Left: Normal geotherm used in the calculations. Center: Viscosity model corresponding to the normal geotherm. Right: Velocity profile of plate motion and counterflow below that minimizes shear dissipation for horizontal flow. This velocity profile was used at the artificial lateral boundary in the calculations.
- Figure 4. Streamlines and isotherms for plate velocity of 1.2 cm/yr in steady-state.
- Figure 5. Heat flow as a function of age. Average heat flow measurements for the North Pacific [Sclater and Francheteau, 1970] are compared with calculated heat flow for Reykjanes 60°N, North Atlantic 32°, South Atlantic 28°, and the East

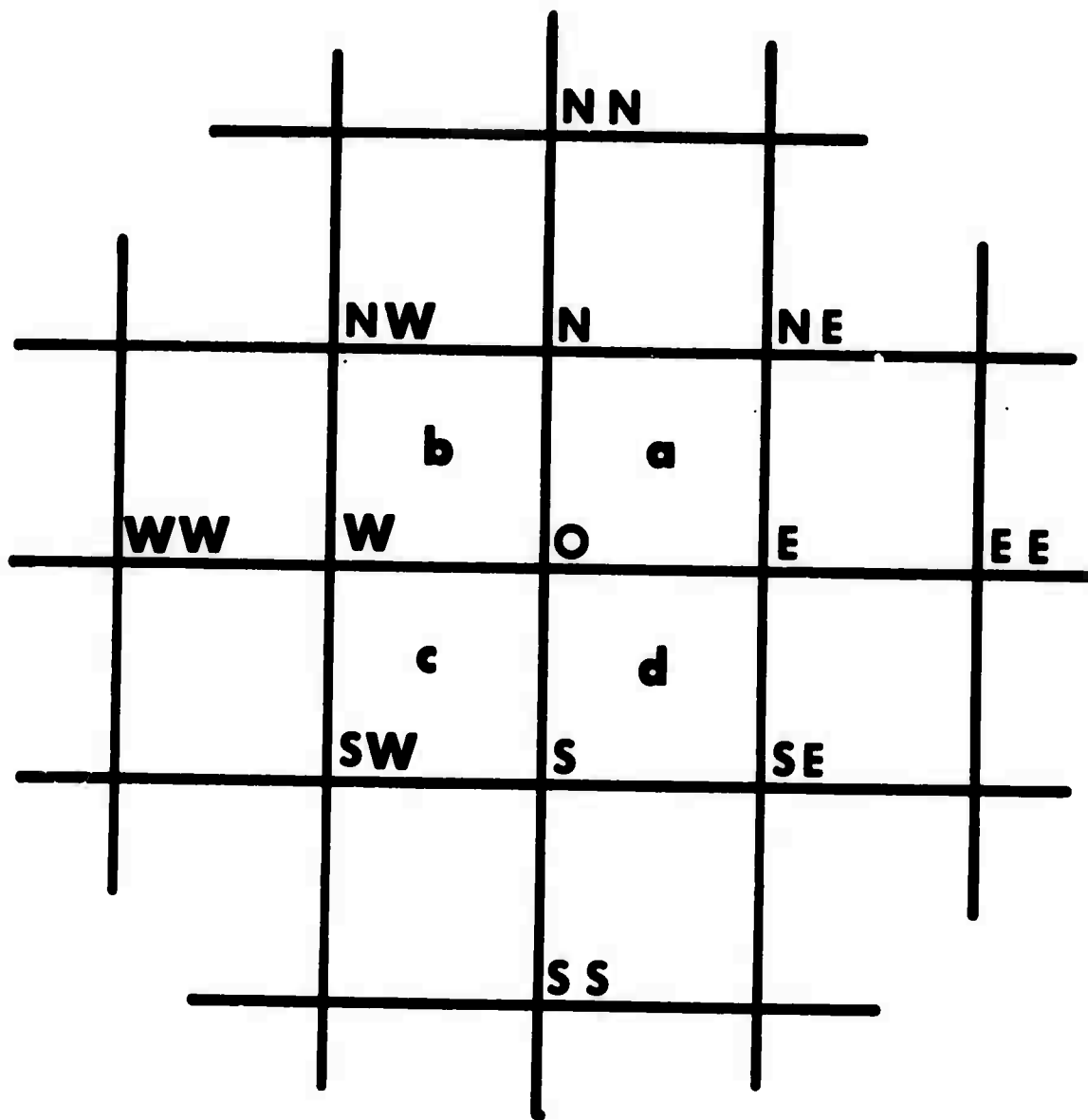
Pacific 43°S. Error bars denote standard deviation of observed heat flow data.

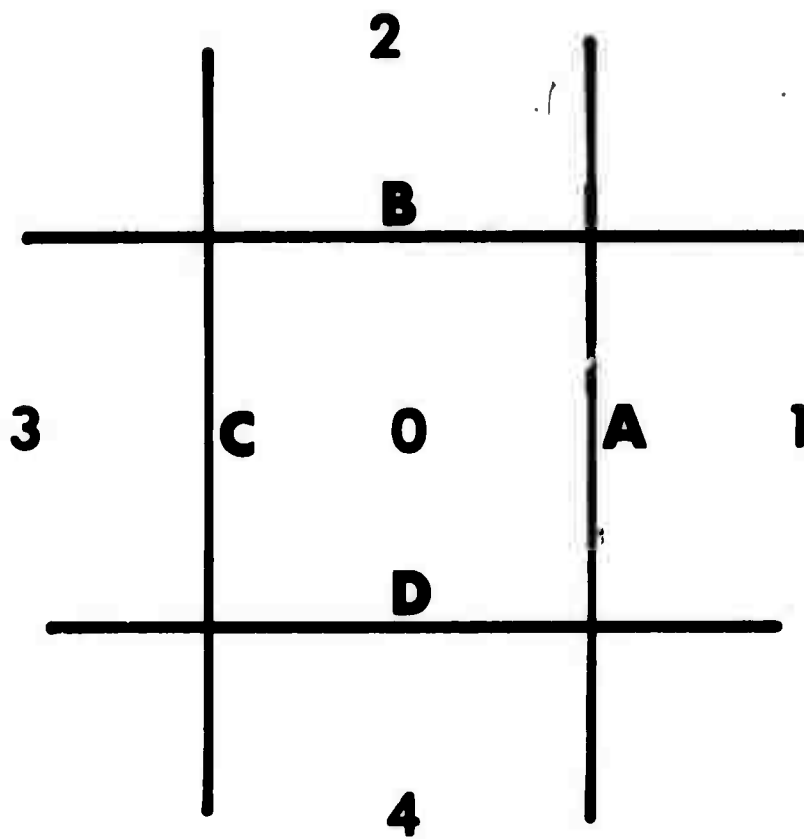
- Figure 6. North Atlantic 32°, topography and gravity. Top: Observed Bouguer anomaly [Talwani and Le Pichon, 1965] is compared to present calculation. Bottom: Observed topography [Talwani, 1970] is compared to calculated isostatic topography (dashed curve) and calculated topography resulting from viscous stresses (solid curve). Sea floor spreading rates were averaged from Pitman and Talwani [1971].
- Figure 7. South Atlantic 28°, topography. Observed topography [Talwani, 1970] is compared to calculated isostatic topography (dashed curve) and calculated topography resulting from viscous stresses (solid curve). Sea floor spreading rates were averaged from Maxwell [1969], Dickson et al. [1968] and Heirtzler et al. [1968].
- Figure 8. Reykjanes 60°N, topography and gravity. Top: Observed Bouguer anomaly [Talwani et al., 1971]

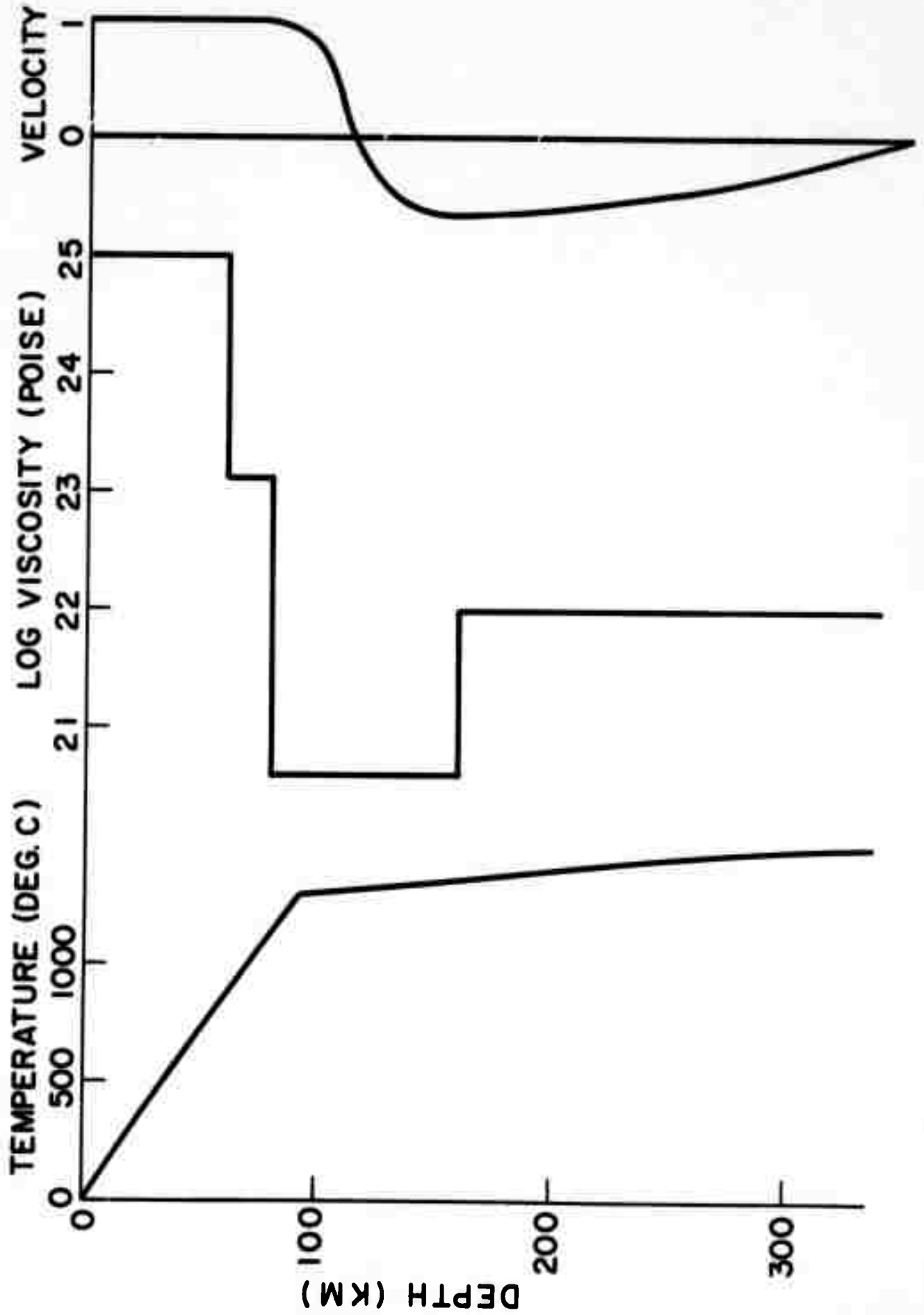
is compared to present calculation. Bottom: Observed topography is compared to calculated isostatic topography (dashed curve) and calculated topography resulting from viscous stresses (solid curve). Sea floor spreading rates were taken from Pitman and Talwani [1971].

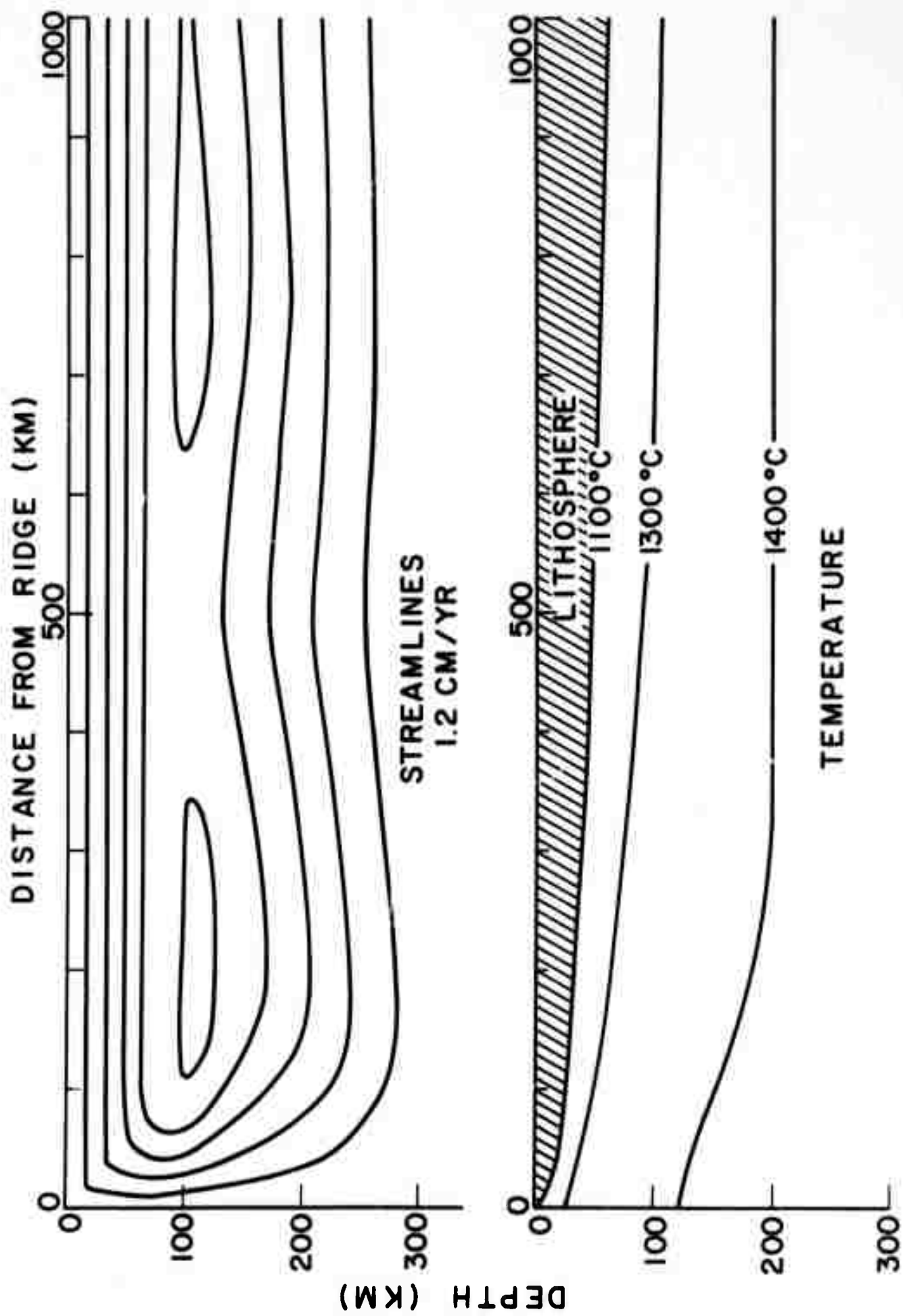
Figure 9. South Pacific 43°, topography. Observed topography [Talwani, 1970] is compared to calculated isostatic topography (dashed curve) and calculated topography resulting from viscous stresses (solid curve). Sea floor spreading rates were obtained from Pitman et al. [1968] and Heirtzler et al. [1968].

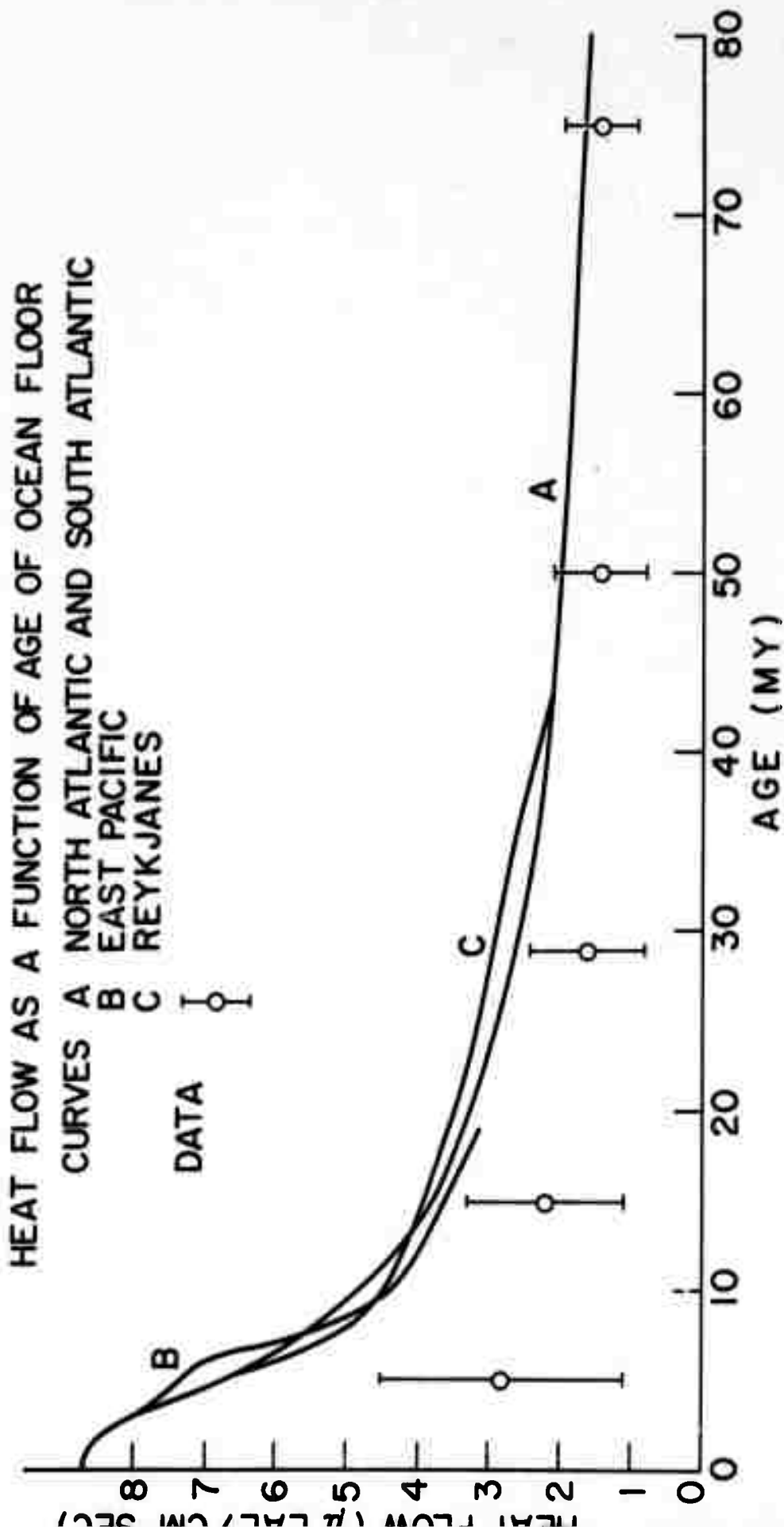
Figure 10. Horizontal stress deviator integrated through the thickness of the plate and divided by 60 km,  $\int s_{xx} dy/60$ , is plotted as a function of distance from the ridge axis.

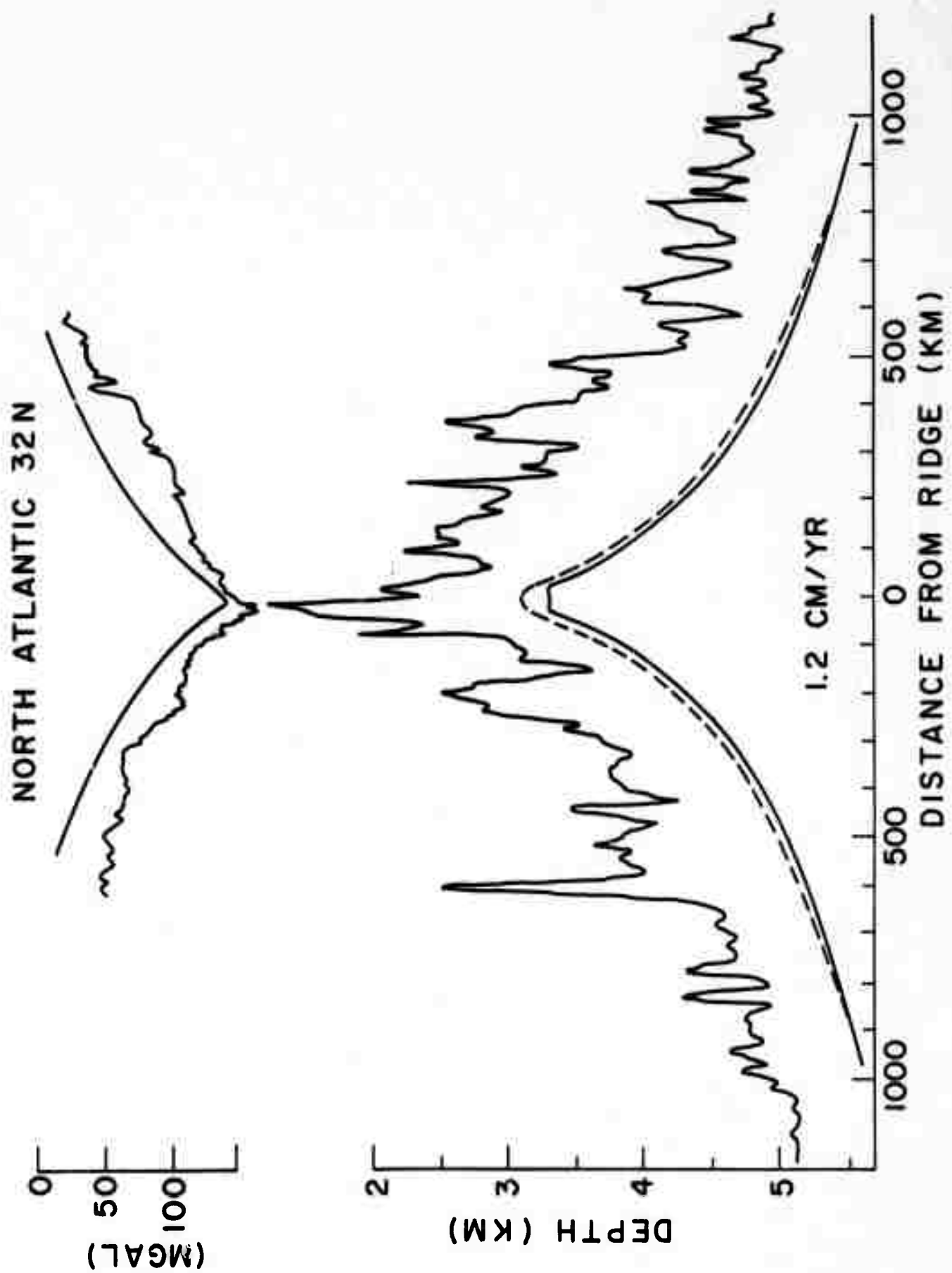


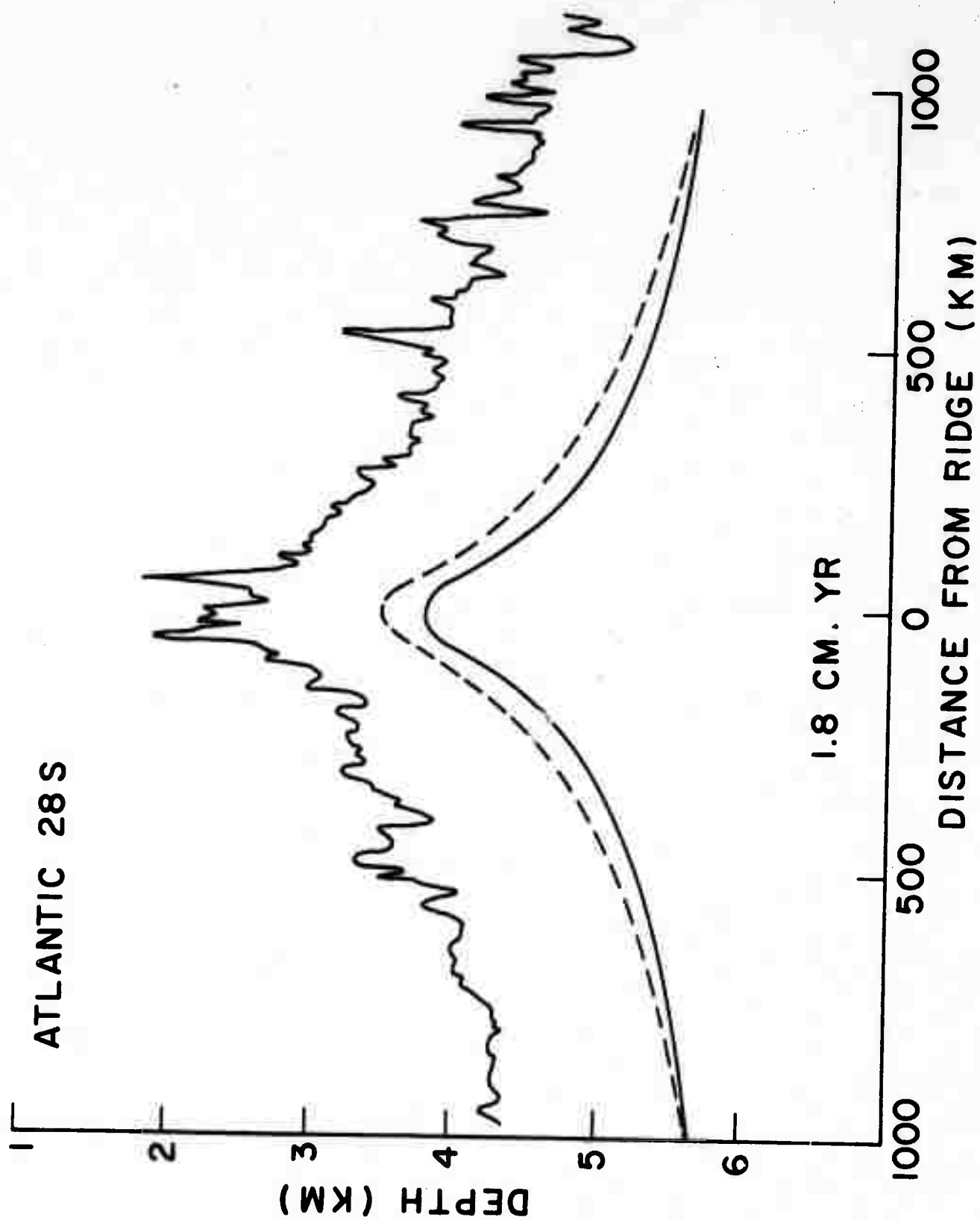


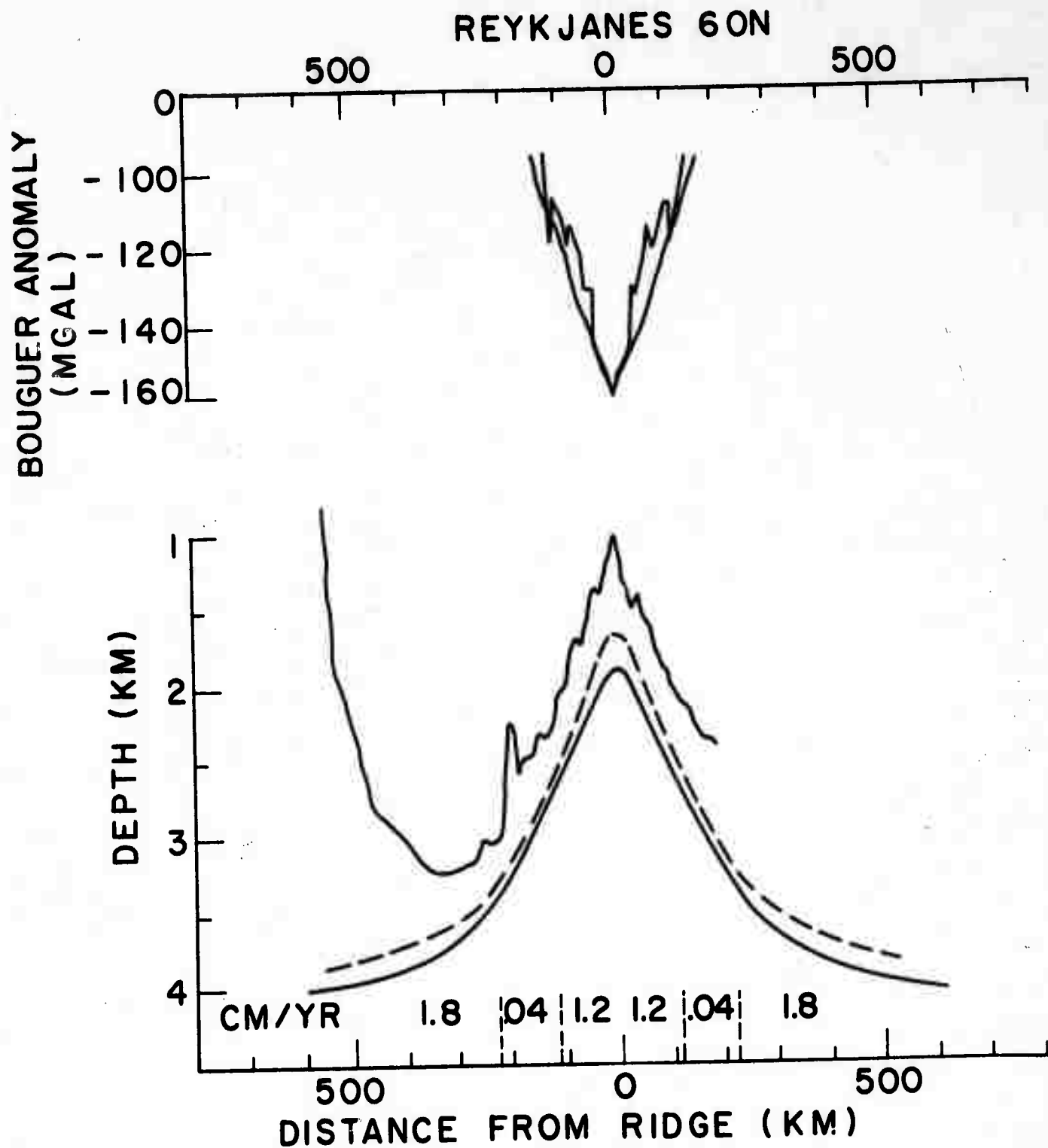


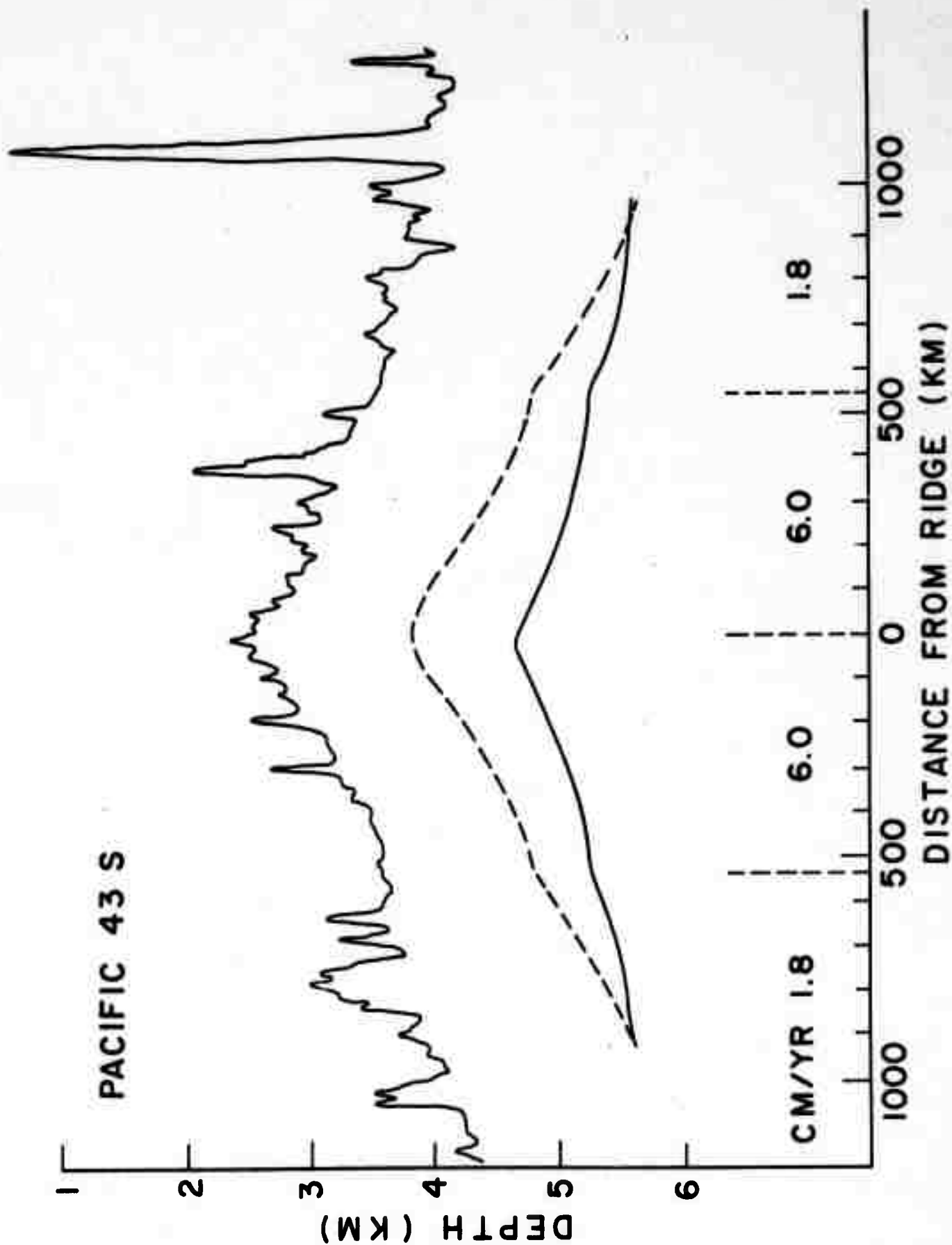


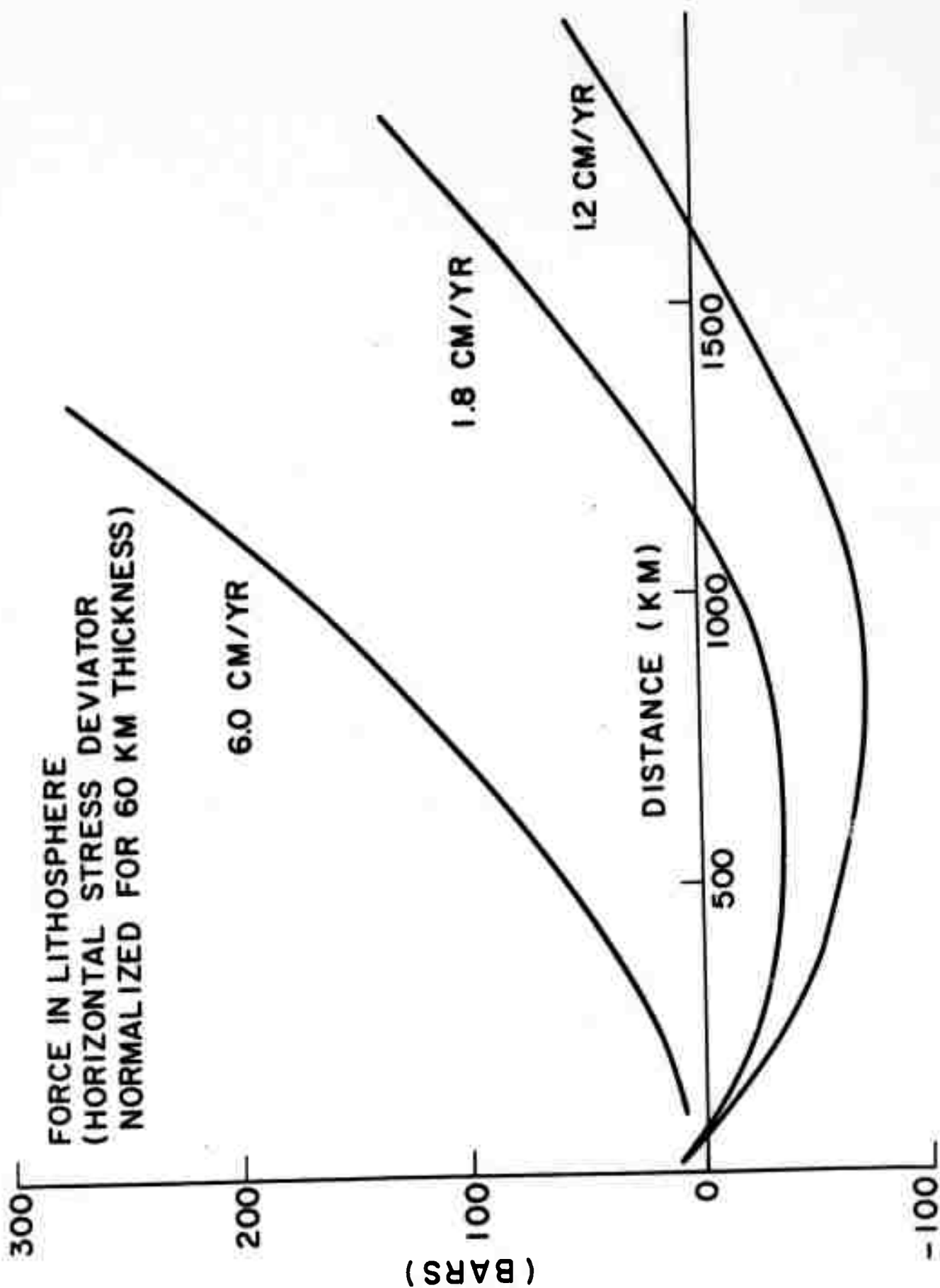












VII.

LIST OF PUBLICATIONS FOR THE PERIOD 1969 THROUGH 1971

- Andrews, D. J., Numerical simulation of sea-floor spreading, submitted to J. Geophys. Res., 1971.
- Andrews, D. J. and S. Shlien, Calculated attenuation of an underground explosion wave in the nearly-elastic range (abstract), Earthquake Notes, 42, 9, 1971.
- Bakun, W. H., Crustal structure beneath LASA from long-period P-wave spectra, submitted to J. Geophys. Res., 1971.
- Bakun, W. H., Focal depths of the 1966 Parkfield, California, earthquakes, J. Geophys. Res., in press, 1971.
- Boore, D. M., K. Aki, and T. Todd, A two-dimensional moving dislocation model for a strike-slip fault, Bull. Seism. Soc. Am., 61, 177-194, 1971.
- Boore, D. M., K. L. Larner, and K. Aki, Comparison of two independent methods for the solution of wave scattering problems: response of a sedimentary basin to vertically incident SH waves, J. Geophys. Res., 76, 558-569, 1971.
- Derr, J. S., Discrimination of earthquakes and explosions by the Rayleigh-wave spectral ratio, Bull. Seism. Soc. Am., 60, 1653-1668, 1970.
- Gilbert, F. and D. V. Helmberger, Generalized ray theory for a layered sphere, J. Geophys. Res., in press, 1971.
- Helmberger, D. and R. A. Wiggins, Upper mantle structure of

- midwestern United States, J. Geophys. Res., 76, 3229-3245, 1971.
- Hirasawa, T., Radiation patterns of S waves from underground nuclear explosions, J. Geophys. Res., 76, 6440-6454, 1971.
- Hirasawa, T. and M. J. Berry, Reflected and head waves from a linear transition layer in a fluid medium, Bull. Seism. Soc. Am., 61, 1-26, 1971.
- Husebye, E. and R. Madariaga, The origin of precursors to core waves, Bull. Seism. Soc. Am., 60, 939-952, 1970.
- Mack, H., Twenty- to eighty-second period characteristics of nuclear explosions recorded at LASA, in Copies of Papers Presented at Woods Hole Conference on Seismic Discrimination, 1, ARPA Working Paper, July 20-23, 1970.
- Mack, H., Multipathing of Rayleigh waves generated by Milrow, in Copies of Papers Presented at Woods Hole Conference on Seismic Discrimination, 2, ARPA Working Paper, July 20-23, 1970.
- Toksöz, M. N., J. W. Minner, and B. R. Julian, Temperature field and geophysical effects of a downgoing slab, J. Geophys. Res., 76, 1113-1138, 1971.

VIII.

RESEARCH ASSOCIATES SUPPORTED BY CONTRACT NO. AF49/638-1763

Below is a brief resume for each of the twelve Research Associates, in alphabetical order, supported by the present contract during the years 1966 to 1971. Included are their periods of tenure, their research interests and the publications that resulted from work done at M. I. T. Their studies and contributions in seismology cover a broad spectrum of problems. They all had some exposure to Large Aperture Seismic Arrays, theoretical techniques and seismic data. A number of these scientists are fully involved with seismic arrays and research on seismic discrimination.

Dudley J. Andrews

Dr. Andrews has been a Research Associate since 1970. He has been working on numerical calculations of wave propagation, crustal movement, and mantle flow. Of particular interest is his work on the shape of the pressure pulse from an underground nuclear explosion in the nearly elastic range of distances.

Publications:

Andrews, D. J., A numerical method for creep deformation of solids (abstract), EOS Trans. Amer. Geophys. Un., 52,

347, 1971.

Andrews, D. J. and S. Shlien, Calculated attenuation of an underground explosion wave in the nearly elastic range (abstract), Earthquake Notes, 42, 9, 1971.

Andrews, D. J., Numerical simulation of sea-floor spreading, submitted to J. Geophys. Res., 1971.

#### William H. Bakun

Dr. Bakun was a Research Associate during 1970-1971. He studied the crustal structure beneath LASA using the Haskell-Thomson theory and he determined the focal depths of earthquakes from near-source observations of various crustal P phases.

#### Publications include:

Bakun, W. H., Focal depths of the 1966 Parkfield, California, earthquakes, J. Geophys. Res., in press, 1971.

Bakun, W. H., Crustal structure beneath LASA from long-period P-wave spectra, submitted to J. Geophys. Res., 1971.

#### David M. Boore

Dr. Boore was a Research Associate during 1969-1970. His interests included numerical and wave theoretical studies of body and surface wave propagation in heterogeneous media

media and theoretical models of the earthquake source.

Publications:

Boore, D., M., K. Aki, and T. Todd, A two-dimensional moving dislocation model for a strike-slip fault, Bull. Seism. Soc. Am., 61, 177-194, 1971.

Boore, D. M., K. L. Larner, and K. Aki, Comparison of two independent methods for the solution of wave scattering problems: response of a sedimentary basin to vertically incident SH waves, J. Geophys. Res., 76, 558-569, 1971.

John S. Derr

Dr. Derr was a Research Associate during 1968-1970. He analyzed data from M.I.T.'s new mercury tiltmeter and studied the amplitude spectra of Rayleigh waves as a discriminant between earthquakes and explosions.

Publications:

Derr, J. S., Discrimination of earthquakes and explosions by the Rayleigh wave spectral ratio, Bull. Seism. Soc. Am., 60, 1653-1668, 1970.

Donald V. Helmberger

Dr. Helmberger was a Research Associate during 1967-1969. He worked on generalized ray theory and its use in the compu-

tation of theoretical seismograms. By comparing theoretical with observed records, he studied the compressional and shear wave velocities of the crust and upper mantle and the fine structure of the crust-mantle transition.

Publications include:

Helmberger, D. V. and G. B. Morris, A travel time and amplitude interpretation of a marine refraction profile: primary waves, J. Geophys. Res., 74, 483-494, 1969.

Helmberger, D. V. and G. B. Morris, A travel time and amplitude interpretation of a marine refraction profile: transformed shear waves, Bull. Seism. Soc. Am., 60, 593-600, 1970.

Helmberger, D. V. and R. A. Wiggins, Upper mantle structure of midwestern United States, J. Geophys. Res., 76, 3229-3245, 1971.

Gilbert, F. and D. V. Helmberger, Generalized ray theory for a layered sphere, in press J. Geophys. Res., 1971.

Tomowo Hirasawa

Dr. Hirasawa was a Research Associate during 1968-1969. His work included wave theoretical studies of compressional waves and an investigation of tectonic strain release by nuclear explosions using shear wave radiation patterns.

Publications include:

Hirasawa, T. and M. J. Berry, Reflected and head waves from a

linear transition layer in a fluid medium, Bull. Seism. Soc. Am., 61, 1-26, 1971.

Hirasawa, T., Radiation patterns of S waves from underground nuclear explosions, J. Geophys. Res., 76, 6440-6454, 1971.

#### Eystein S. Husebye

Dr. Husebye was a Research Associate during 1966-1968. He was interested in the seismic array as a tool for studying the earth. He developed methods for measuring  $dT/d\Delta$  and  $d^2T/d\Delta^2$  using LASA and applied the techniques to study core phases. Husebye is currently on the staff of NORSAR.

Publications include:

Husebye, E. S., Direct measurement of  $dT/d\Delta$ , Bull. Seism. Soc. Am., 59, 717-727, 1969.

Husebye, E. and R. Madariaga, The origin of precursors to core waves, Bull. Seism. Soc. Am., 60, 939-952, 1970.

Toksöz, M. N., E. S. Husebye, and R. A. Wiggins, Structure and properties of the earth's core, in preparation, 1971.

#### Bruce R. Julian

Dr. Julian was a Research Associate during 1969-1970. His work focused on ray theory for heterogeneous media with applications to lateral variations of seismic velocity in the mantle. Particular emphasis was placed on understanding the

effect on body-wave travel-times and amplitude radiation patterns of downgoing plates. Dr. Julian is currently a member of the Seismic Discrimination Group at M. I. T. Lincoln Laboratory.

Publications include:

Julian, B. R., Regional variations in upper mantle structure in North America (abstract), EOS Trans. Amer. Geophys. Un., 51, 359, 1970.

Toksöz, M. N., J. W. Minear, and B. R. Julian, Temperature field and geophysical effects of a downgoing slab, J. Geophys. Res., 76, 1113-1138, 1971.

Harry Mack

Dr. Mack was a Research Associate during 1969-1970. He worked on array processing of seismic and microbarograph data. In particular, using frequency-wave number analysis, he studied the spectral characteristics of Rayleigh waves from several nuclear explosions and earthquakes and the problem of surface-wave multipathing. Dr. Mack is currently with the Array Analysis Center at Teledyne.

Publications include:

Mack, H., Twenty- to eighty-second period characteristics of nuclear explosions recorded at LASA, in Copies of Papers Presented at Woods Hole Conference on Seismic Discrimina-

tion, 1 (ARPA), July 20-23, 1970.

Mack, H., Multipathing of Rayleigh waves generated by Milrow,  
in Copies of Papers Presented at Woods Hole Conference  
on Seismic Discrimination, 2 (ARPA), July 20-23, 1970.

John W. Minear

Dr. Minear was a Research Associate during 1968-1969. He constructed numerical models for mantle convection and lithosphere subduction. Particularly important work was his temperature models for downgoing slabs of lithosphere and the associated effects on such geophysical properties as seismic wave propagation.

Publications include:

Minear, J. W. and M. N. Toksöz, Thermal regime of a downgoing slab and new global tectonics, J. Geophys. Res., 75, 1397-1419, 1970.

Minear, J. W. and M. N. Toksöz, Thermal regime of a downgoing slab, Tectonophysics, 10, 367-390, 1970.

Toksöz, M. N., J. W. Minear, and B. R. Julian, Temperature field and geophysical effects of a downgoing slab, J. Geophys. Res., 76, 1113-1138, 1971.

Masanori Saito

Dr. Saito was a Research Associate during 1966-1968. His

work included a technique for synthesizing dilatational and rotational seismograms from an array of three-component stations and the computation of variational parameters and excitation functions for surface waves and free oscillations in layered media. His computer programs from his latter studies have been used extensively by students and staff at M.I.T. and elsewhere to study earth structure and source properties from surface wave dispersion and amplitude data.

Publications include:

- Saito, M., Excitation of free oscillations and surface waves by a point source in a vertically heterogeneous earth, J. Geophys. Res., 72, 3689-3699, 1967.
- Saito, M., Synthesis of rotational and dilatational seismograms, J. Phys. Earth, 16, 53-61, 1968.
- Saito, M., Partial derivatives of the phase velocity of surface waves with respect to anisotropy factors, in preparation, 1971.

#### Roger Turpening

Dr. Turpening was a Research Associate during 1966-1967. He studied particle motion-mode filter and designed a digital filter to enhance rectilinear motion in the presence of retrograde elliptical motion.